Appendix B: Evaluation of Stratification and Mixed Layer Depth in San Francisco Bay

Introduction

Salinity driven density changes is a fundamental process of estuarine hydrodynamics. The density structure has a first-order effect on vertical and lateral transport processes that modulate light and nutrients and phytoplankton productivity. Density is directly linked with momentum and scalar mixing as it can inhibit or induce vertical mixing depending on its vertical structure. Furthermore, horizontal density gradients induce basin-scale baroclinic motions. Hence, the success of any numerical simulation directly depends on proper modeling of density and needs to be verified with observed data.

Many complex physical processes control the properties of the upper part of the water body, including the density, (e.g., see Figure B.1), and hence it is a complicated task to predict the density in a numerical model. Density stratification can change rapidly due to external forcings such as atmosphere fluxes (e.g. wind, heat fluxes), precipitation, freshwater flow, etc. A model's ability to predict density stratification depends on several parameters including the model grid resolution, correct implementation of the boundary and initial conditions, proper modeling of sub-grid scale turbulent processes, and parameterization of evaporation in shallow areas.

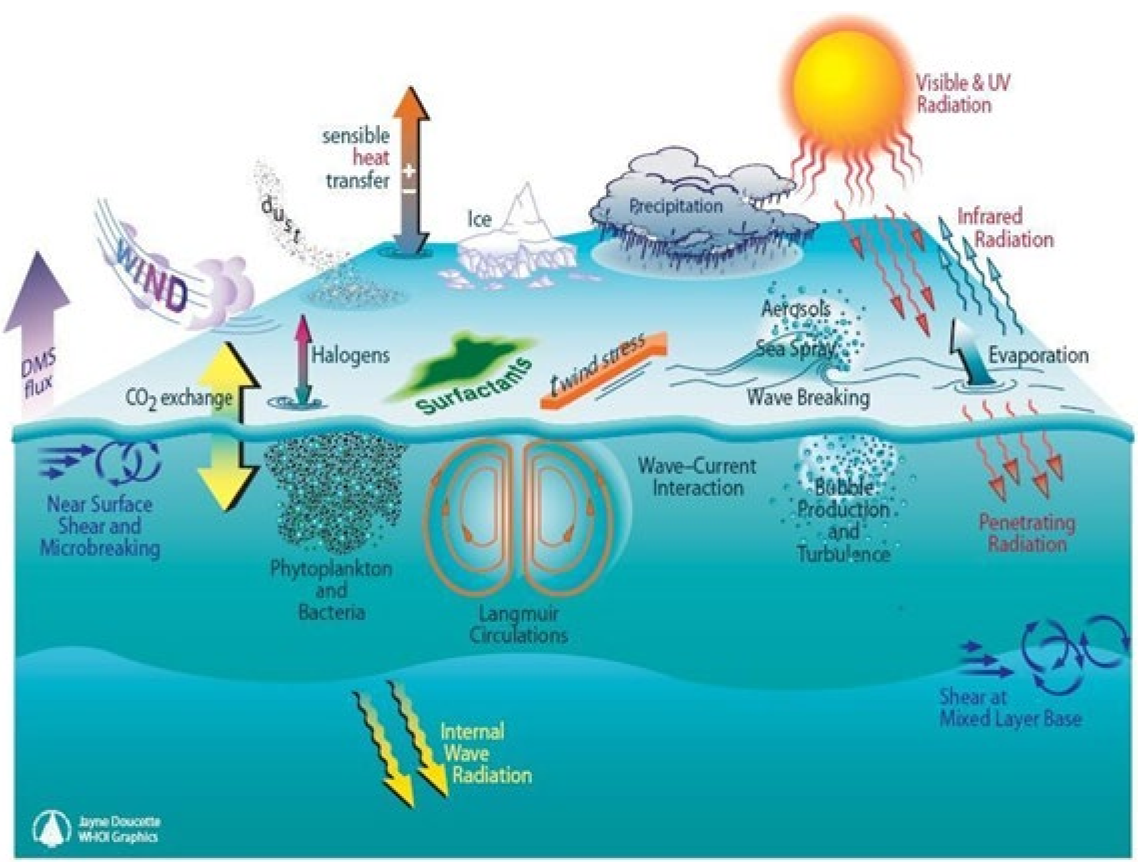

Figure B.1. Conceptual diagram illustrating phenomena affecting physical and biogeochemical processes especially in the upper part of the water body

The unstructured nature of the DFM grid allows for efficient and flexible resolution of flow features ranging from small perimeter sloughs and ponds up to a regional representation of the coastal ocean. This range of features is resolved without explicit seams or nesting boundaries as would be required for a structured grid model applied to the same area.

Like any other model, DFM has errors and inaccuracy due to many factors such as the discretization schemes, model spatial and temporal resolution, model inputs like initial and boundary conditions, and turbulence parameterizations. Hence, the model results need to be verified against observations.

The validation of the velocity, water surface elevation, density and stratification variability are important for evaluation of the coupled hydrodynamic-biogeochemical processes that affect primary production and nutrient cycling within SFB. It is relatively straightforward to validate model predictions of velocity, water surface elevation, salinity and temperature against direct field observations. Many of these were presented in the report. Other hydrodynamic models of SFB have been predominantly calibrated to these basic observations similar to those presented in the previous report.

The focus of this section will be on validating derived metrics of stratification and mixing that cannot be directly measured in the field, but that are nonetheless very useful in furthering the understanding of biogeochemistry in the system. This includes density, buoyancy frequency (N^2) and mixed layer depth (MLD). These derived parameters allow an evaluation of density stratification strength over depth. The buoyancy frequency is proportional to the vertical density gradient, and is a measure of the stability of fluid parcels in a water column. It shows the natural frequency of a water parcel when displaced from its position. The mixed layer (ML) is defined as the upper portion of the water column where turbulent mixing results in a fairly uniform vertical density profile. The generated turbulence can be caused by air-sea interactions (e.g. wind stress, heat fluxes) or other estuarine processes (e.g. slump of density fronts). MLD and its temporal/spatial variability is an important parameter which controls the mixing and fate of scalars, which in turn has implications on biogeochemical processes and nutrient cycling.

Some derived estimates such as density are relatively straightforward to validate because of standard relationships that can be used to calculate these parameters from direct observations (e.g. the equation of state for calculating density). However, other derived estimates such as MLD are more challenging to validate because of the inherent uncertainty introduced in the methods used to derive these estimates from either the field observations or the corresponding predictions in the model.

The peer-reviewed literature on the verification of estuarine MLD is also fairly limited (Irby *et al.* 2016). Therefore, in this section we have used more complicated validation methods to assess whether model predictions of stratification are reasonable, and the fundamental hydrodynamic processes provided by DFM are reliable for simulation of biogeochemistry within DWAQ. These methods are based on data collected at select USGS stations (Figure B.2). The observations of salinity and temperature were obtained from USGS CTDs deployed from R/V Polaris and R/V Peterson at the stations. Using salinity and temperature data along the navigational channel, and the corresponding predicted values from the model, we calculated and compared additional metrics such as density, N^2 and MLD between the model results and the data. To our knowledge it is the first time that such an extensive comparison of fundamental physical parameters has been undertaken to assess the performance of a hydrodynamic model of SFB. The results -- especially the MLD calculations -- will be used to assess the influence of stratification and other physical drivers on the formation and propagation of phytoplankton blooms within SFB.

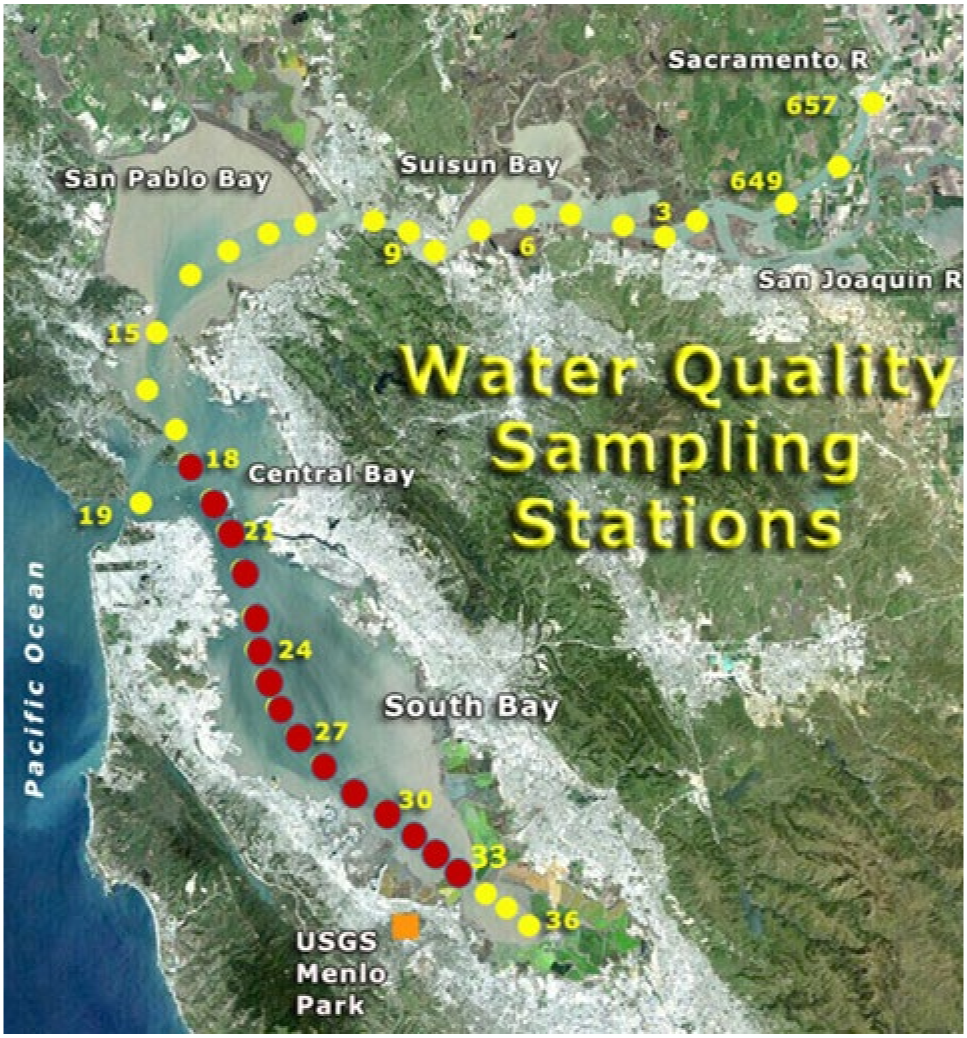

Figure B.2. USGS cruise sampling stations. Studied locations are shown in red circles

WY2018, 2017 and 2013 are the focus of the validation and analysis presented herein because these years represent a range of hydrological conditions and bloom events of interest. Similar analyses were also developed for WY2014, 2015 and 2016 and are presented in the Appendix B, and generally fall within the range of hydrological and biogeochemical conditions represented between WY2013, 2017 and 2018.

Analysis Methods

As mentioned previously, we have previously validated the hydrodynamic model for elevation, velocity and also have done some evaluation of the density by calculation of top vs. bottom salinity difference (SFEI 2017, 2020). The results showed that the model performed well in capturing the physical properties of the flow. Correct prediction of physical parameters and the hydrodynamics is imperative for the biogeochemical model in which the mixing and velocity, density stratification and hence the MLD prediction have first order effect on the success of the model. In this study we focus first on the prediction of the density stratification and its effects, by studying the *density and other derived parameters such as MLD,* instead of the more basic and separate comparisons to *salinity* and *temperature*. MLD is commonly used in oceanic studies (Irby *et al.* 2016) to indicate the top of the stratified portion of the water column. There is no universal definition for the MLD so different methods are used for finding it. Wilson *et al.* (2020) investigated five different methods for defining MLD using results from numerical simulations and data and concluded that a density difference method which estimates the MLD based on the difference between the surface and the MLD location is more robust and generic.

In the current analysis, the following density-based methods were used to study and evaluate the robustness of the SFB hydrodynamic model:

- Comparison of the modeled density time series to the density calculated from observational data. For both model and data, density was calculated using the Gibbs Seawater (GSW) oceanographic toolbox (McDougall and Baker 2011) based on the predicted temperature and salinity at each layer or the depths where the temperature and salinity measurements were made, respectively. To enable comparisons of the model at the depths where data were measured, model predictions of salinity and temperature were interpolated linearly between the layers prior to the calculation of density.
- Comparison of depth-averaged buoyancy frequency estimated from model predictions and observational data:
    - 2 was calculated as $-g/\rho_0\,(\partial\rho/\partial z)$, where $g = -9.81\ (m^2/s)$ is the gravitational acceleration, ρ_0 is the reference density. $N^2 > 0$ means stable density stratification (i.e., density increases with depth and lighter fluid overlies heavier fluid), and $N^2 < 0$ means unstable density stratification, where heavier fluid overlies lighter fluid, tending to overturn. Density at each depth for model and data were derived as noted in the first bullet. Time series of depth averaged $N^2(t)$ (i.e. ${N_{avg}}^2(t)$) between the model and data were compared to assess how well the model predicted the density stratification.
- Comparison of the vertical density and buoyancy frequency with data:
    - The model density vertical profile ρ(z) was compared with observed data to assess model accuracy and its suitability for predicting other scalars. Also, the vertical profile of N^2 was studied to access the model's ability to predict stratification.
- MLD calculation: Two widely accepted methods from Wilson *et al.* (2020) were compared for determining MLD:
    - The calculation of the MLD based on density difference criteria - MLD was defined based on a critical density value calculated as $\rho_{cr} = \rho_{surf} + d\rho_{cr}$, where ρ_{surf} is the density at the surface; $d\rho_{cr}$ is the difference between the density of the MLD and the surface density. The depth which corresponds to this critical density value was defined as the MLD. For stable stratification, the density below the MLD should be significantly greater than density at the MLD. Figure B.3 shows how the location of MLD is defined using the critical density method. The choice of $d\rho_{cr}$ is important in determining the MLD because a small $d\rho_{cr}$ may be too sensitive and underestimate the actual MLD, and a large $d\rho_{cr}$ may not be sensitive enough to density changes with depth and may lead to a conclusion of the entire column as being well mixed. $d\rho_{cr}$ was determined

through sensitivity analysis using a range of $d\rho_{cr}$ values following the approach in Wilson et al. (2020). Empirical cumulative density functions (CDFs) were constructed for each $d\rho_{cr}$ value, and the $d\rho_{cr}$ where the empirical CDFs provided a good match between the model and data, while still preserving the ability to sufficiently characterize stratification (based on multiple lines of evidence described above), was selected for further analysis.

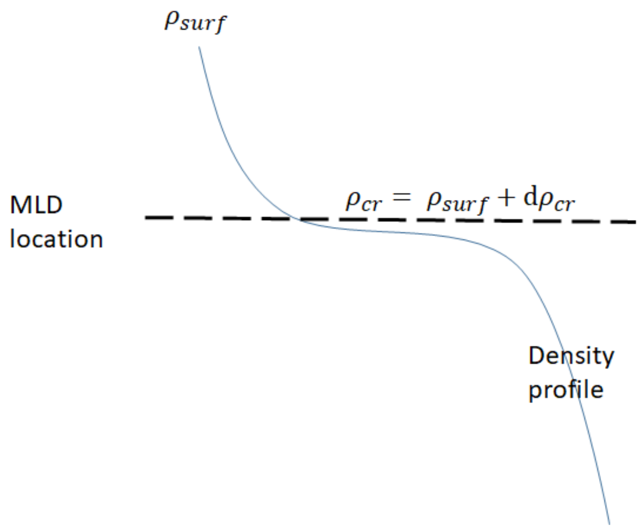

Figure B.3. Calculation of MLD based on the critical density difference (ρ_{cr})

- Calculation of the MLD based on density gradient criteria - MLD was defined as the depth at which a critical density gradient value $(d\rho/dz)_{cr}$ was exceeded such that immediately below the MLD, the density gradient is significantly greater than the critical density gradient (Figure B.4). Similar to the first method, the critical density gradient was determined through sensitivity analysis following the approach adopted in Wilson *et al.* (2020), and CDFs were compared for a range of critical density gradients.

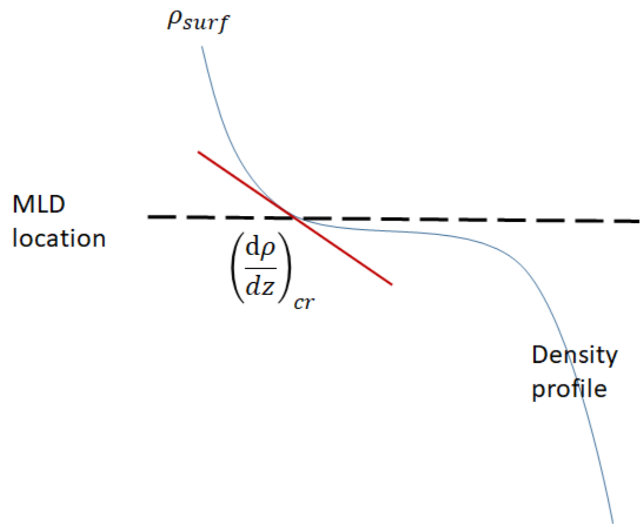

Figure B.4. Calculation of MLD based on the critical density gradient $(d\rho/dz)_{cr}$

In this study, ultimately the first method (critical density criteria, $d\rho_c$) for calculation of the MLD was adopted because as discussed subsequently based on multiple lines of evidence this method proved more reliable than the density gradient method.

Finally, when comparing MLDs from model predictions of salinity and temperature to point measurements of R/V Polaris and R/V Peterson cruise data-based MLD estimates, the 24 hour moving average (MA) model results, along with the 24-hour moving percentiles (10th and 90th) were used because the corresponding paired, point predictions from the model may not provide a complete picture of the model performance in case the model is slightly off phase in simulating the diurnal tides. Moreover, the formation of ML is often a result of sustained stratification, over a time frame longer than diurnal tidal cycle. By comparing the 24-hour MA and the moving percentiles, the objective is to assess whether the model predicted MLDs are within the range of snapshot estimates from the data and generally represent the variations observed over a spring-neap cycle (approximately the same as the USGS Petersen Cruise frequency of every 2 weeks).

Results Summary

Averaged Buoyancy Frequency and Density Time Series

The depth-averaged buoyancy frequency and density, and the near-surface and bottom density time series are compared with collected data. The model results from WY2013, WY2017 and WY2018 are presented, and additional Water Years are presented in Appendix B1. The hydrographs for the boundary inflows into SFB for WY2013-WY2018 are shown in Figure B.5 to help with interpreting the stratification.

WY2018

Figures B.6 through B.11 show a comparison of time series of model- and measurement-based estimates of density and N^2 at the USGS stations 18, 22, 24, 27, 30 and 32, spanning central through south bay (see Figure B.2 for locations). Each figure shows the surface, bottom and the depth averaged density, and N^2 on the left panels, and corresponding scatter plots of paired model-measured data estimates on the right panels. In these figures, σ_i is the density anomaly calculated as $\sigma_i = \rho_i - \rho_0$, where ρ_i is the density for *i* = surface, bottom or depth-averaged and $\rho_0 = 1000\ (kg/m^3)$ is the reference density.

Freshwater inflows in WY2018 peaked in early April, with flows from the Delta and North Bay significantly larger than elsewhere. The comparison shows that the average, surface and bottom density are well predicted. Specifically, in all locations, the model reproduces the observed seasonal variation in density differences resulting from freshwater runoff in the spring months. The model also captures the longitudinal differences in the density from Central Bay (saltier and denser overall) to South Bay (fresher and lighter overall). Furthermore, the differences in the surface and bottom densities indicates that the relative strength of stratification is stronger in April in Central Bay (Stations 18 and 22) compared to the South Bay and Lower South Bay stations. The scatter plots on the right panels show that the model estimates of density align well with the measurements along the 1:1 line.

The N^2 panel shows that both the timing and strength of stratification are predicted well. In these comparisons the relative differences within the model-estimates and the N^2 calculated from the measurements are more important than the absolute magnitude because these comparisons aim to identify the timing and duration of stratification events from the changes in N^2. The N^2 results show that moving towards the South Bay regions, the stratification becomes weaker (stations 24 and 27). N^2 is noticeably higher from March to June indicating stratified conditions and is closer to zero in other months (Oct/2012 – Mar/2013 and June/2013 – Oct/2013) implying weak or no stratification. During spring, the N^2values calculated from measurements show that restratification occurs frequently in April and May reflecting the spring-neap cycles and/or freshwater runoff events, consistent with the evidence from the surface and bottom density differences. The model also predicted a similar pattern of restratification during these months. After August, the stratification diminishes (low N^2), meaning a well-mixed water column as shown by both the model and the data. In the southern stations (30 and 32) the stratification becomes stronger in cold months compared to stations 24 and 27, showing they are less influenced by freshwater inputs (see Figure B.5).

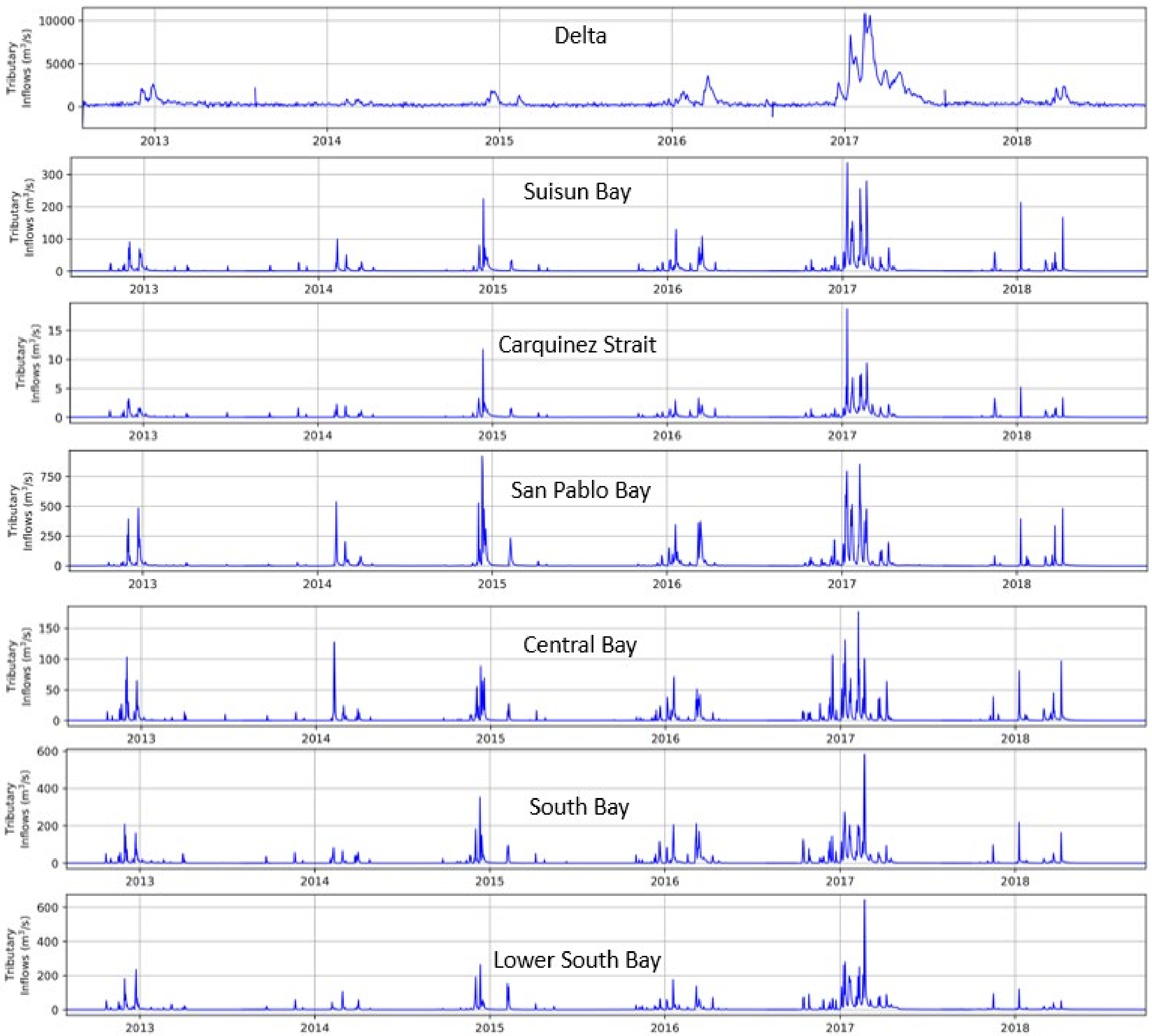

Figure B.5. Boundary inflows for WY2013-WY2018

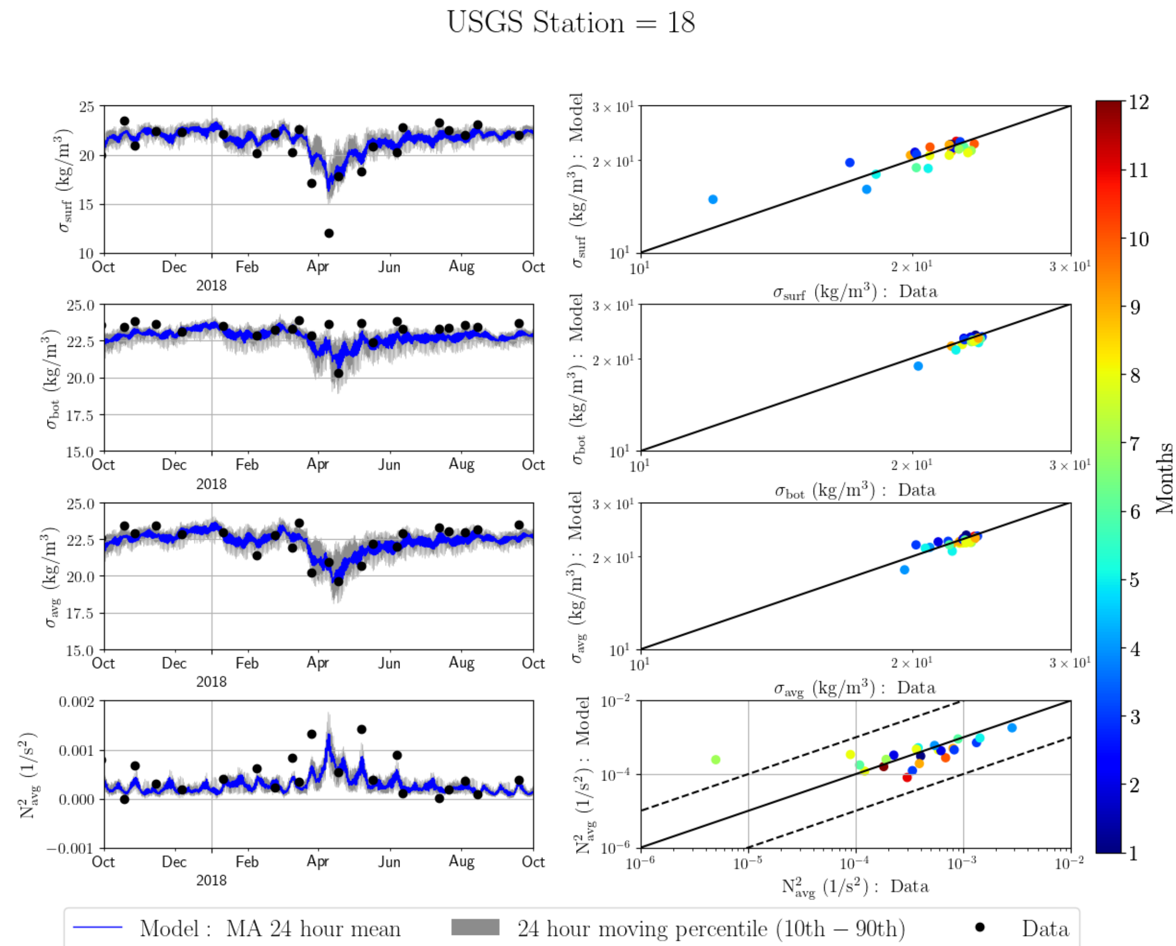

Notes: Left panels show the time series and the right panels are scatter plots comparing the model results with the measurements. The solid black line on the right panels is the 1:1 line, and the two dashed lines on either side show an order of magnitude difference relative to 1:1.

Figure B.6. Comparison of model results with USGS data at station 18 for WY2018

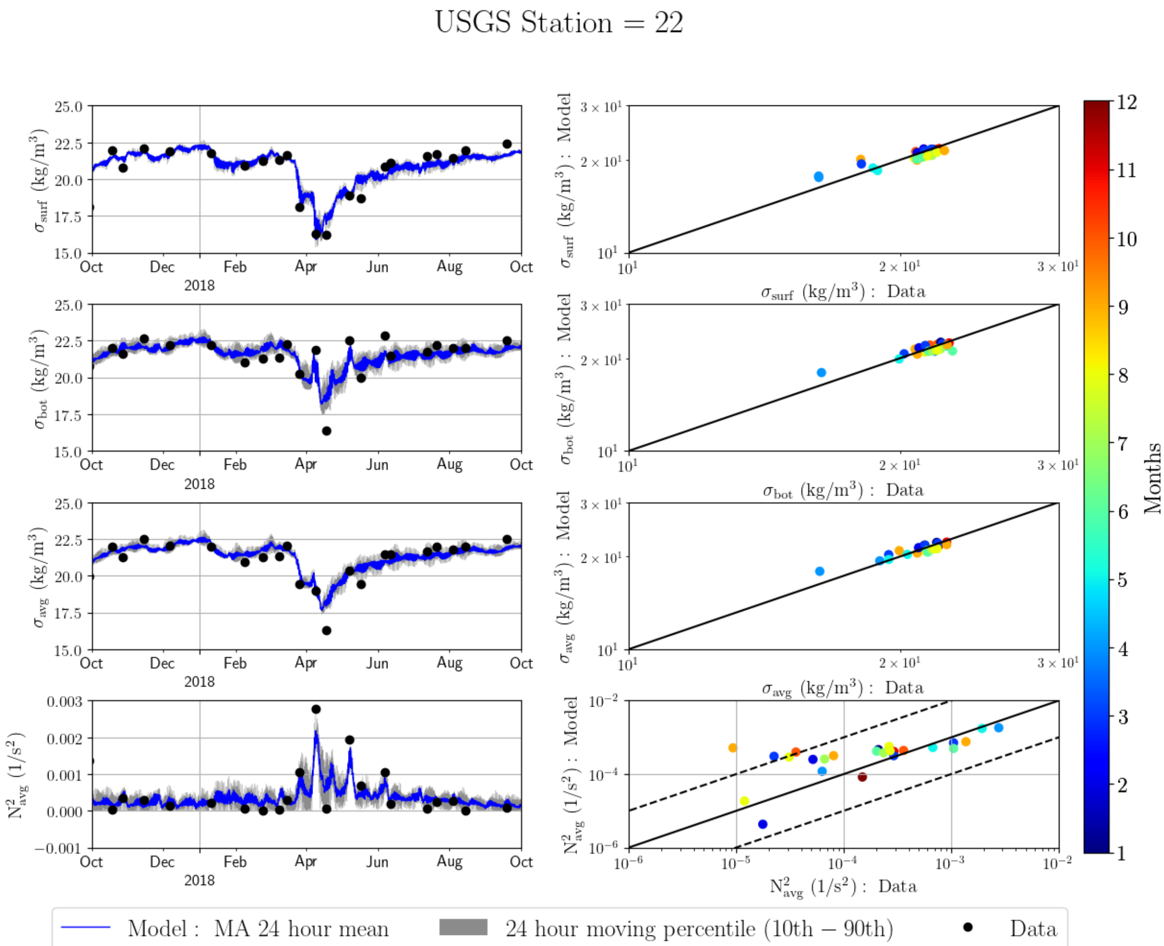

Notes: Left panels show the time series and the right panels are scatter plots comparing the model results with the measurements. The solid black line on the right panels is the 1:1 line, and the two dashed lines on either side show an order of magnitude difference relative to 1:1.

Figure B.7. Comparison of model results with USGS data at station 22 for WY2018

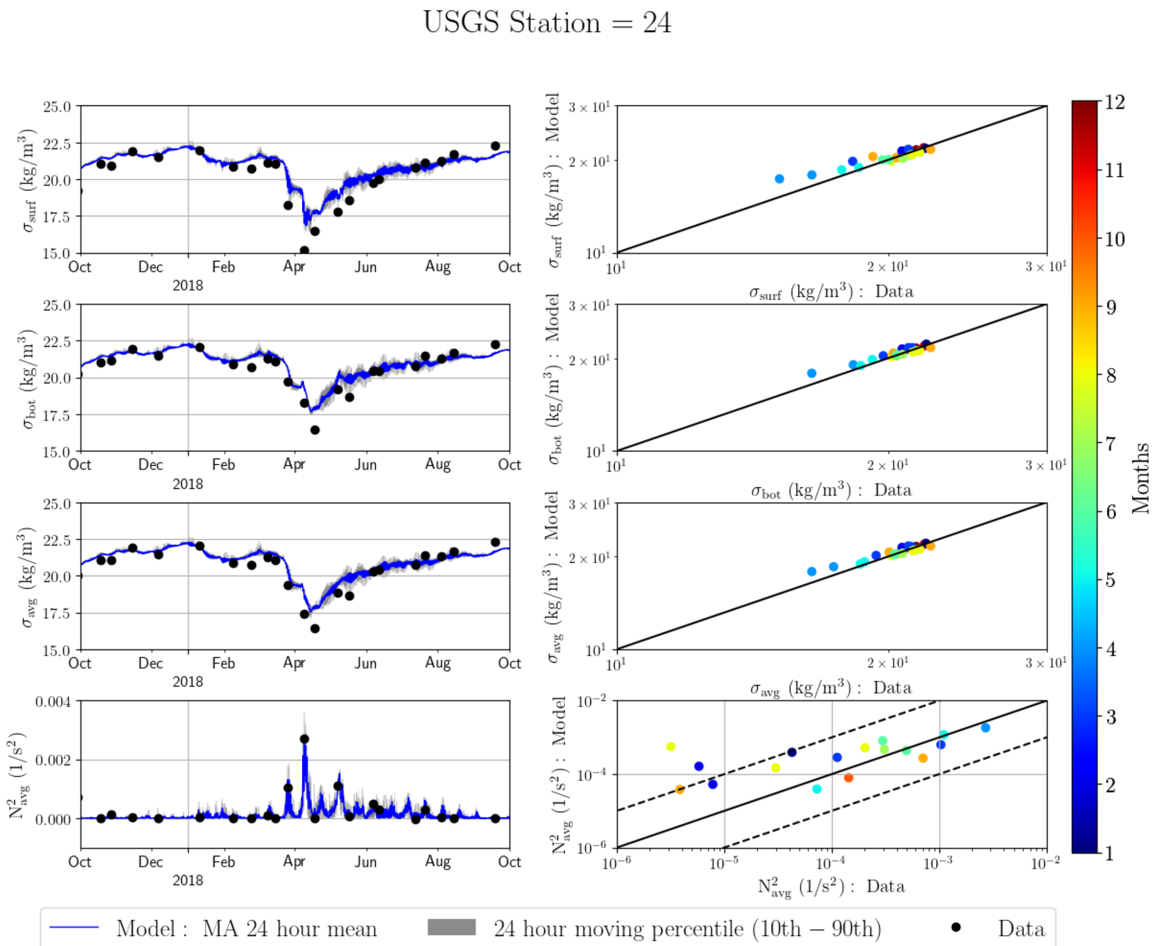

Notes: Left panels show the time series and the right panels are scatter plots comparing the model results with the measurements. The solid black line on the right panels is the 1:1 line, and the two dashed lines on either side show an order of magnitude difference relative to 1:1.

Figure B.8. Comparison of model results with USGS data at station 24 for WY2018

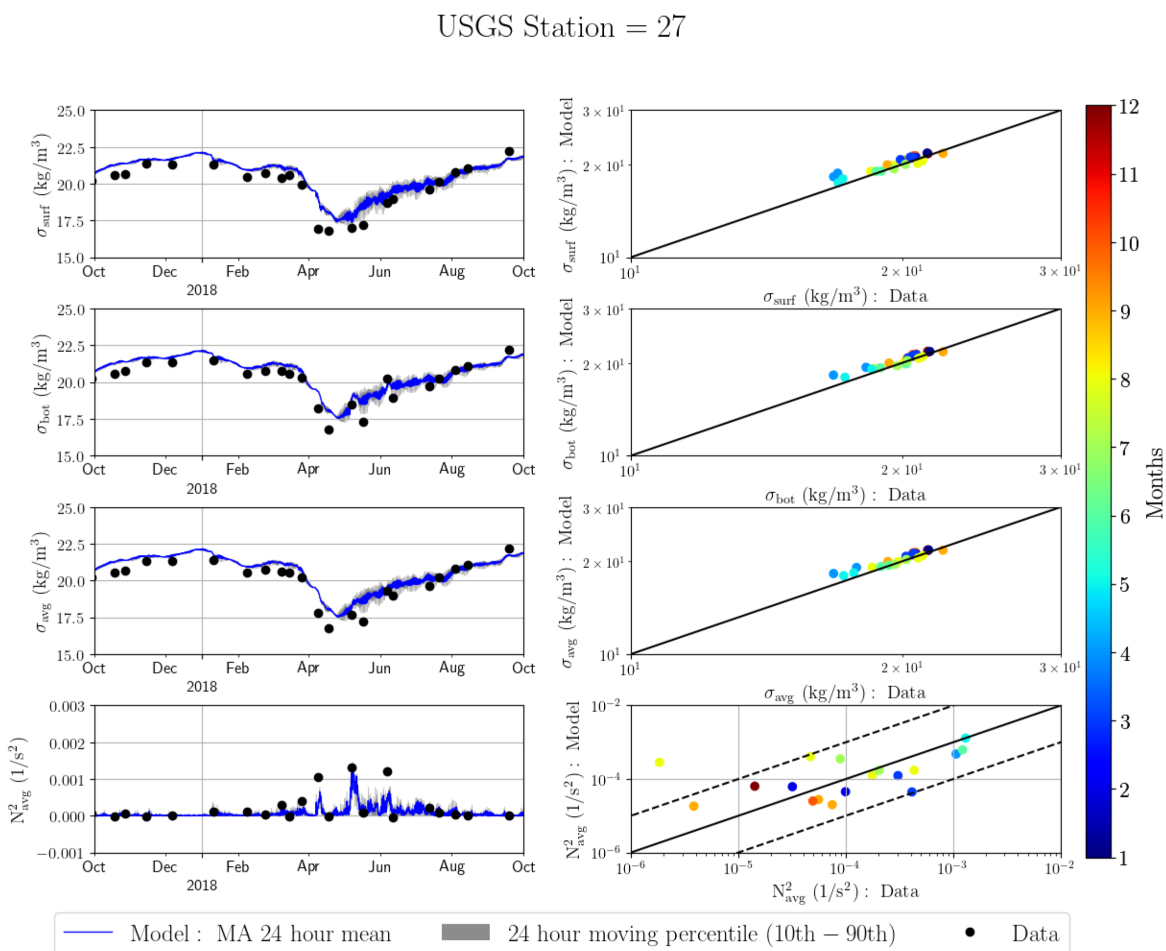

Notes: Left panels show the time series and the right panels are scatter plots comparing the model results with the measurements. The solid black line on the right panels is the 1:1 line, and the two dashed lines on either side show an order of magnitude difference relative to 1:1.

Figure B.9. Comparison of model results with USGS data at station 27 for WY2018

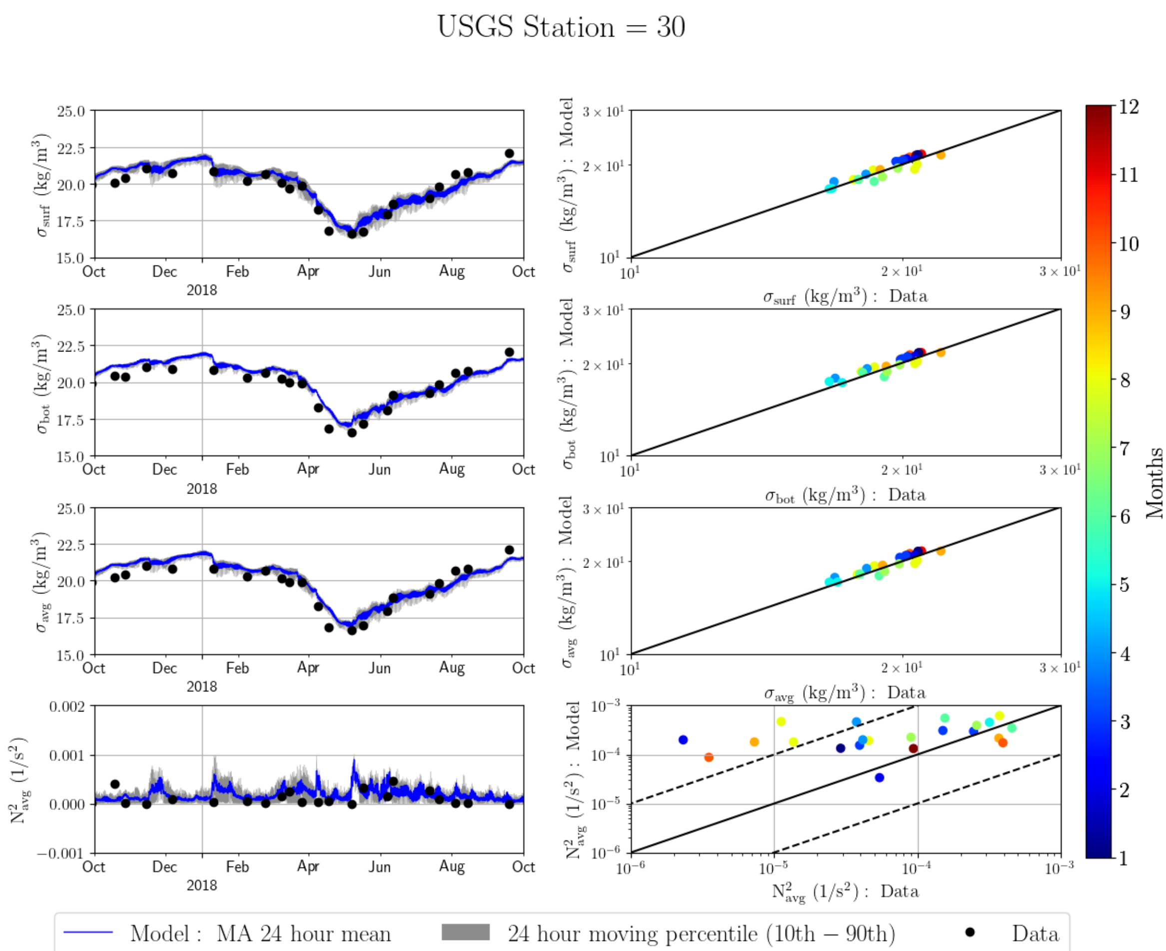

Notes: Left panels show the time series and the right panels are scatter plots comparing the model results with the measurements. The solid black line on the right panels is the 1:1 line, and the two dashed lines on either side show an order of magnitude difference relative to 1:1.

Figure B.10. Comparison of model results with USGS data at station 30 for WY2018

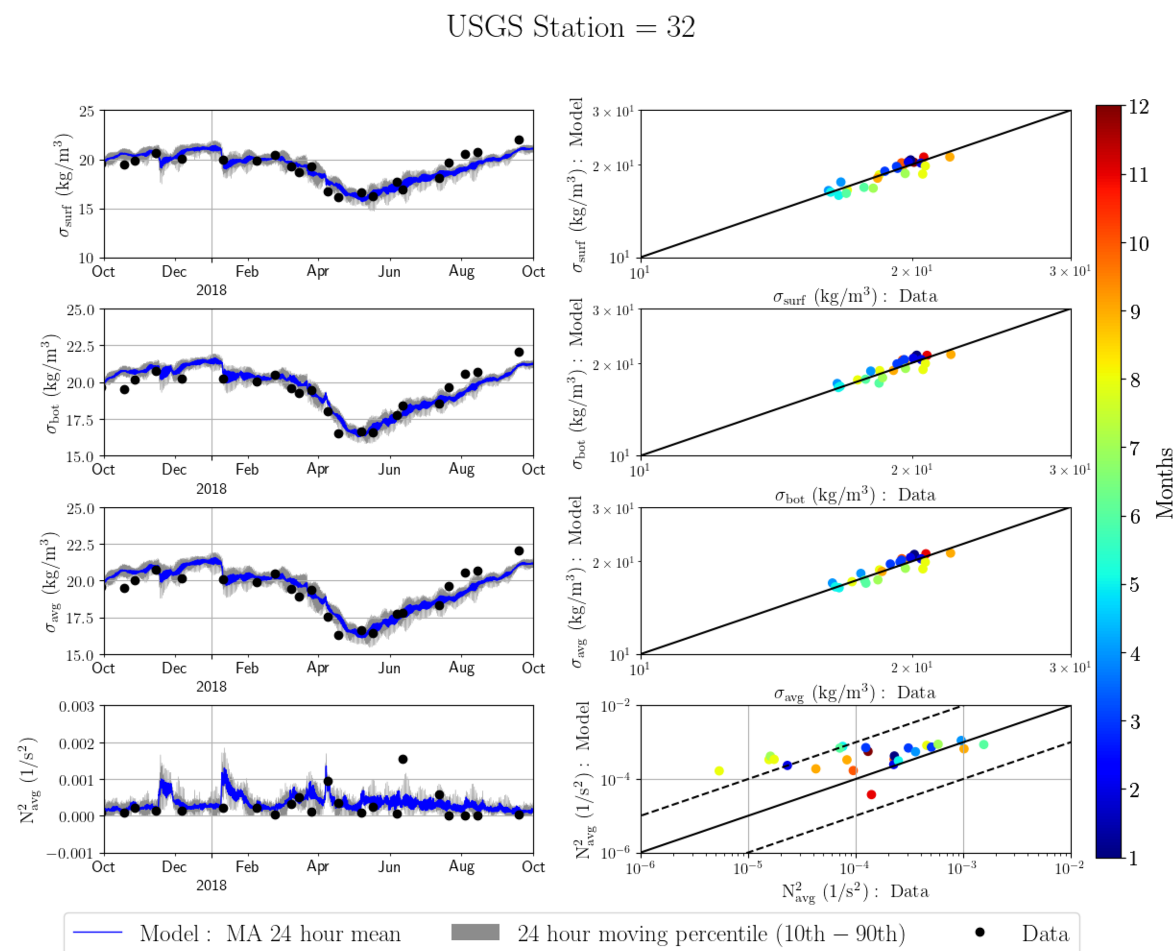

Notes: Left panels show the time series and the right panels are scatter plots comparing the model results with the measurements. The solid black line on the right panels is the 1:1 line, and the two dashed lines on either side show an order of magnitude difference relative to 1:1.

Figure B.11. Comparison of model results with USGS data at station 32 for WY2018

WY2017

WY2017 was a wet year with large freshwater runoff events in the winter and spring months (Figure B.5). Similar to WY2018, the comparison of the model results with data for WY2017 shows good agreement for both buoyancy frequency and density timing and magnitude, especially for density (Figures B.12 through B.17). The N^2 results at stations 18-24 show that the restratification initiates earlier compared to WY2018 and occurs in mid-January and reaches its maximum strength in March (compared to mid-April for WY2018). Also, the results show that the N^2 in WY2017 can be up to almost three times larger that N^2 in WY2018, meaning that the WY2017 has a stronger difference in the bottom and surface density caused by freshwater input at the surface. These differences are apparent in both the measurement- and model-derived N^2 values at all the stations shown, which illustrates the ability of the hydrodynamic model to capture inter-annual differences in stratification.

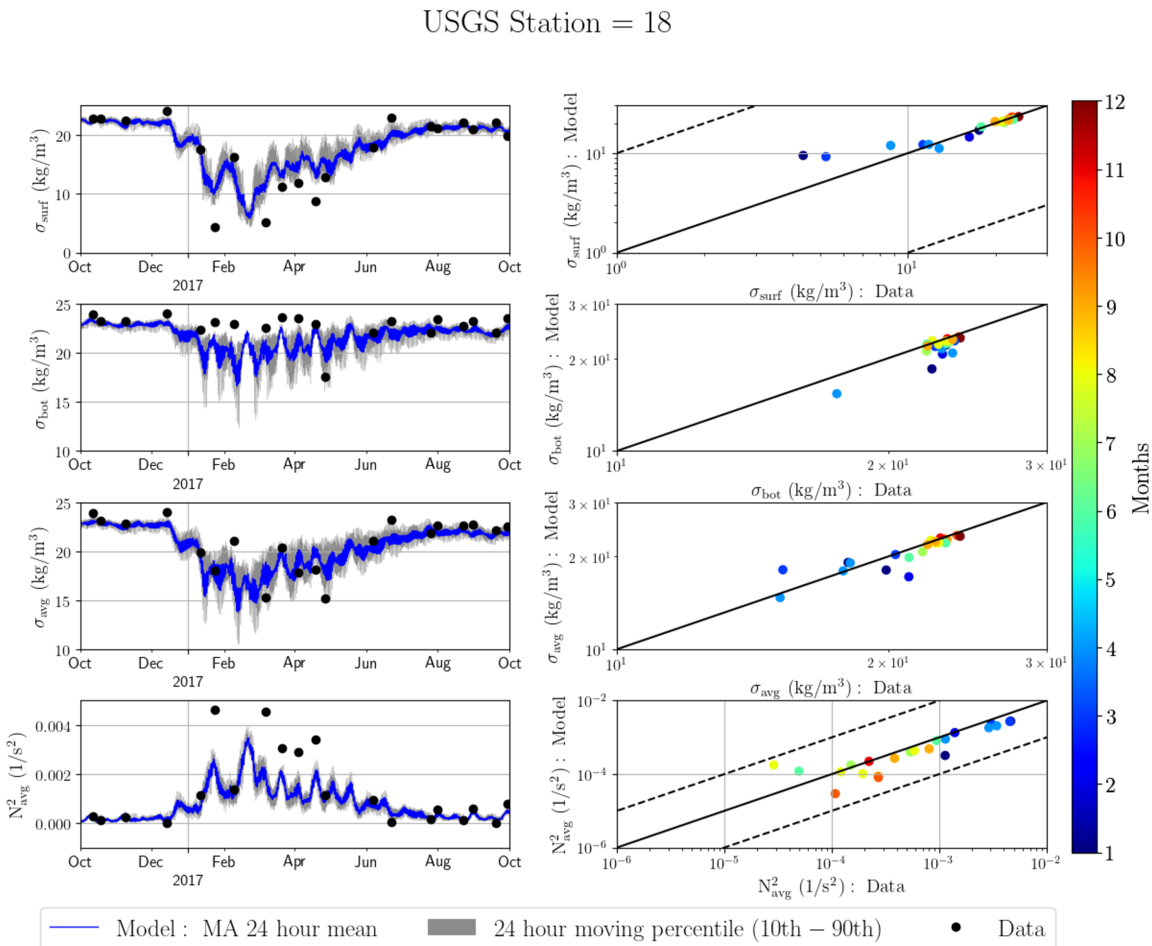

Notes: Left panels show the time series and the right panels are scatter plots comparing the model results with the measurements. The solid black line on the right panels is the 1:1 line, and the two dashed lines on either side show an order of magnitude difference relative to 1:1.

Figure B.12. Comparison of model results with USGS data at station 18 for WY2017

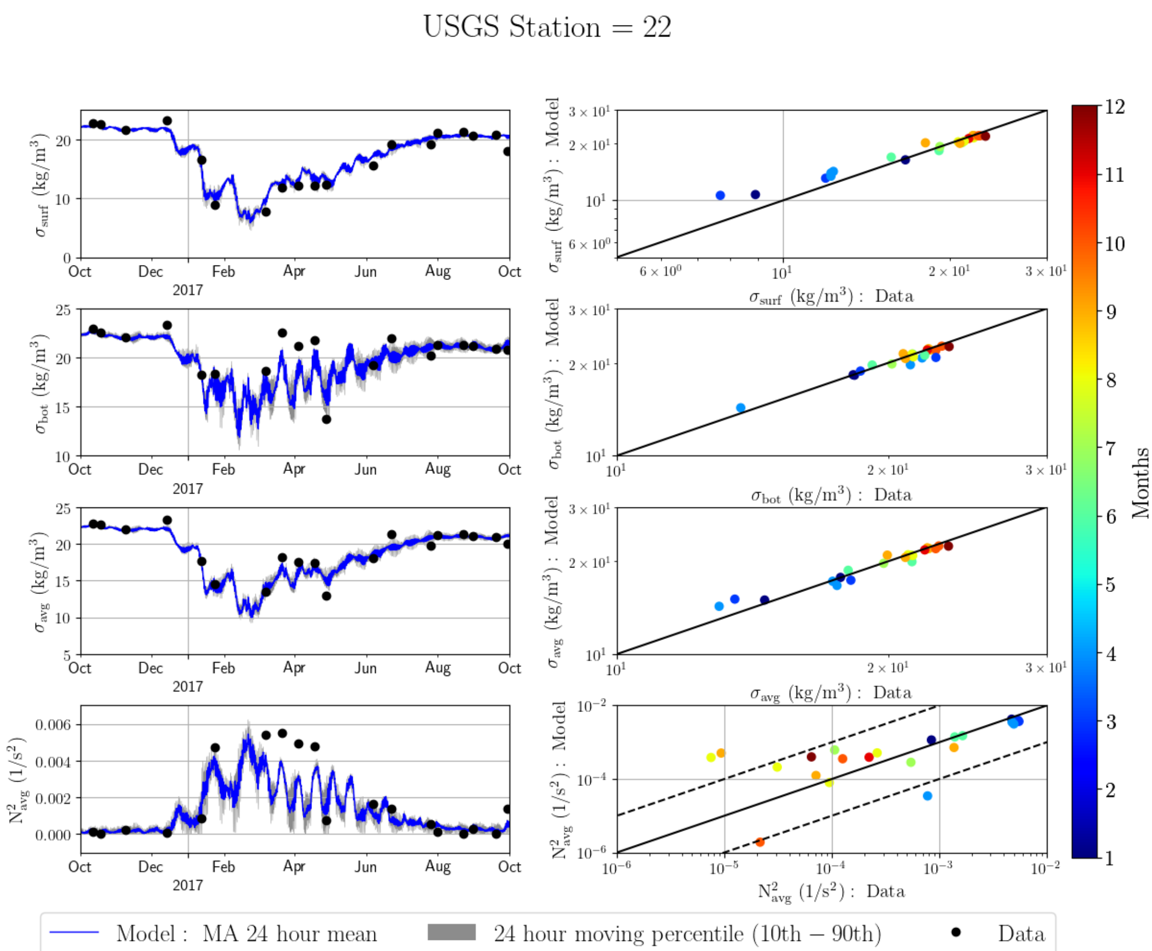

Notes: Left panels show the time series and the right panels are scatter plots comparing the model results with the measurements. The solid black line on the right panels is the 1:1 line, and the two dashed lines on either side show an order of magnitude difference relative to 1:1.

Figure B.13. Comparison of model results with USGS data at station 22 for WY2017

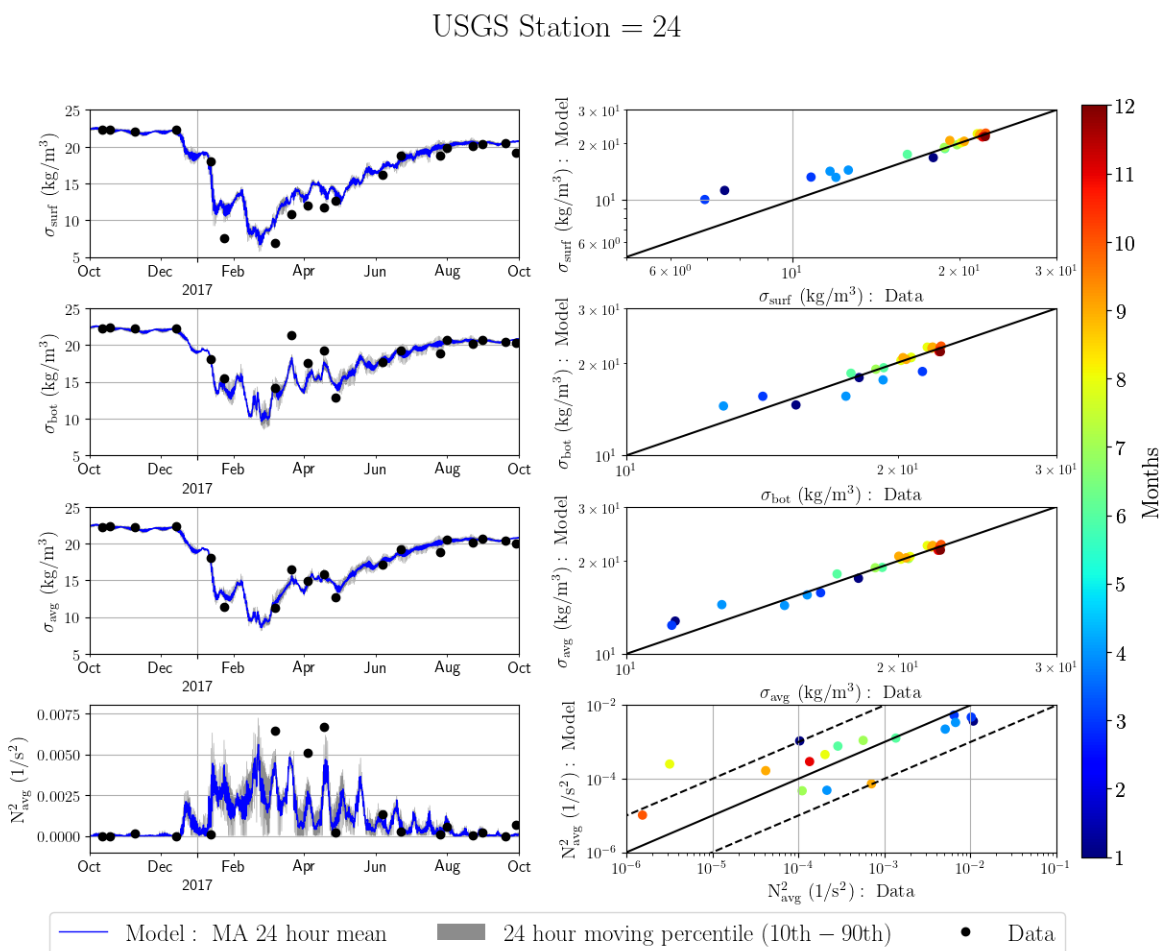

Notes: Left panels show the time series and the right panels are scatter plots comparing the model results with the measurements. The solid black line on the right panels is the 1:1 line, and the two dashed lines on either side show an order of magnitude difference relative to 1:1.

Figure B.14. Comparison of model results with USGS data at station 24 for WY2017

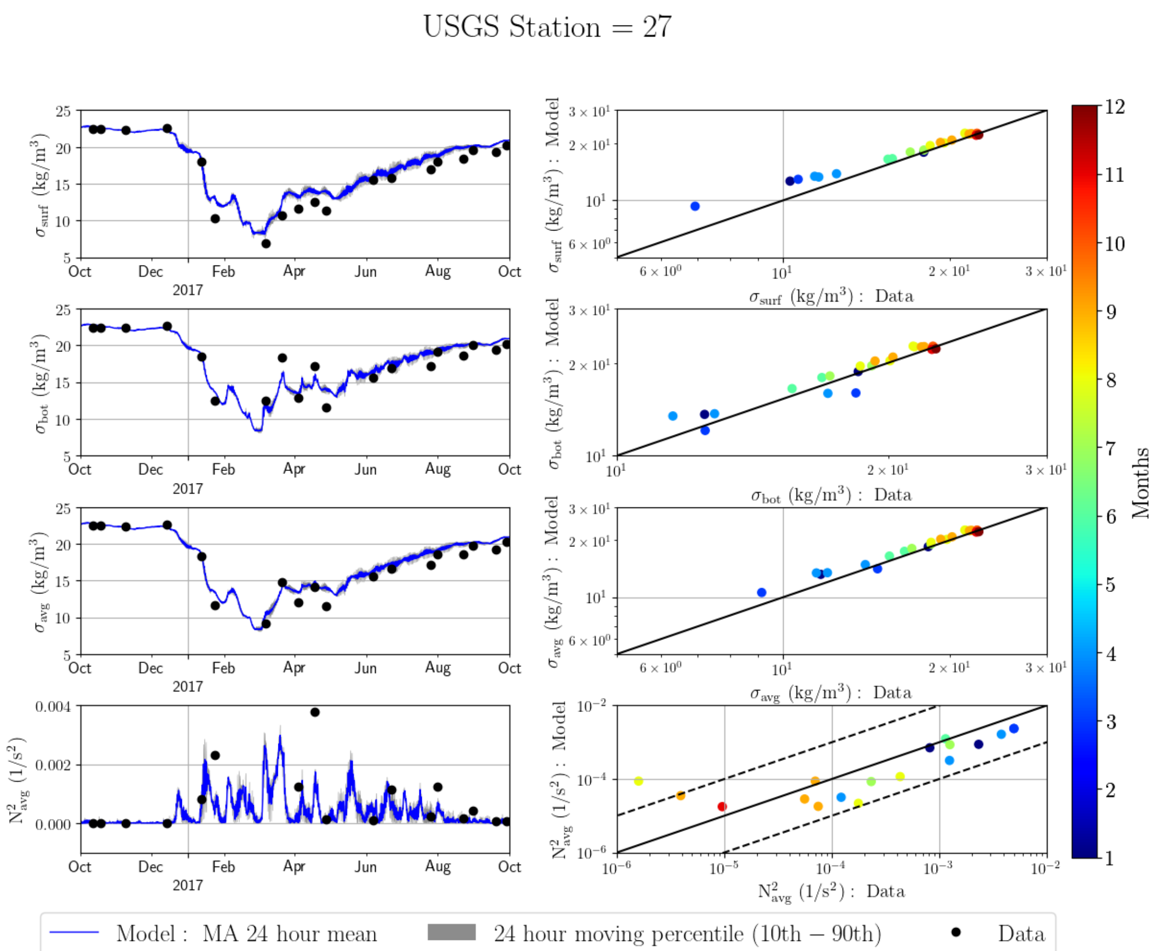

Notes: Left panels show the time series and the right panels are scatter plots comparing the model results with the measurements. The solid black line on the right panels is the 1:1 line, and the two dashed lines on either side show an order of magnitude difference relative to 1:1.

Figure B.15. Comparison of model results with USGS data at station 27 for WY2017

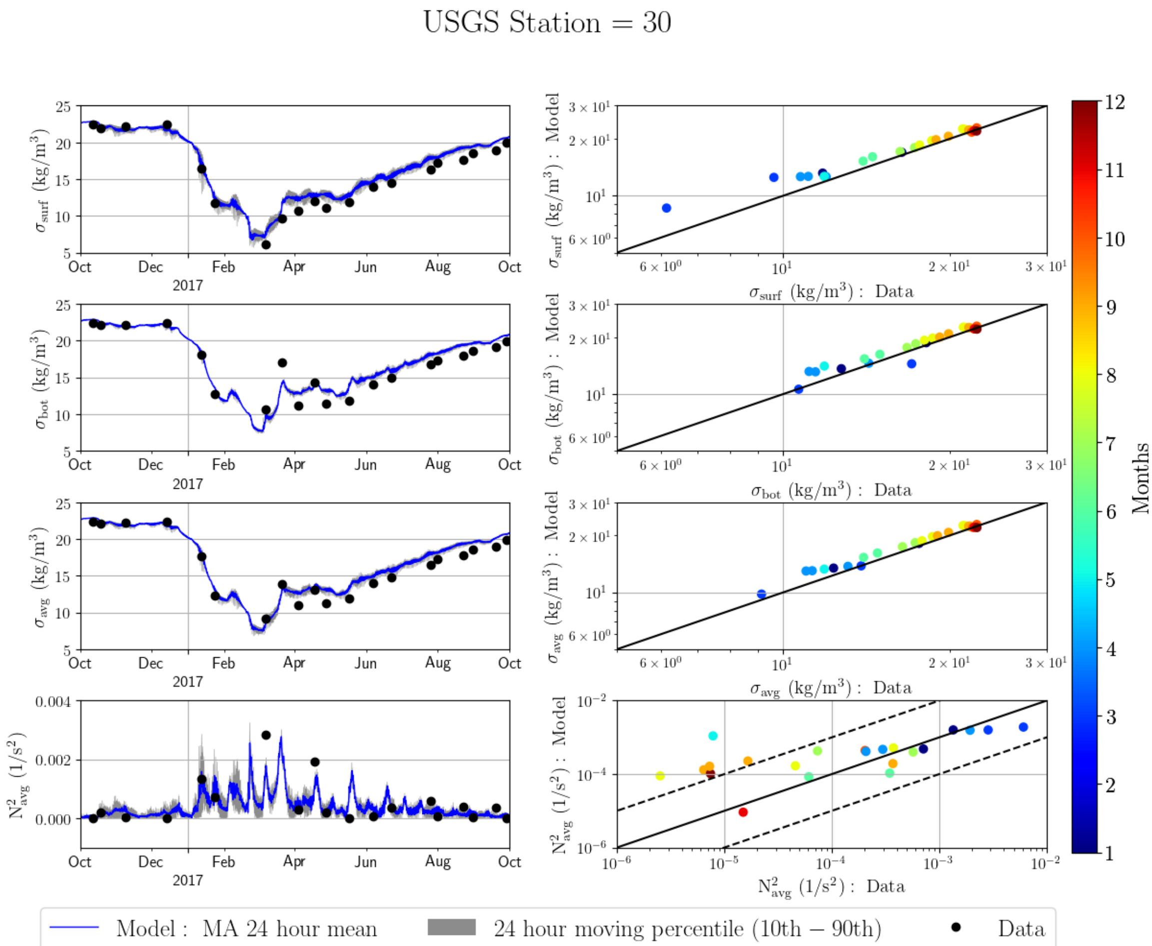

Notes: Left panels show the time series and the right panels are scatter plots comparing the model results with the measurements. The solid black line on the right panels is the 1:1 line, and the two dashed lines on either side show an order of magnitude difference relative to 1:1.

Figure B.16. Comparison of model results with USGS data at station 30 for WY2017

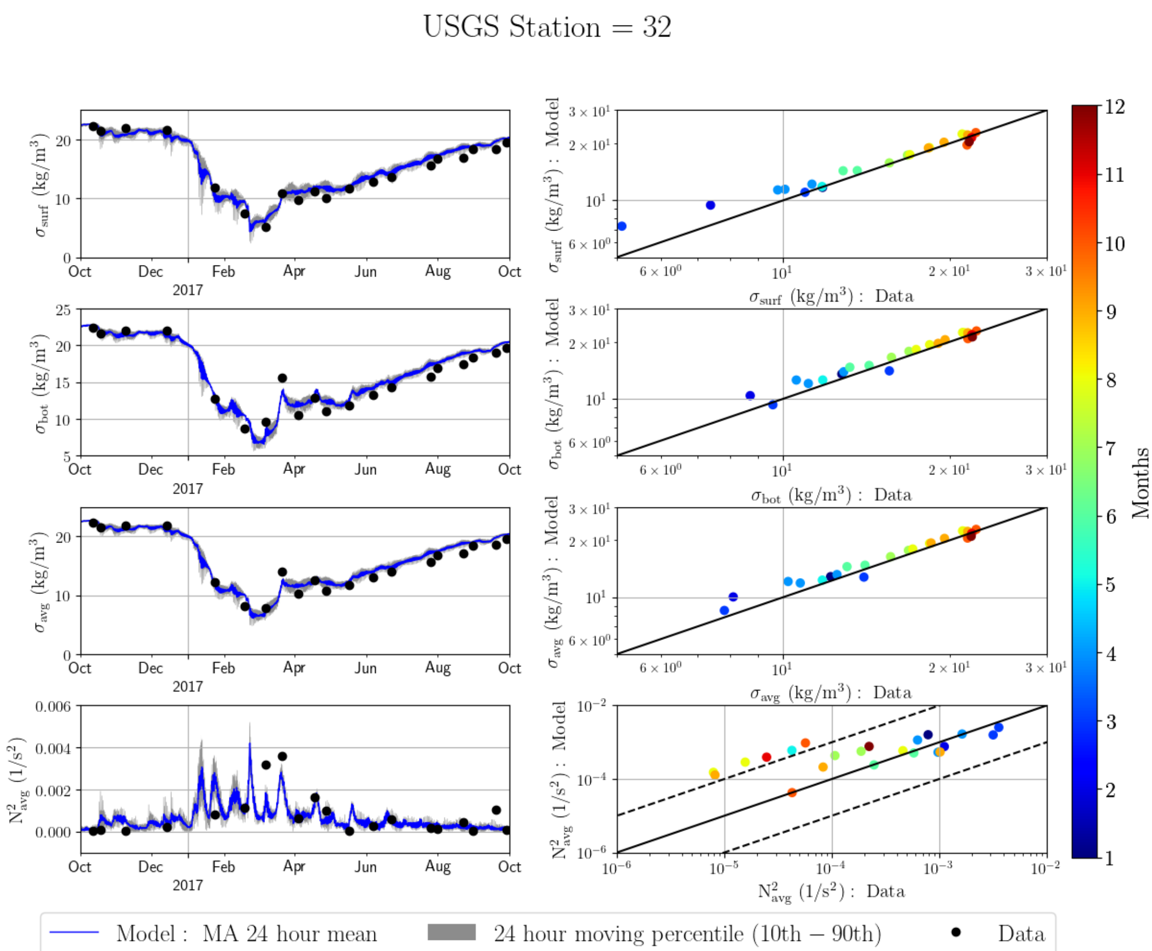

Notes: Left panels show the time series and the right panels are scatter plots comparing the model results with the measurements. The solid black line on the right panels is the 1:1 line, and the two dashed lines on either side show an order of magnitude difference relative to 1:1.

Figure B.17. Comparison of model results with USGS data at station 32 for WY2017

WY2013

WY2013 results also show good agreement for both buoyancy frequency and density (Figures B.18 through B.23). Both model and measurement-based N^2 values show that stratification occurs early in WY2013, starting around end of November 2012, and the maximum stratification is seen around end of December 2012. WY2013 stratification is weaker than WY2017 but comparable to WY2018 (e.g., in station 22 the maximum N^2 in WY2013 is about a third of the maximum N^2 in WY2017, but roughly equal to WY2018).

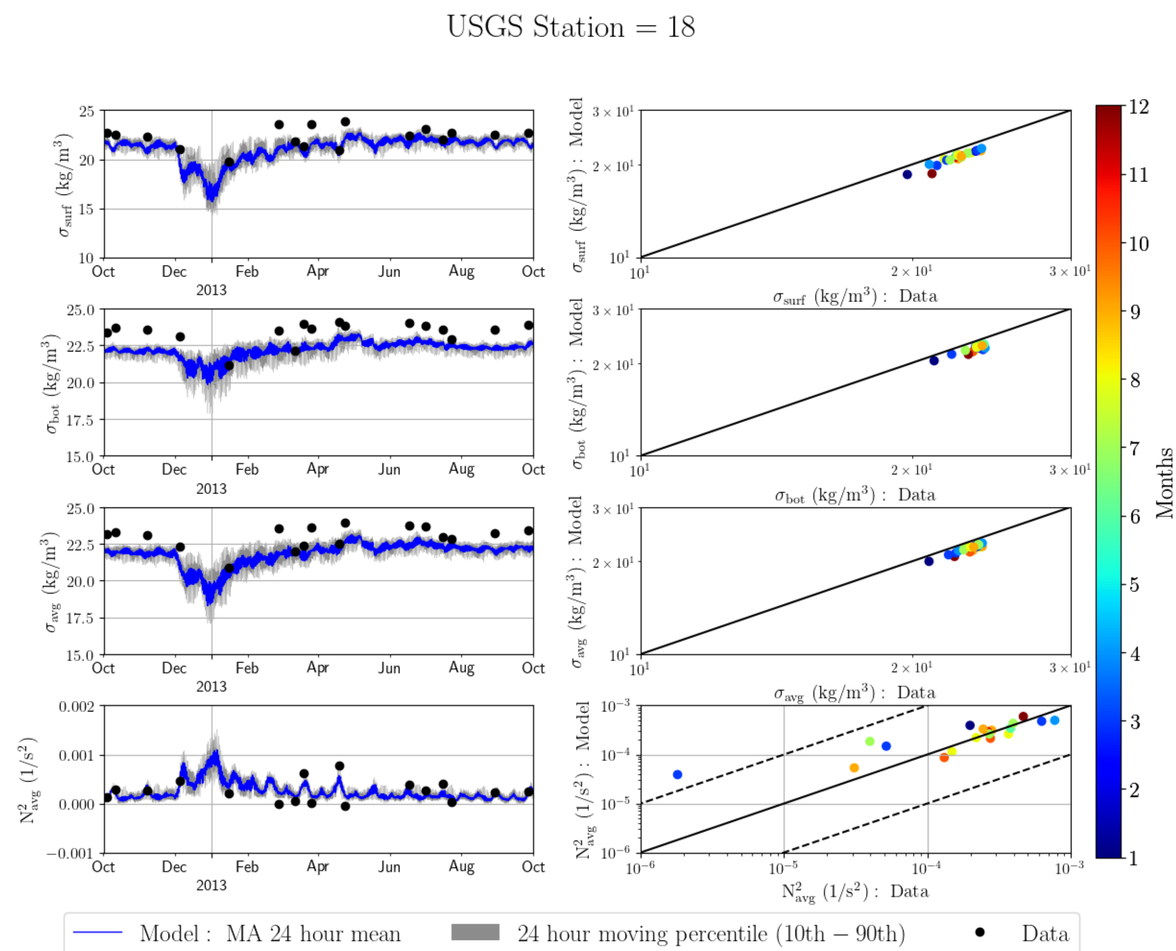

Notes: Left panels show the time series and the right panels are scatter plots comparing the model results with the measurements. The solid black line on the right panels is the 1:1 line, and the two dashed lines on either side show an order of magnitude difference relative to 1:1.

Figure B.18. Comparison of model results with USGS data at station 18 for WY2013

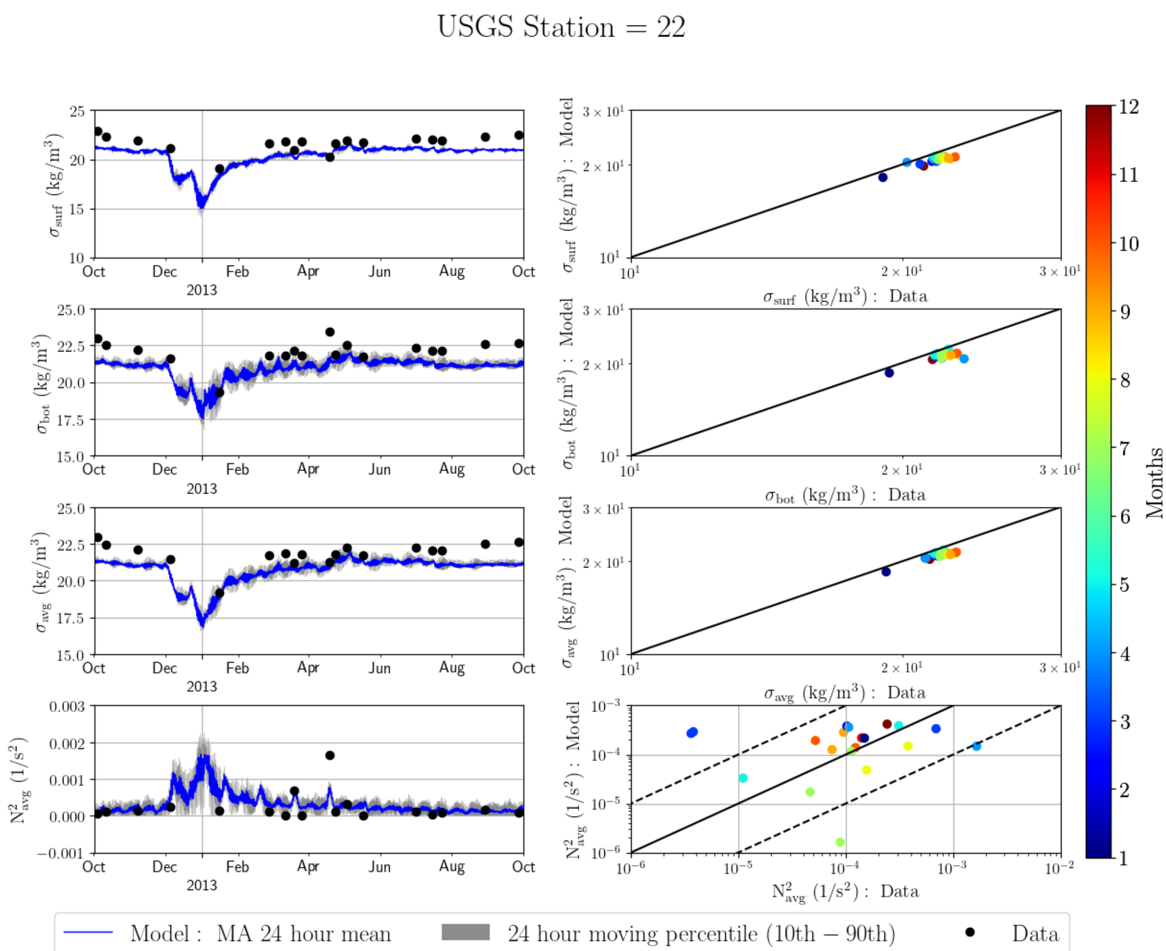

Notes: Left panels show the time series and the right panels are scatter plots comparing the model results with the measurements. The solid black line on the right panels is the 1:1 line, and the two dashed lines on either side show an order of magnitude difference relative to 1:1.

Figure B.19. Comparison of model results with USGS data at station 22 for WY2013

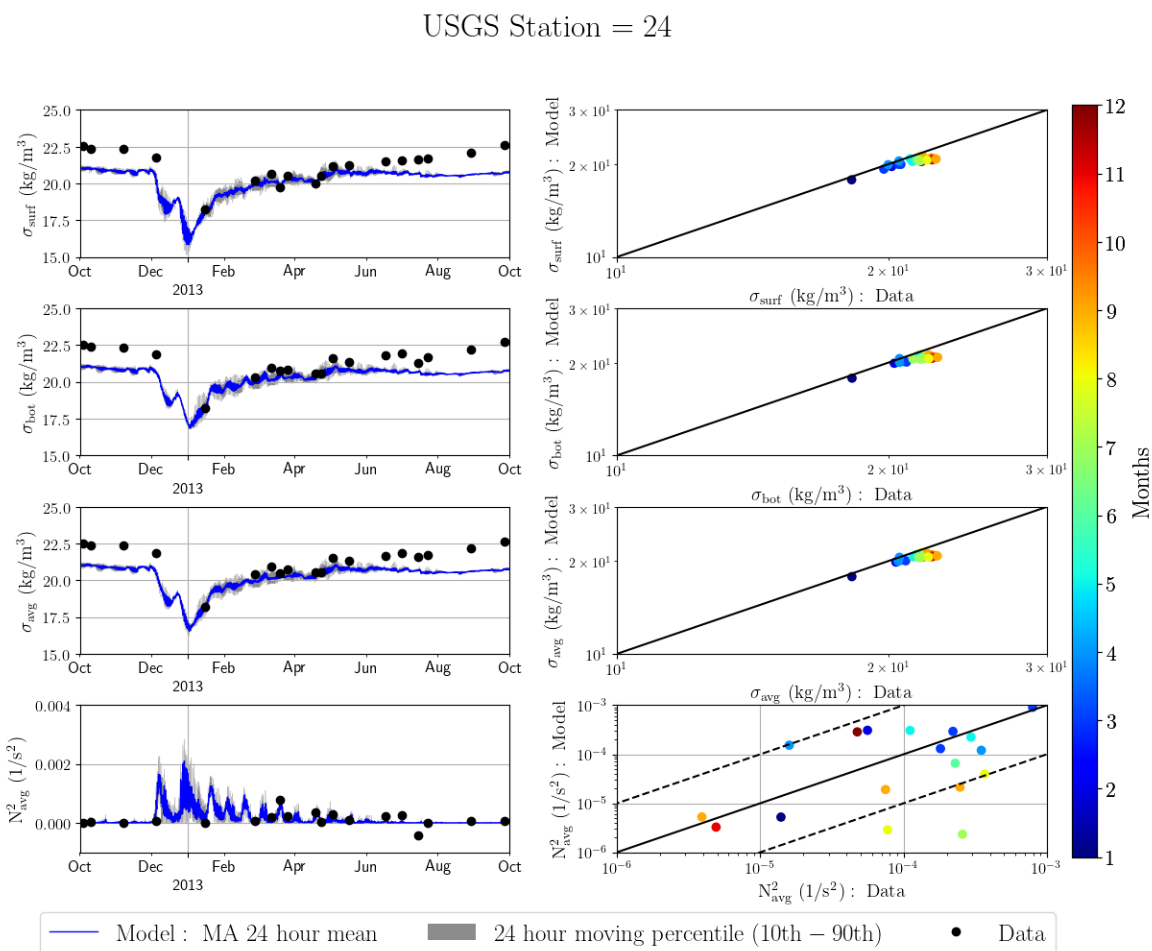

Notes: Left panels show the time series and the right panels are scatter plots comparing the model results with the measurements. The solid black line on the right panels is the 1:1 line, and the two dashed lines on either side show an order of magnitude difference relative to 1:1.

Figure B.20. Comparison of model results with USGS data at station 24 for WY2013

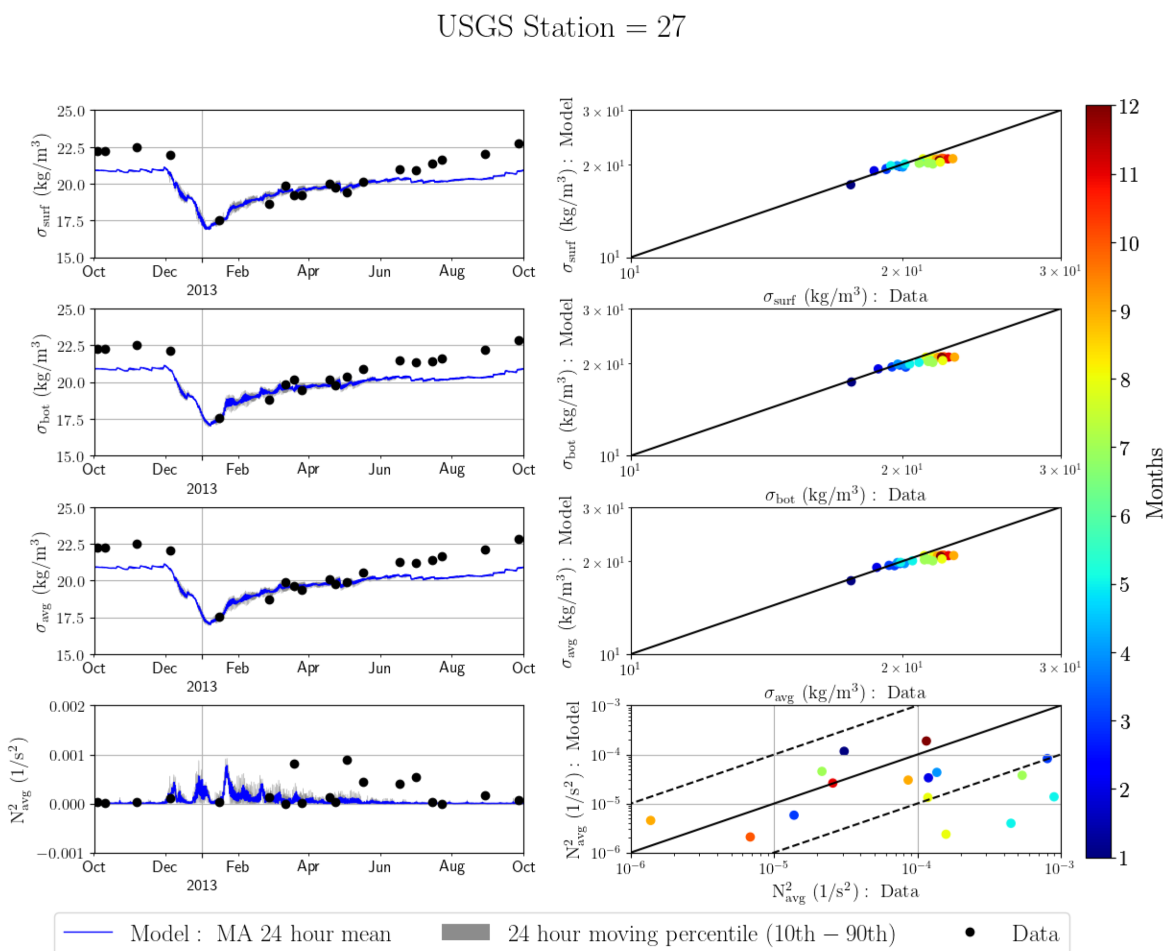

Notes: Left panels show the time series and the right panels are scatter plots comparing the model results with the measurements. The solid black line on the right panels is the 1:1 line, and the two dashed lines on either side show an order of magnitude difference relative to 1:1.

Figure B.21. Comparison of model results with USGS data at station 27 for WY2013

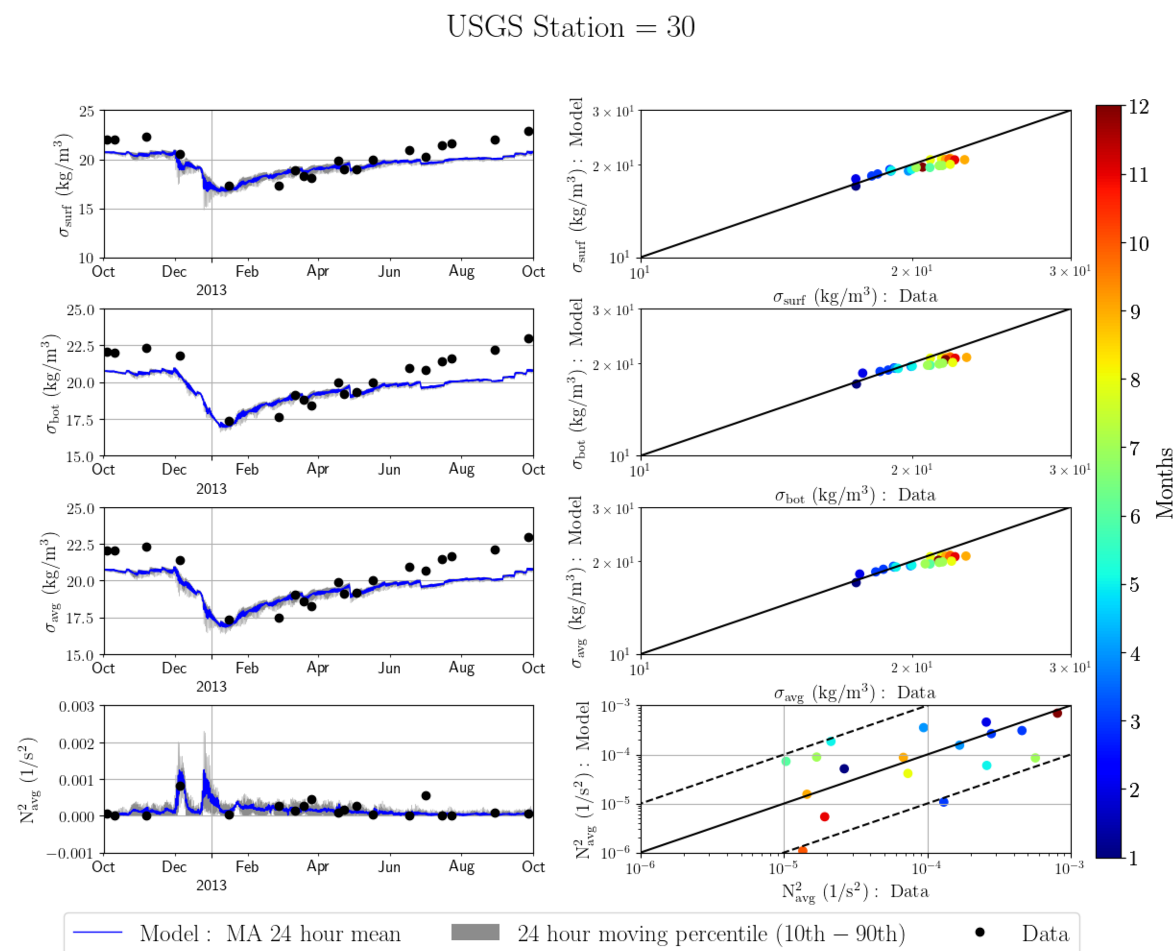

Notes: Left panels show the time series and the right panels are scatter plots comparing the model results with the measurements. The solid black line on the right panels is the 1:1 line, and the two dashed lines on either side show an order of magnitude difference relative to 1:1.

Figure B.22. Comparison of model results with USGS data at station 30 for WY2013

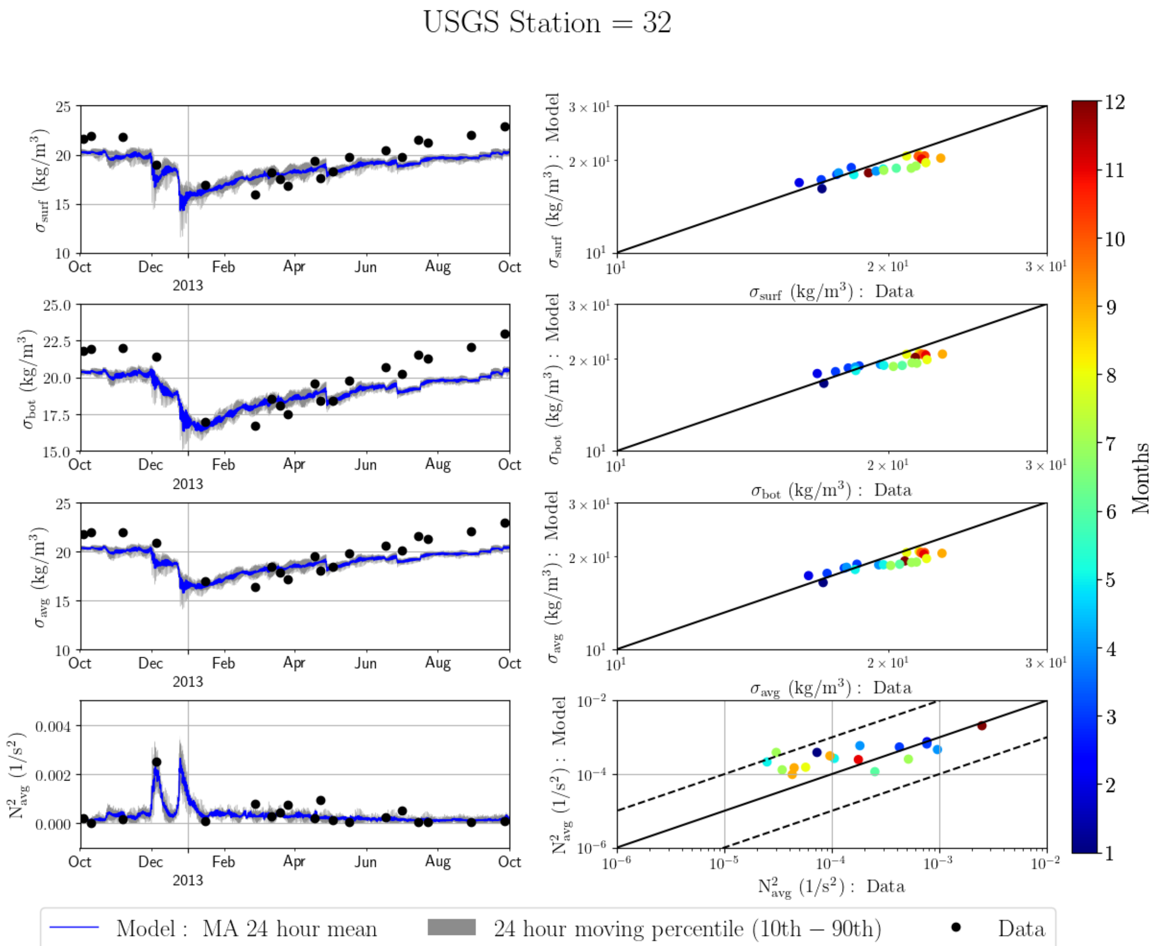

Notes: Left panels show the time series and the right panels are scatter plots comparing the model results with the measurements. The solid black line on the right panels is the 1:1 line, and the two dashed lines on either side show an order of magnitude difference relative to 1:1.

Figure B.23. Comparison of model results with USGS data at station 32 for WY2013

Comparison for N^2 for Different Water Years

In this section, we present the comparison of the results between WY2018, 2017 and 2013 at stations 24 and 27 (Figures B.24 and B.25). The comparisons for other stations are shown in Appendix B.1. It is clear that the strongest stratification occurs in WY2017 compared to the other two WYs. Moreover, in WY2018 the stratification initiates in late March which is a few months later compared to the other two years.

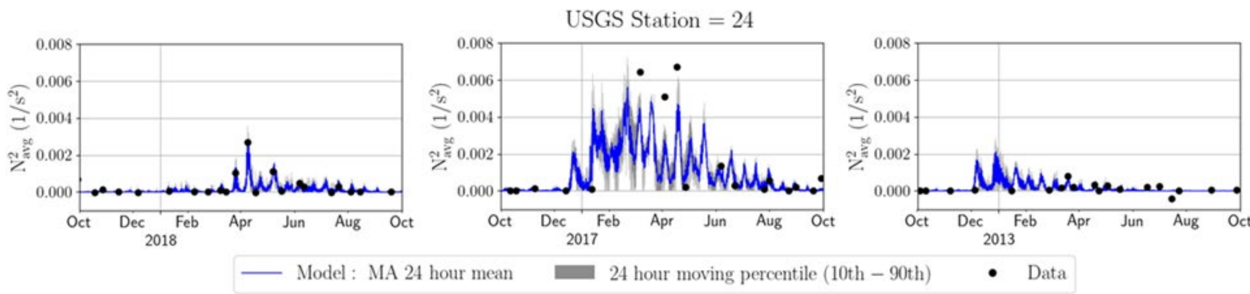

Figure B.24. Comparison of N^2 for WY2018, 2017 and 2013 at station 24

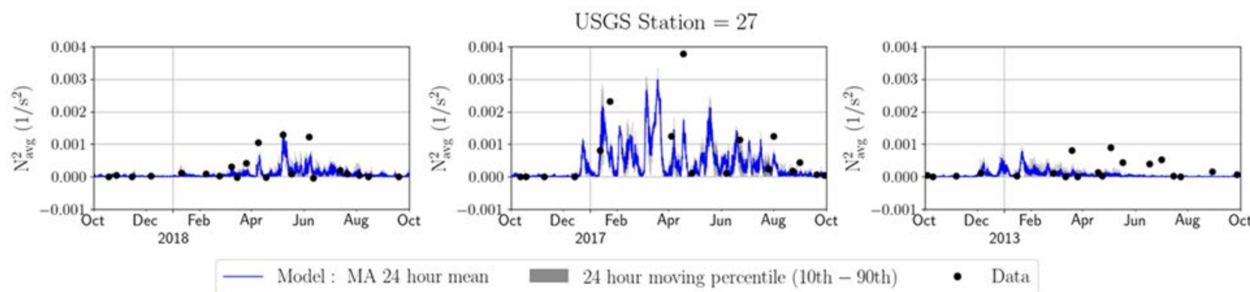

Figure B.25. Comparison of N^2 for WY2018, 2017 and 2013 at station 27

Profiles of Buoyancy Frequency and Density

Vertical profiles of density and N^2 were constructed to assess model performance at each location. These comparisons were developed for four specific dates to show the capability of the model in capturing the density profile in different seasons. Results at station 24 are shown in Figures B.26 through B.28 for WY2018, WY2017 and WY2013 respectively. Results for other stations are shown in the Appendix B.2.

The vertical profiles of density show that density structure differs between the seasons, and the years, depending on the timing and magnitude of freshwater runoff (Figure B.5). In particular, WY2018 and WY2013 show relatively mild depth gradients of density (Figures B.26 and B.28 respectively) whereas WY2017 shows stronger depth gradients of density particularly in January and April (Figure B.27). The model successfully reproduces the vertical gradients as well as the differences in density timing between the seasons.

The N^2 depth profiles show that while there are mismatches between the data and the model, the difference is acceptable, especially considering the uncertainty in data and highly sensitive nature of the buoyancy frequency arising from its calculation (i.e., taking the density gradient and the depth gradient and their division). Nonetheless, for all three years the depths at which the peak N^2 values are predicted are comparable across years and seasons, particularly for the periods with stratification.

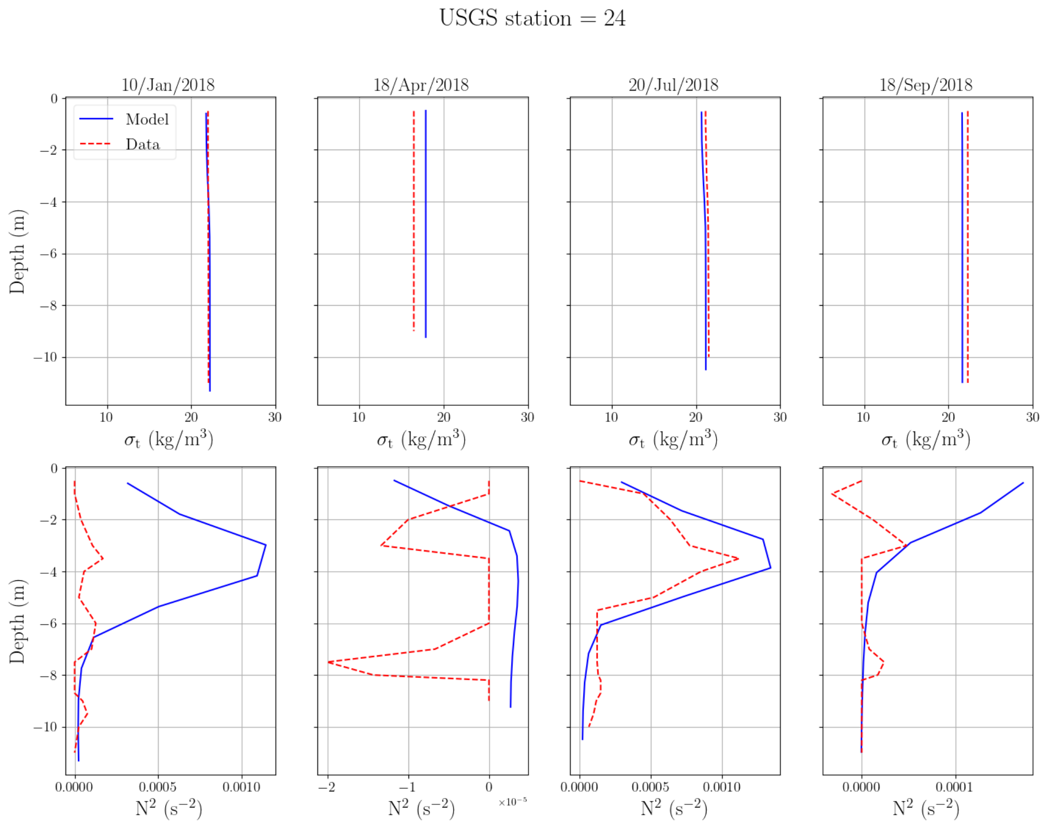

Figure B.26. Density profiles (top panels) and N^2 profiles (bottom panels) at station 24 for WY2018

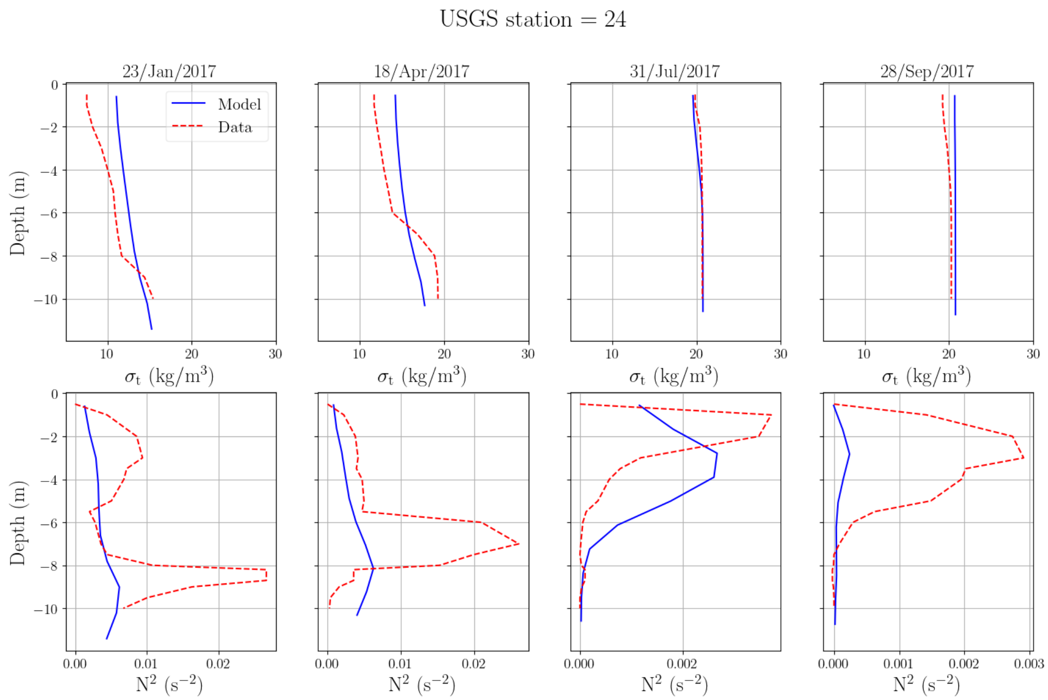

Figure B.27. Density profiles (top panels) and N^2 profiles (bottom panels) at station 24 for WY2017

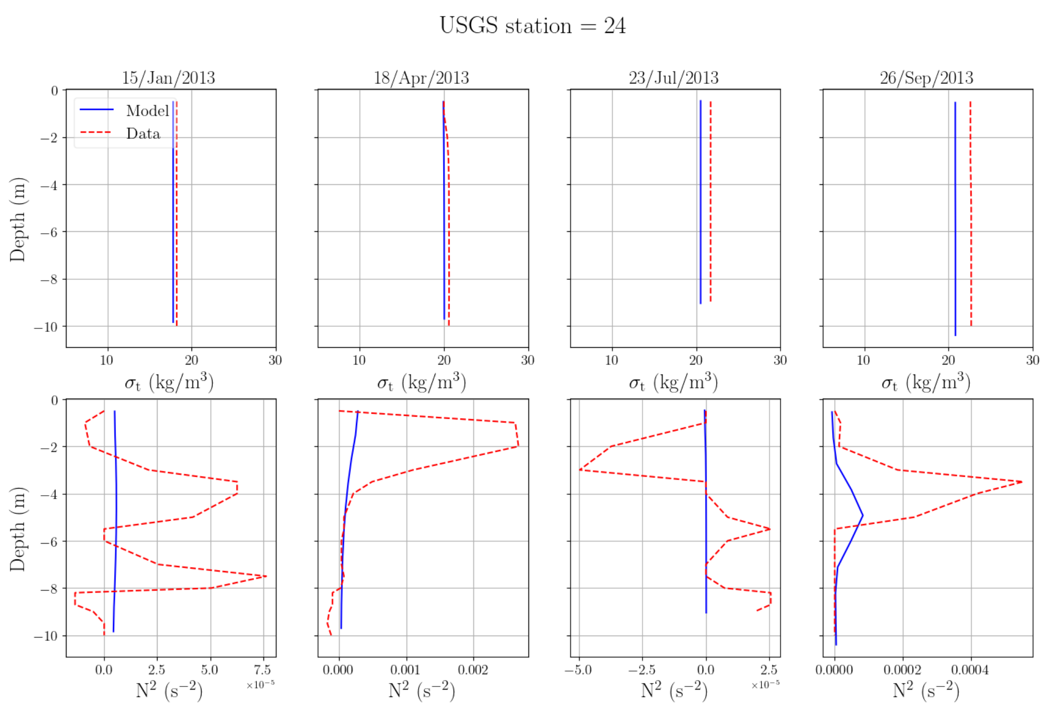

Figure B.28. Density profiles (top panels) and N^2 profiles (bottom panels) at station 24 for WY2013

Mixed Layer Depth - Identification of Critical Density Cutoff

The cumulative density of MLDs estimated from the model and the corresponding USGS data-based estimates for critical density criterion ranging from 0.01 kg/m^3 to 1 kg/m^3 are shown in Figures B.29-B.31. These figures also show the overall cumulative density for all model results that are not paired (model outputs are available at a higher frequency than field measurements). These figures illustrate that for small critical density criteria, an overwhelming majority of the model and data-derived MLD (more than 80%) show a very shallow MLD, but the MLD begins to stabilize to a more consistent distribution at a critical density criterion of 0.75 kg/m^3 and higher. The shape of the CDF does not change appreciably past a critical density criterion of 1 kg/m^3 for all three years. At the higher end of the range of critical density criteria evaluated (1.5 - 2.0 kg/m^3) the upper tail of the CDF begins to exhibit greater deviations between the model- and the measurement-derived MLDs. Therefore, 1 kg/m^3 was used as the critical density criterion for the MLD comparisons presented herein.

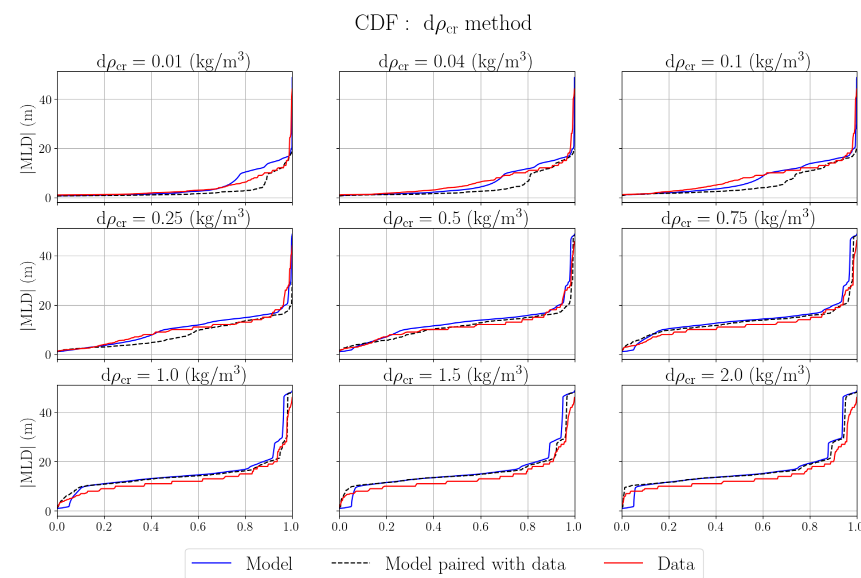

Figure B.29. The MLD cumulative distribution functions (CDF) for WY2018 and for various $d\rho_c$

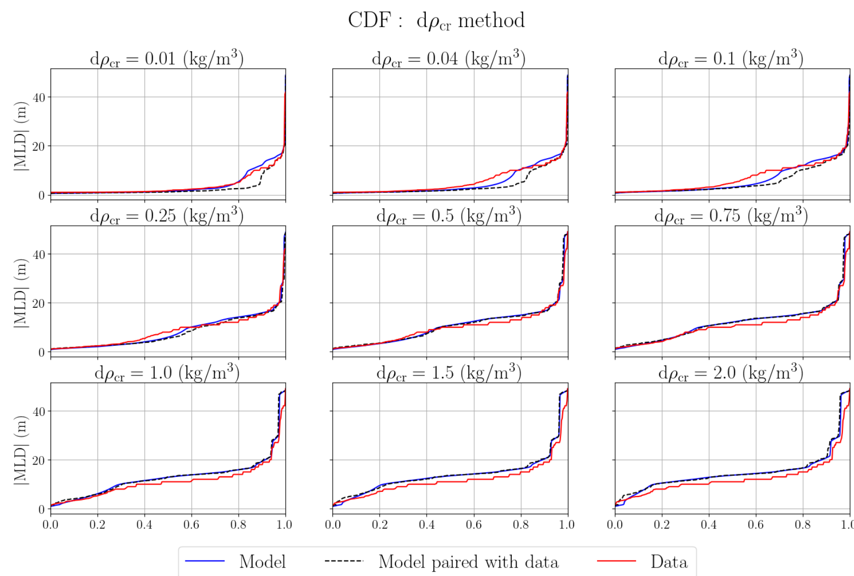

Figure B.30. The MLD cumulative distribution functions (CDF) for WY2017 and for various $d\rho_c$

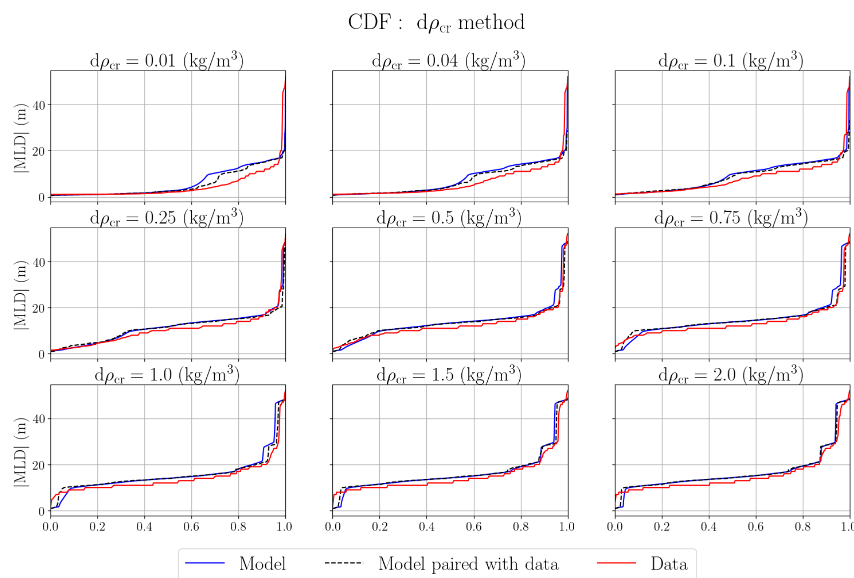

Figure B.31. The MLD cumulative distribution functions (CDF) for WY2013 and for various $d\rho_c$

As indicated in Section B.2, a similar comparison of the CDFs for the model- and measurement-based MLDs were also performed based on the critical density gradient criterion ranging from 0.01 kg/m^4 to 1 kg/m^4 (Figures B.32-B.34). This method also indicates that a sufficiently high critical density gradient (0.5 kg/m^4 or higher) is necessary to produce a stable distribution for both the model and measurement-based MLDs, but when this value is near the upper end of the range evaluated the upper tail of the CDFs between the model- and measurement-derived MLDs begin to show appreciable deviation. Overall, the results between the two methods are comparable, and a similar distribution of the MLD is obtained when the cutoff is not overly sensitive. The results discussed subsequently in this section are based on the critical density method with a cutoff of 1 kg/m^3.

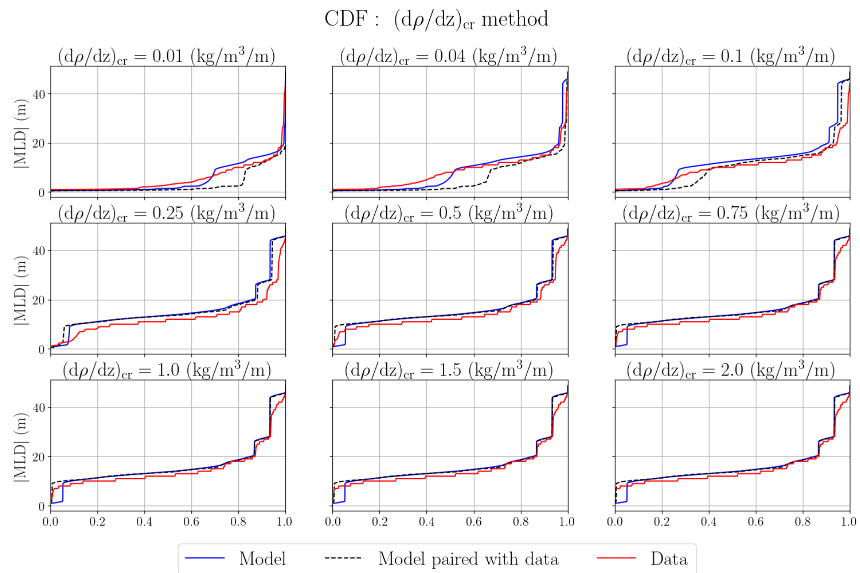

Figure B.32. The MLD cumulative distribution functions (CDF) for WY2018 and for various $(d\rho/dz)_c$

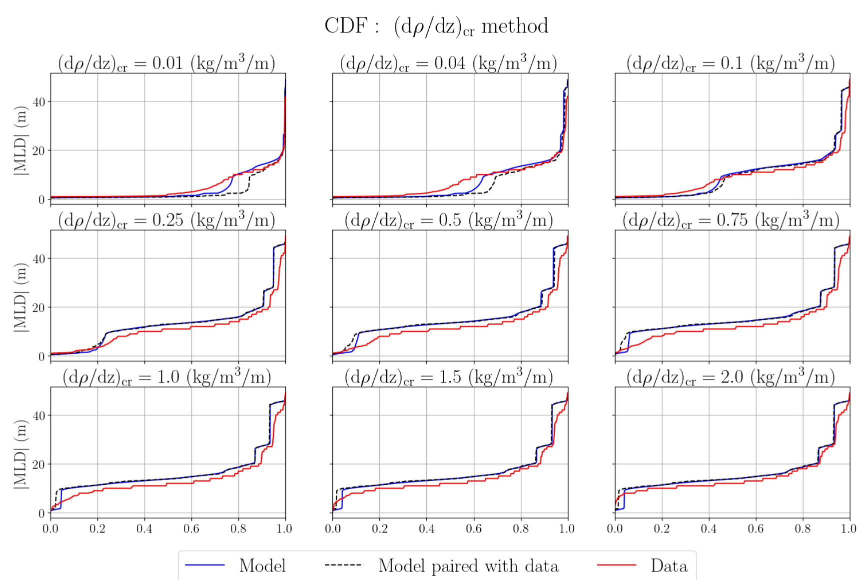

Figure B.33. The MLD cumulative distribution functions (CDF) for WY2017 and for various $(d\rho/dz)_c$

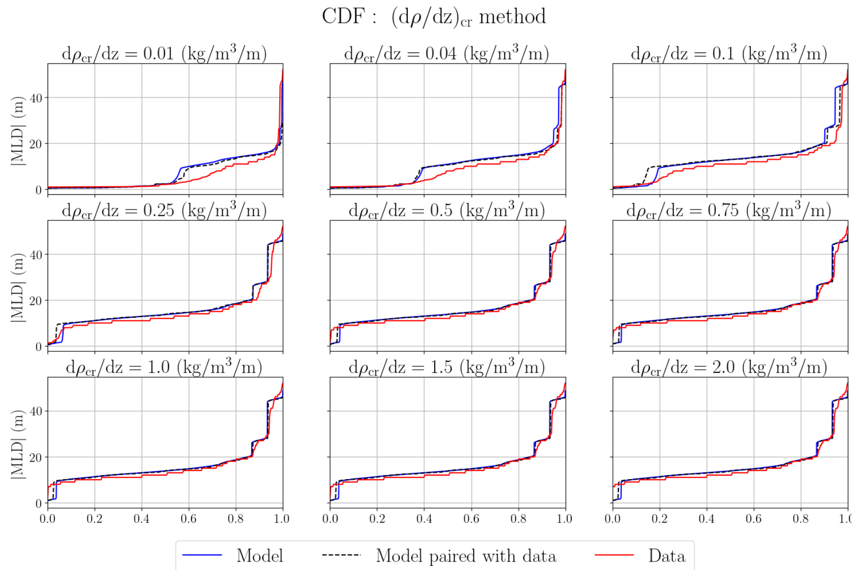

Figure B.34. The MLD cumulative distribution functions (CDF) for WY2013 and for various $(d\rho/dz)_c$

Mixed Layer Depth Time Series

In this section, we compare the MLD estimated from the model predictions of salinity and temperature against the MLD estimates from USGS measurements of temperature and salinity for WY2018, 2017 and 2013. As indicated in Section B.2 model-based MLDs are 24-hour MA and 10th and 90th moving percentiles.

MLD Time Series for WY2018

Figures B.35 through B.40 show a comparison of the model- and measurement-derived MLD results for WY2018. The changes in MLD over season and during sustained stratification events are most relevant in these comparisons. For biogeochemistry and primary production, time periods where the MLD shrinks considerably to within the top 10 m (i.e., limiting the availability of nutrients within the photic zone) is much more significant than time periods where the MLD changes by a substantial magnitude (for example, by 10 m) but is within the bottom half of the water column. Figures B.35 to B.40 illustrate that model reproduces the large scale seasonal changes in the MLDs relative to the measurement-derived estimates including: consistent shrinking of the MLD during spring runoff period (Mar-Jun); the relative differences in MLD over space (deeper in Central Bay and upper portions of South Bay and shallower in South Bay and Lower South Bay); and the relative lack of sustained stratification events in south of San Mateo Bridge (see Figures B.38 - B.40). These findings are also consistent with the density and N^2 results presented earlier. For example, in station 22 (see Figure B.6 that shows density and N^2 and Figure B.35 that shows MLD) the model has predicted the restratification and shoaling of the MLD from March to June. After June the stratification is weak, the water column is mixed and the MLD is deep, showing little variation in time. An evaluation of the performance over all stations (18 to 32) is shown in Figure B.41 for different times in WY2018 as a model-data scatter plot. It shows that while there are some points that are dispersed and generally overpredicted, however most of them are clustered around the 1:1 line, showing generally good agreement between the model and the measurement based MLDs.

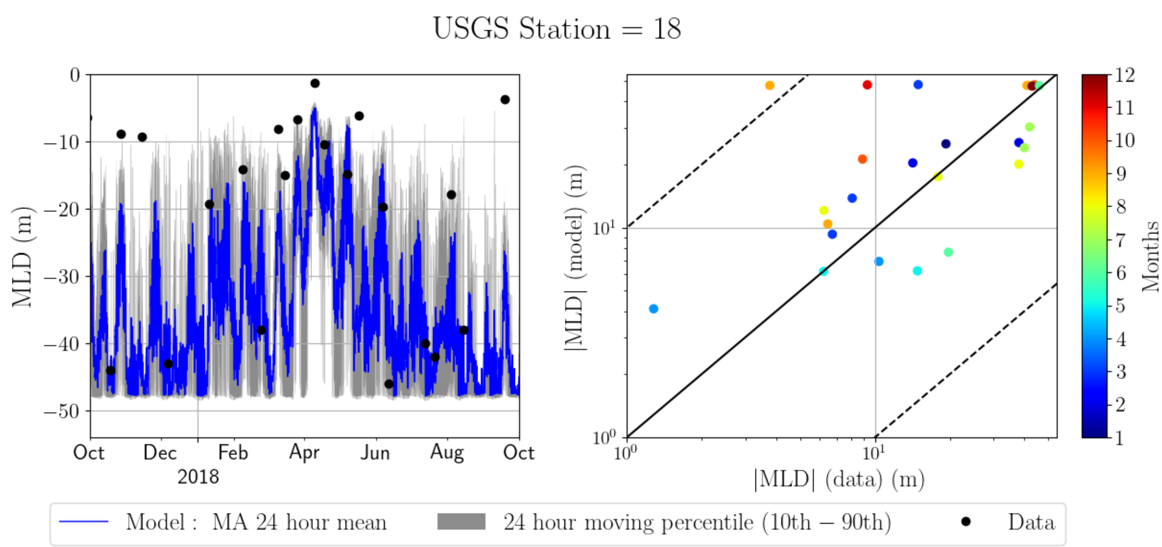

Figure B.35. The MLD for WY2018 at station 18. Left panel shows the time series and the right panel shows the comparison of the model and density results, colored by the month

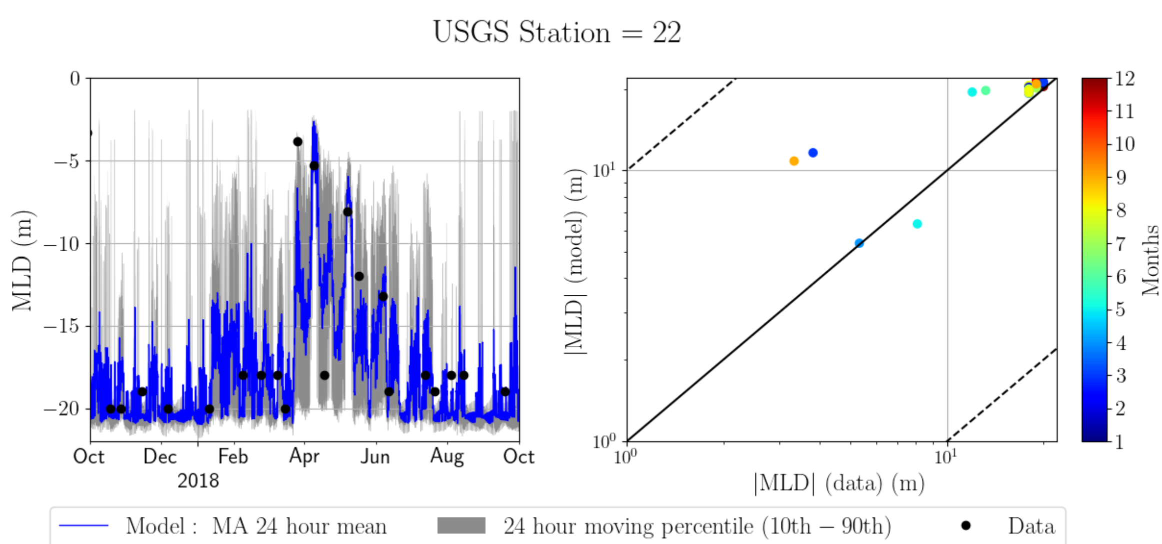

Figure B.36. The MLD for WY2018 at station 22. Left panel shows the time series and the right panel shows the comparison of the model and density results, colored by the month

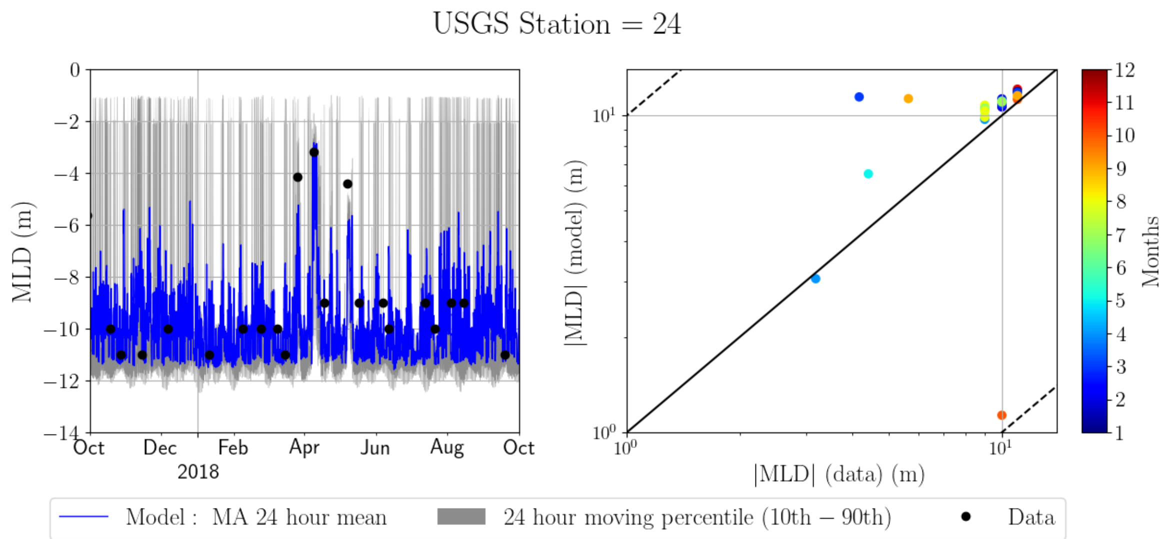

Figure B.37. The MLD for WY2018 at station 24. Left panel shows the time series and the right panel shows the comparison of the model and density results, colored by the month

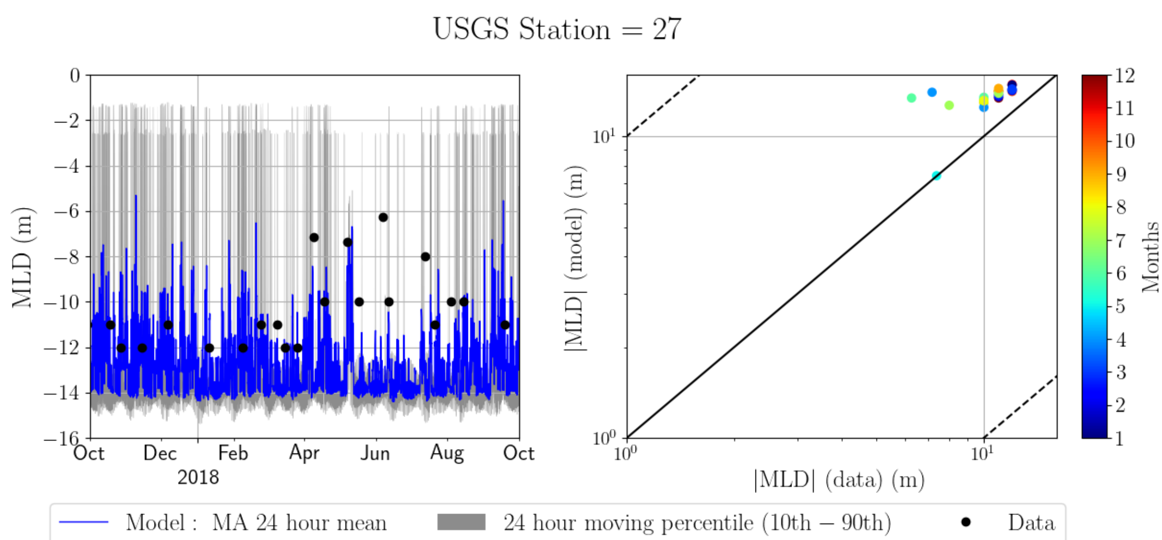

Figure B.38. The MLD for WY2018 at station 27. Left panel shows the time series and the right panel shows the comparison of the model and density results, colored by the month

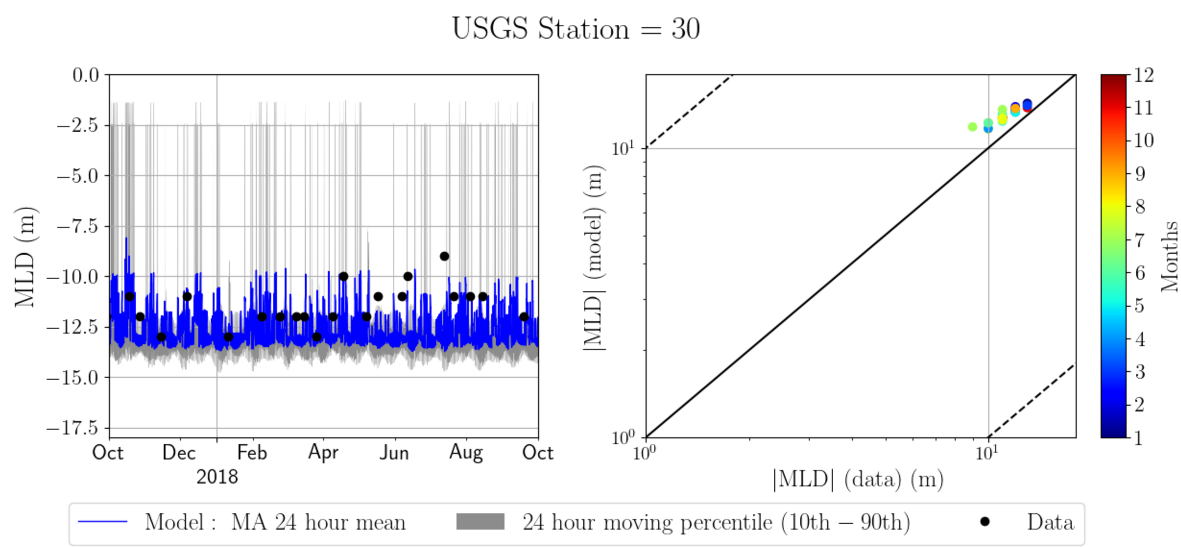

Figure B.39. The MLD for WY2018 at station 30. Left panel shows the time series and the right panel shows the comparison of the model and density results, colored by the month

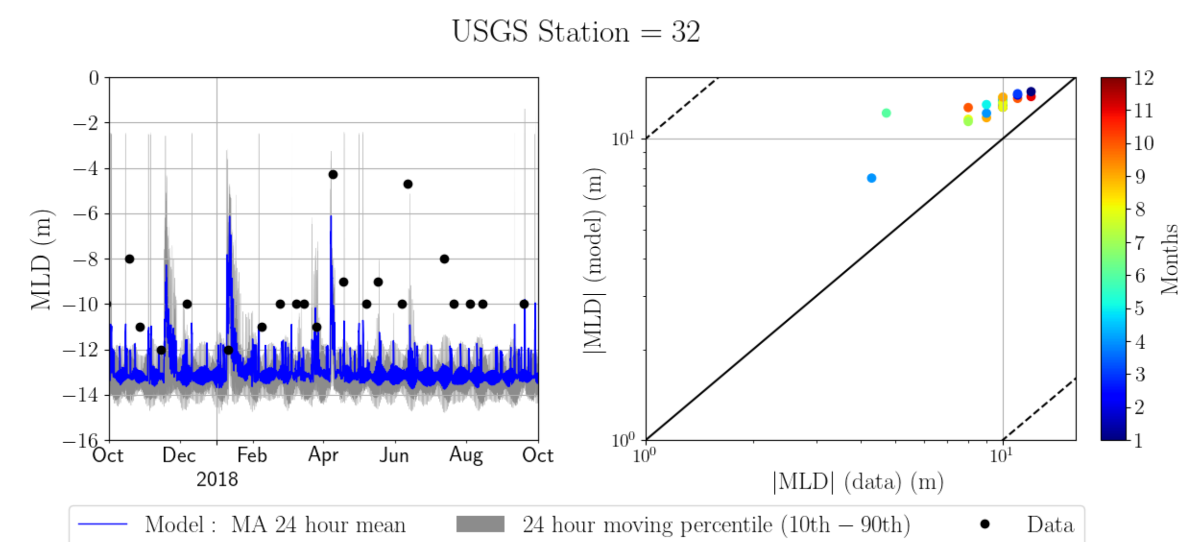

Figure B.40. The MLD for WY2018 at station 32. Left panel shows the time series and the right panel shows the comparison of the model and density results, colored by the month

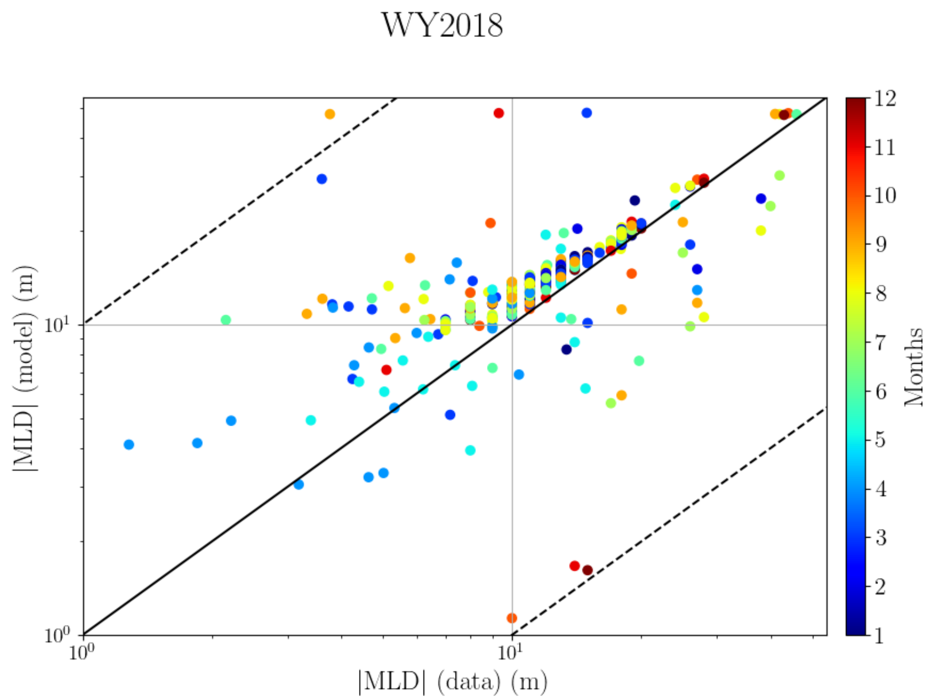

Figure B.41. The comparison of the model and density results, colored by the month for WY2018

MLD Time Series for WY2017

WY2017 was a high flow year, with larger freshwater runoff in the winter and spring months (Jan - May). The results show good performance of the model in capturing the temporal variability in the MLD as well as the MLD magnitude compared to data (Figure B.42 - B.47). In particular, the model-based MLD reproduces the extended period (January-June) of relatively strong stratified conditions that is evident in the correspondingly shallow measurement-derived MLDs. Moreover, the sustained stratification event is evident as far south as Station 32 and is successfully captured in the model-based MLD. Coincidentally a relatively large bloom event occurred in the spring of this year, which was also reproduced in the DWAQ model (SFEI 2020). Further explorations of the effect of extended stratification on the potential for triggering a bloom is planned in FY2022. Similar to WY2018, the scatter plot of the model and measurement derived MLDs for all stations at different times in WY2017 shows that most of the points are clustered around the 1:1 line (Figure B.48).

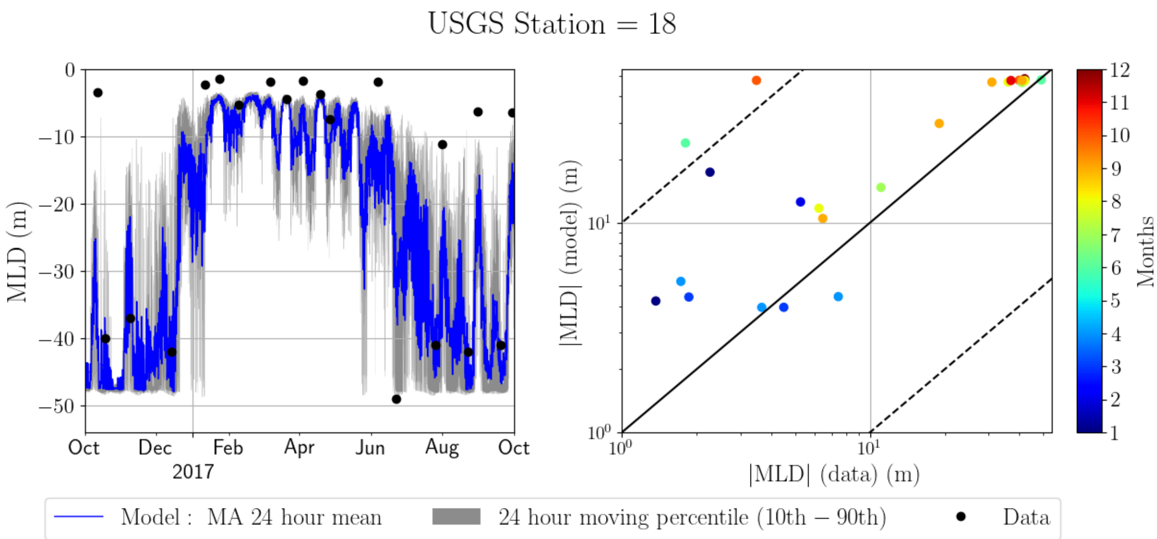

Figure B.42. The MLD for WY2017 at station 18. Left panel shows the time series and the right panel shows the comparison of the model and density results, colored by the month

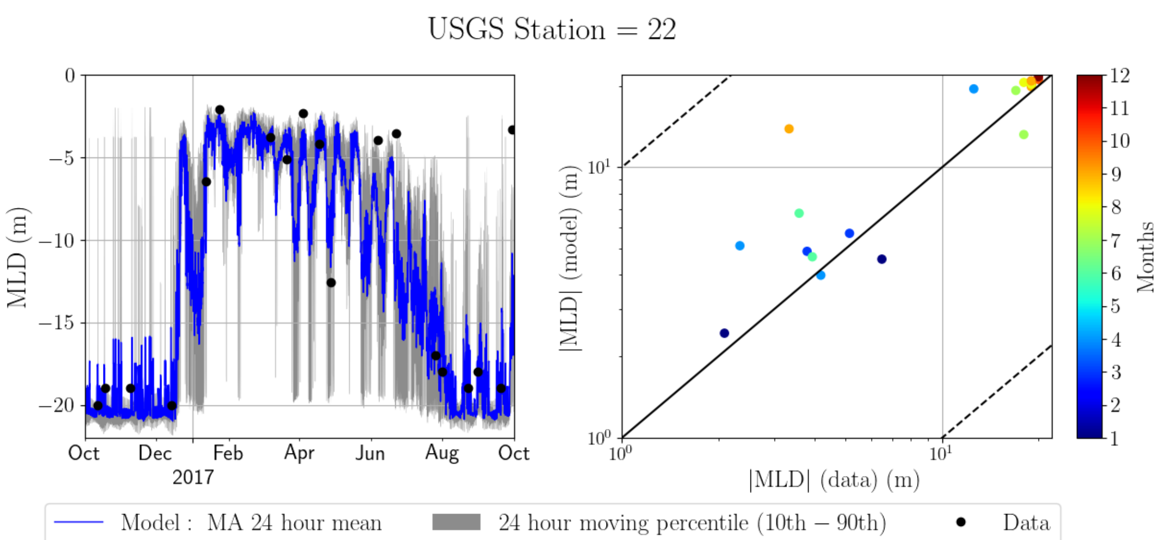

Figure B.43. The MLD for WY2017 at station 22. Left panel shows the time series and the right panel shows the comparison of the model and density results, colored by the month

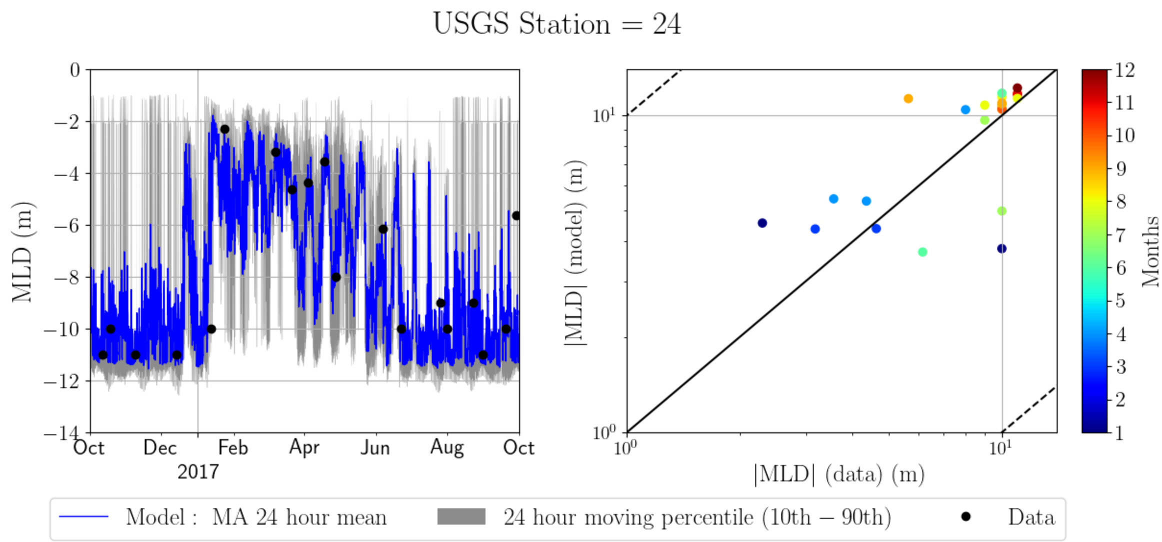

Figure B.44. The MLD for WY2017 at station 24. Left panel shows the time series and the right panel shows the comparison of the model and density results, colored by the month

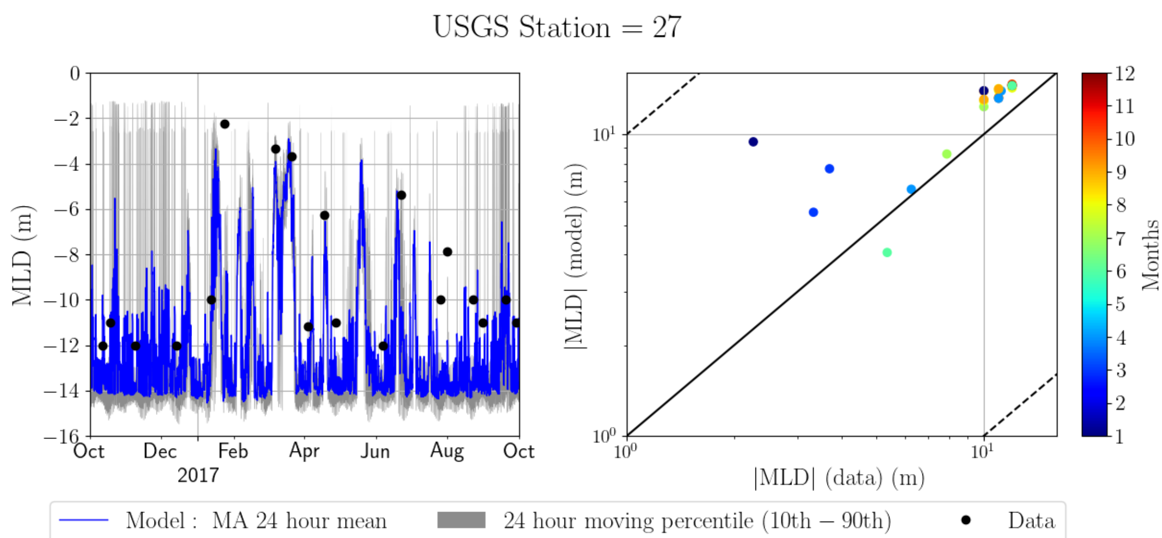

Figure B.45. The MLD for WY2017 at station 27. Left panel shows the time series and the right panel shows the comparison of the model and density results, colored by the month

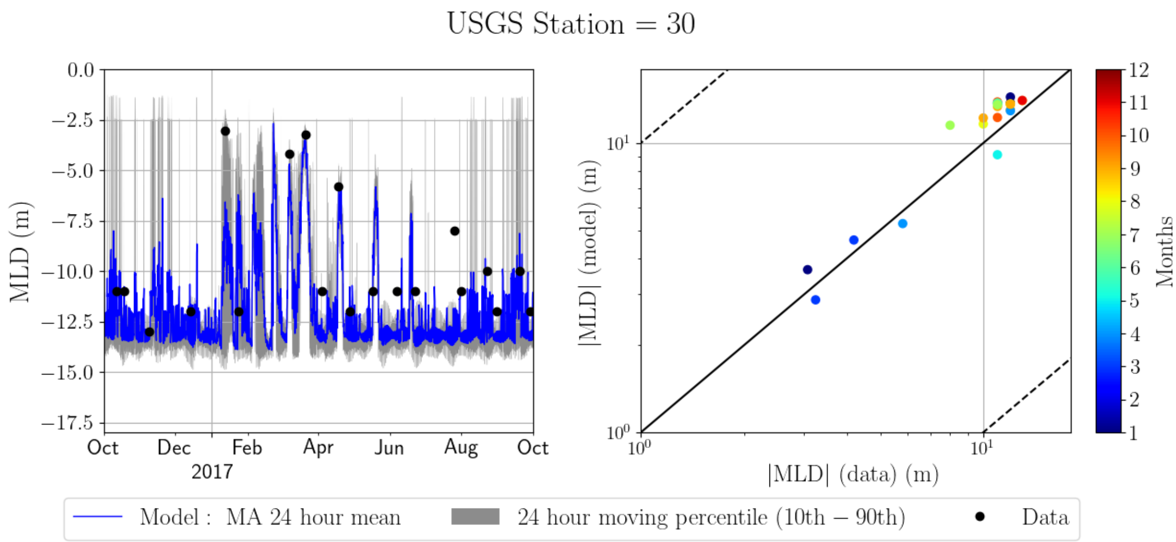

Figure B.46. The MLD for WY2017 at station 30. Left panel shows the time series and the right panel shows the comparison of the model and density results, colored by the month

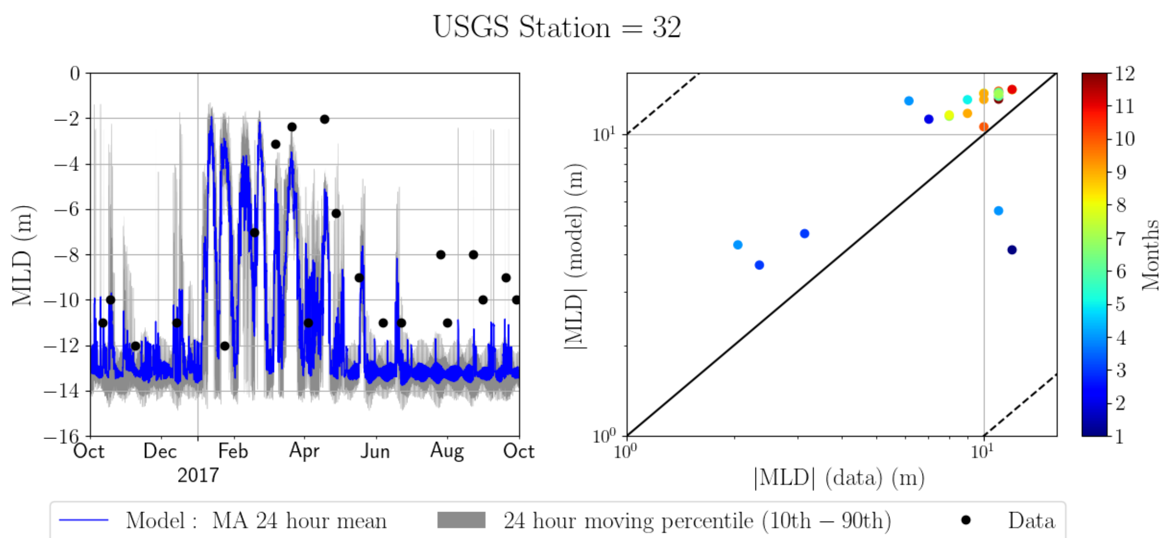

Figure B.47. The MLD for WY2017 at station 32. Left panel shows the time series and the right panel shows the comparison of the model and density results, colored by the month

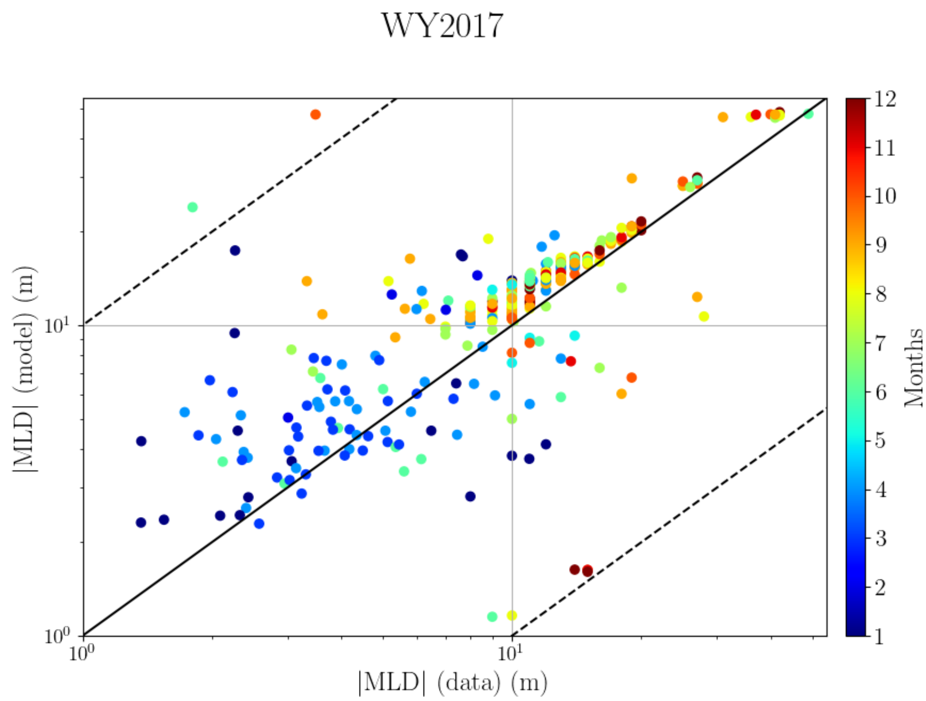

Figure B.48. The comparison of the model and density results, colored by the month for WY2017

MLD Time Series for WY2013

Similar to other years, the MLD agrees acceptably well with data (Figures B.49 - B.54). However, in WY2013 the stratification is weak, with a few transient restratification events, for example around December 2012 (see Figure B.18 - B.23). As such, the MLD is generally deep with little variation. Where the data are available and showed evidence of sustained stratification (shallow MLDs in December-January), the model-based MLD captured these observations (e.g., stations 30 and 32 in Figures B.53 and 54). As in WY2017 the period with shallow MLDs (particularly in South and Lower South Bay) coincided with a larger bloom event which was reasonably reproduced in the DWAQ model (SFEI 2020), providing further evidence of the successful reproduction of observed hydrodynamics. Figure B.55 shows a reasonable scatter around the 1:1 line for WY2013 over all the stations, like the other water years.

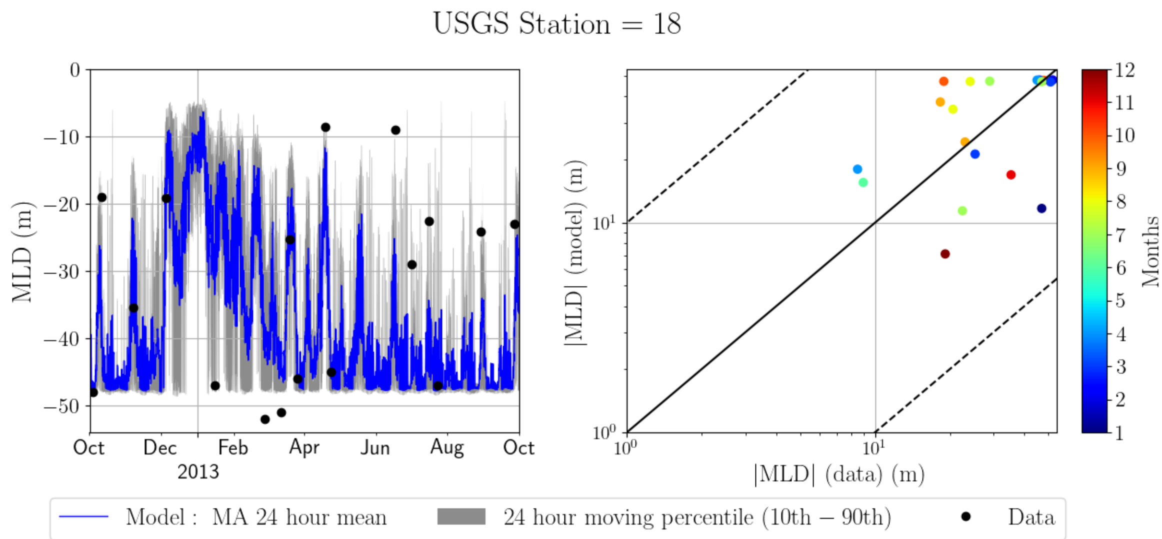

Figure B.49. The MLD for WY2013 at station 18. Left panel shows the time series and the right panel shows the comparison of the model and density results, colored by the month

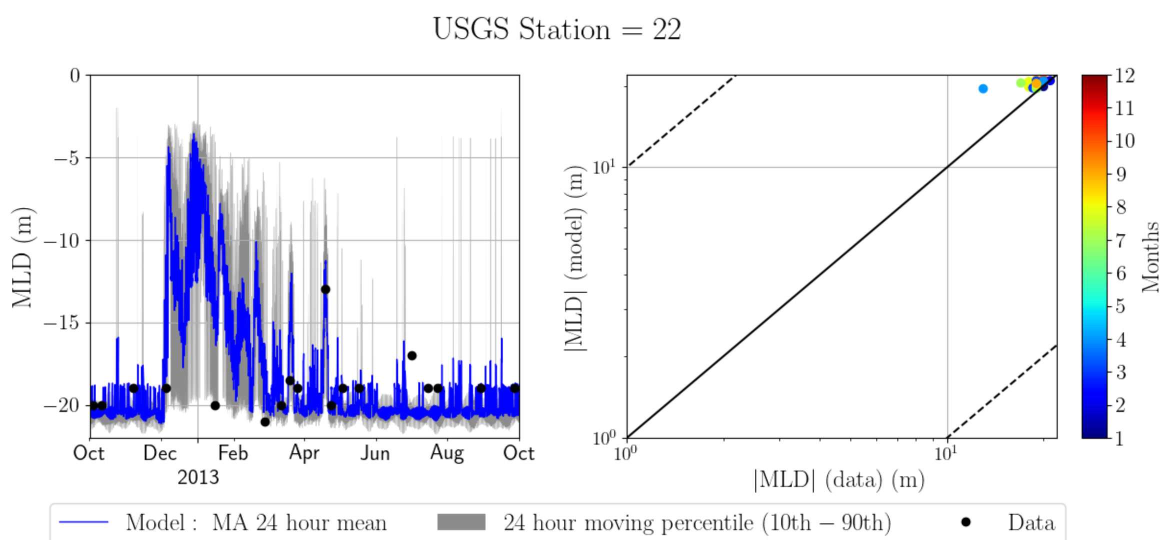

Figure B.50. The MLD for WY2013 at station 22. Left panel shows the time series and the right panel shows the comparison of the model and density results, colored by the month

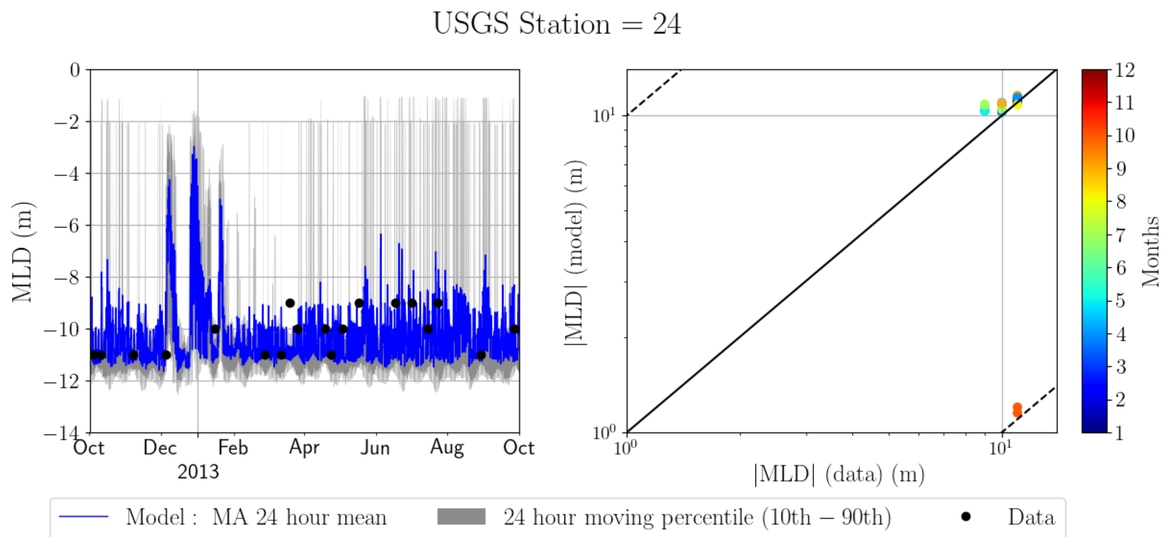

Figure B.51. The MLD for WY2013 at station 24. Left panel shows the time series and the right panel shows the comparison of the model and density results, colored by the month

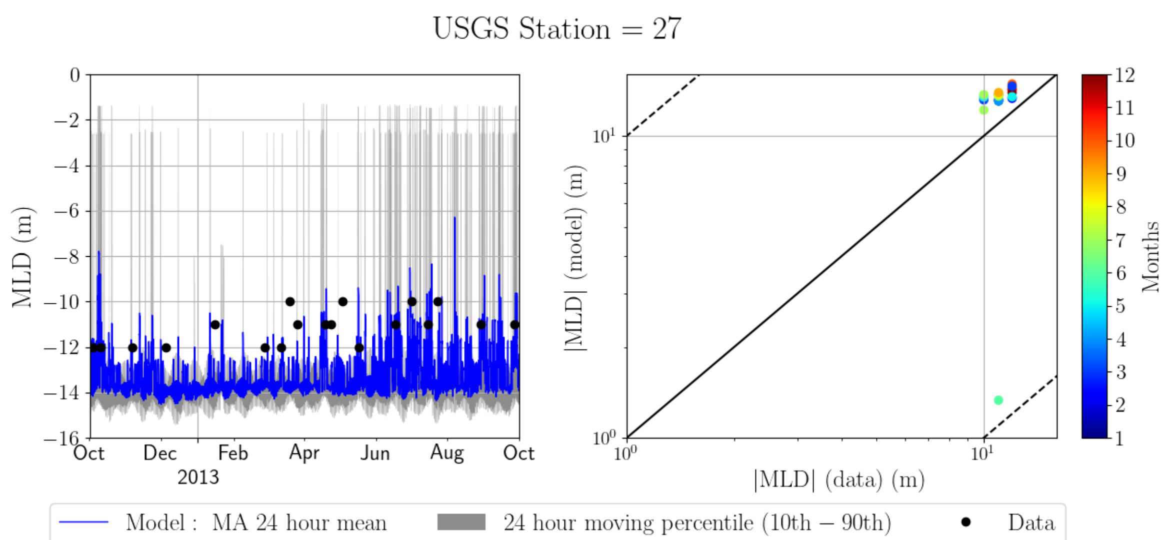

Figure B.52. The MLD for WY2013 at station 27. Left panel shows the time series and the right panel shows the comparison of the model and density results, colored by the month

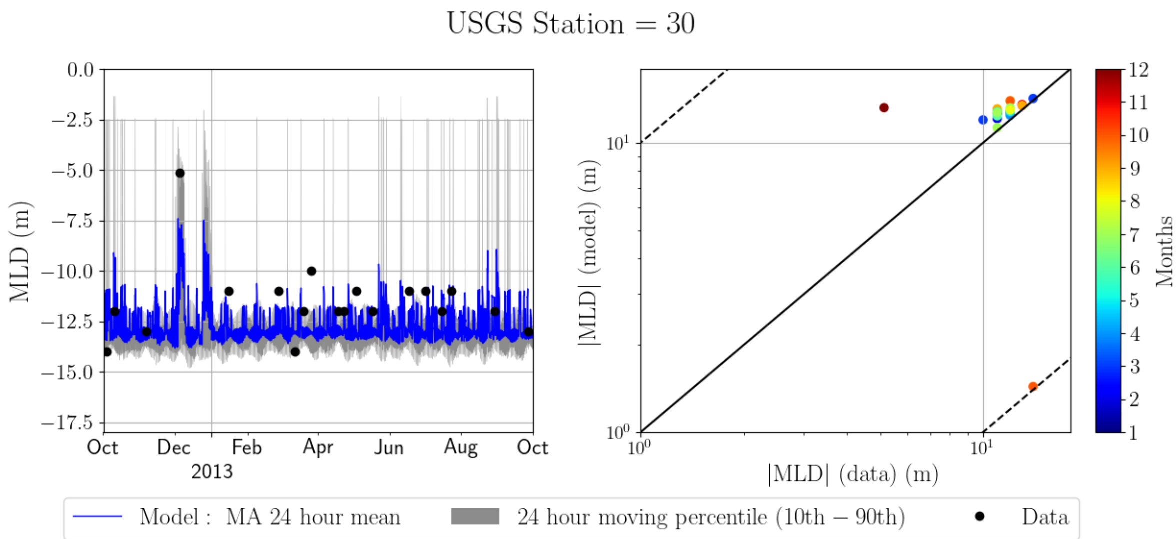

Figure B.53. The MLD for WY2013 at station 30. Left panel shows the time series and the right panel shows the comparison of the model and density results, colored by the month

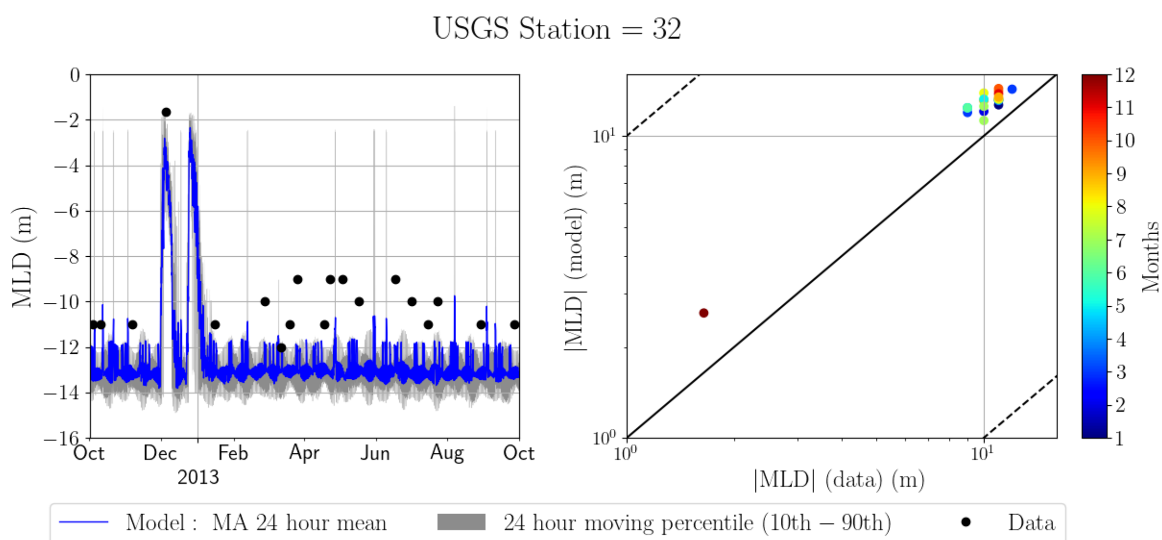

Figure B.54. The MLD for WY2013 at station 32. Left panel shows the time series and the right panel shows the comparison of the model and density results, colored by the month

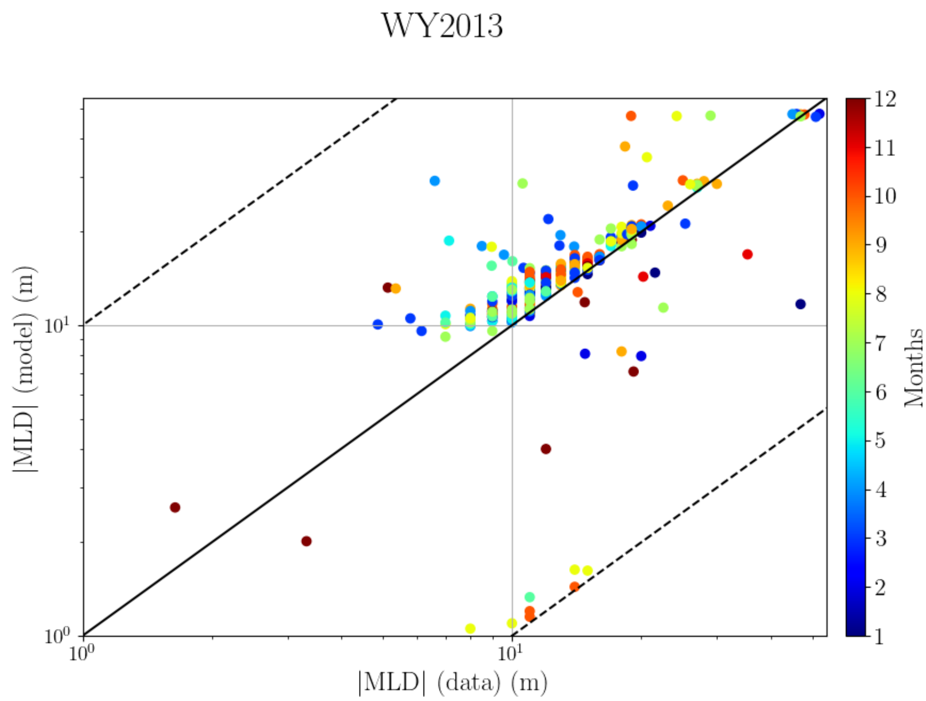

Figure B.55. The comparison of the model and density results, colored by the month for WY2013

Summary

In this study we evaluated the capability of DFM for modeling the density stratification. We used different water years (WY2018, 2017, and 2013) with distinctive characteristics to examine the performance of the model for simulating density stratification under different hydrological conditions. We calculated the time series of the density and buoyancy frequency, the density and buoyancy frequency vertical profiles at different times, and ultimately the mixed layer depth time series. The results were compared with USGS observed data at different locations. The comparison of the buoyancy frequency, density and MLD over multiple water years showed that the model is predicting the temporal variability of the density as well as its magnitude.

Different thresholds for commonly accepted approaches (based on density differences) for estimating MLD were compared to identify optimal threshold values that were suited for SFB. These comparisons are useful for future model validations as well.

The findings of this study will be used to investigate the onset of chlorophyll blooms in SFB and the correlation between the stratification and other factors that play a role in chlorophyll blooms.

Appendix B.1: Supplemental Results for Stratification and MLD Analysis

Comparison of N^2 across different water years

The following plots and figures depict N^2 results for the WY2018, WY2017 and WY2013.

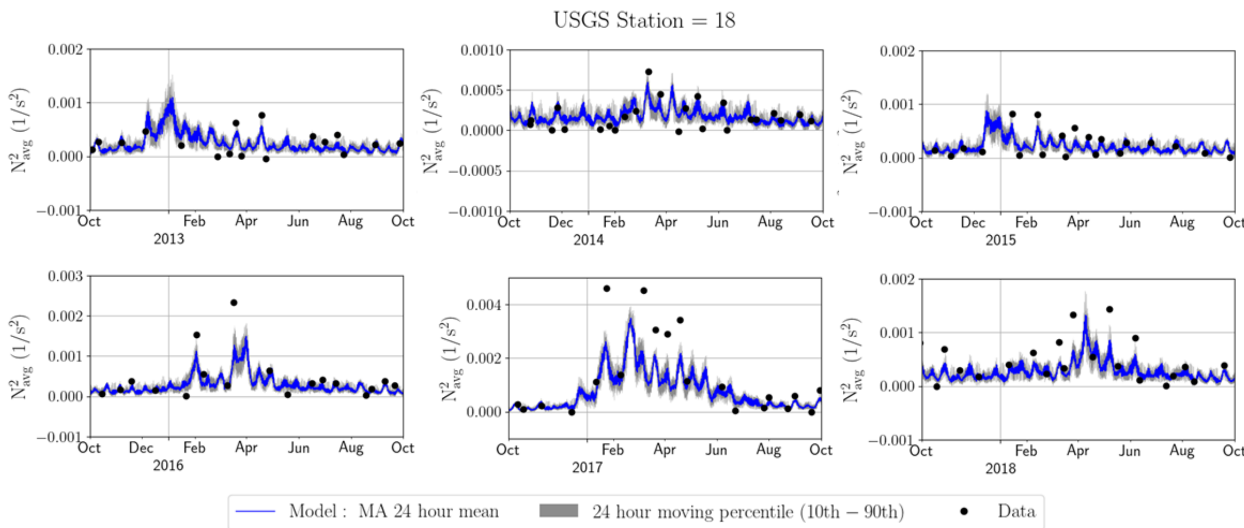

Figures B.1.1. Depth-averaged N^2 at station 18 for WY2013-WY2018

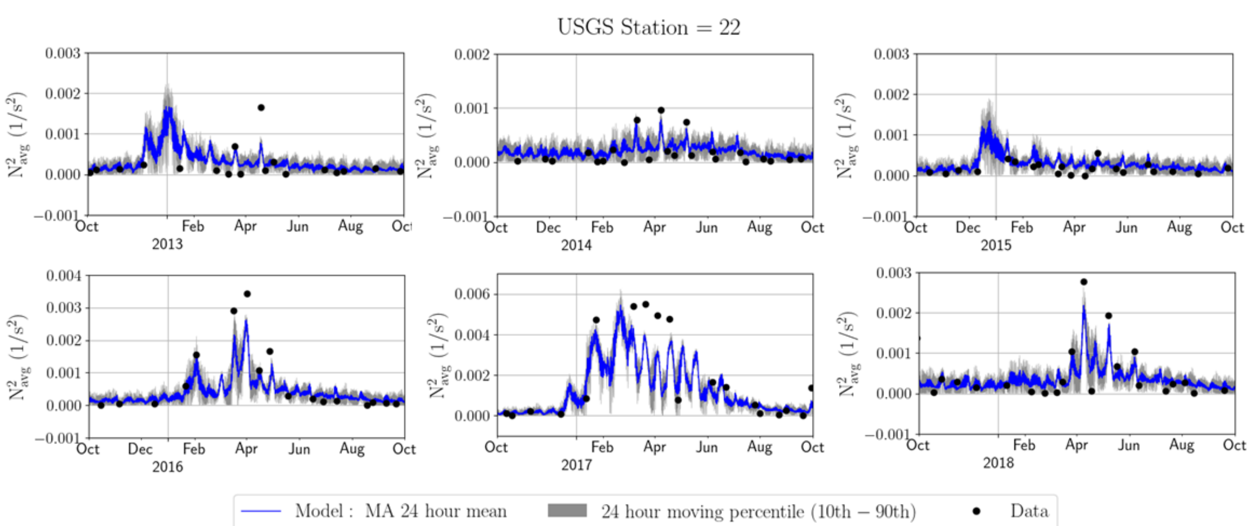

Figures B.1.2. Depth-averaged N^2 at station 22 for WY2013-WY2018

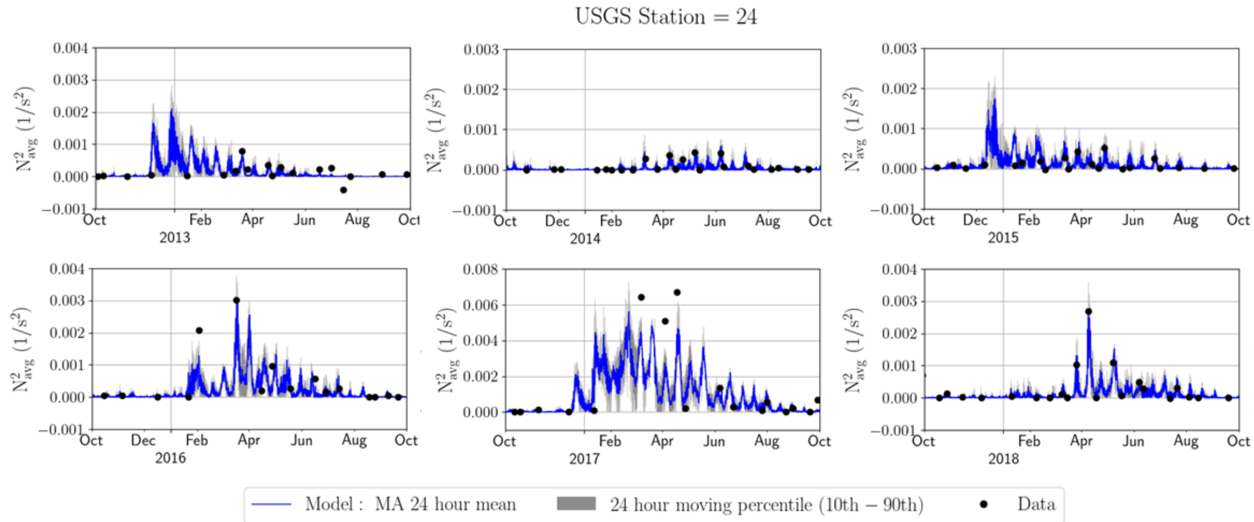

Figures B.1.3. Depth-averaged N^2 at station 24 for WY2013-WY2018

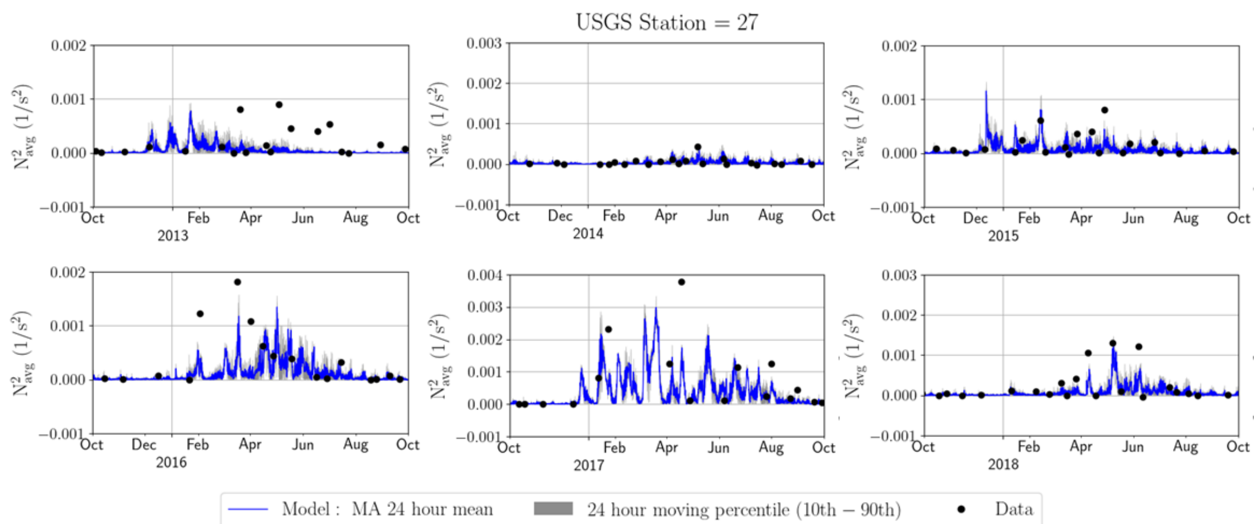

Figures B.1.4. Depth-averaged N^2 at station 27 for WY2013-WY2018

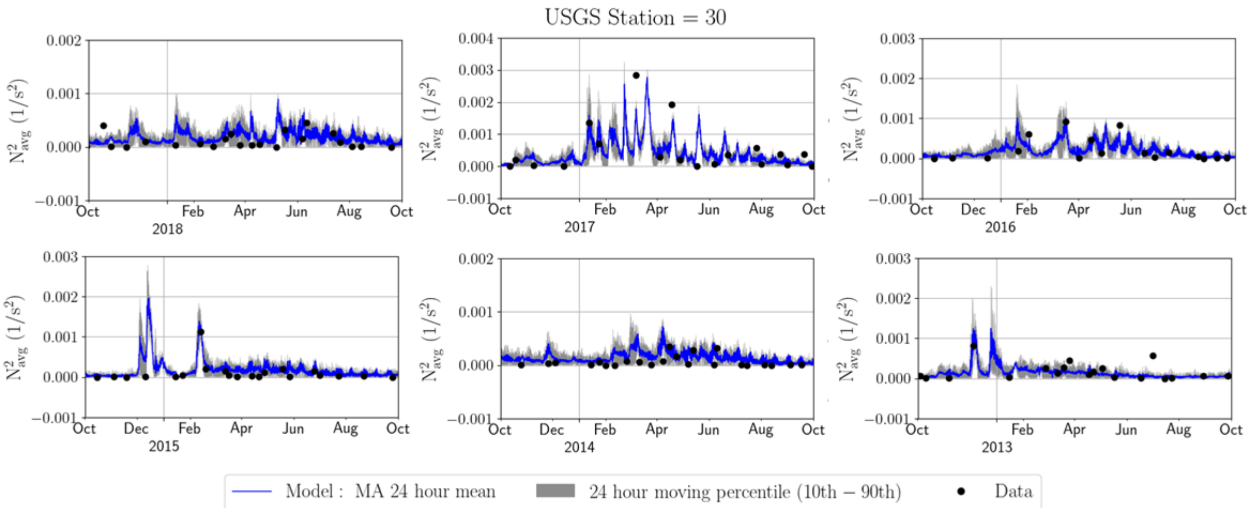

Figures B.1.5. Depth-averaged N^2 at station 30 for WY2013-WY2018

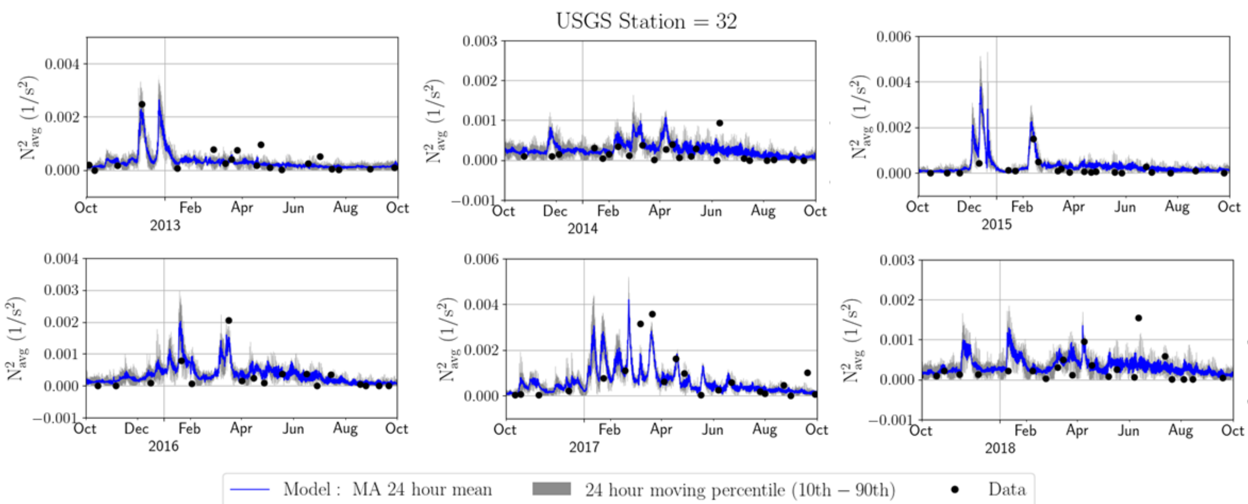

Figures B.1.6. Depth-averaged N^2 at station 32 for WY2013-WY2018

Density and N^2 profiles

The following plots and figures depict density and N^2 profiles for WY2018, WY2017 and WY2013.

WY2018

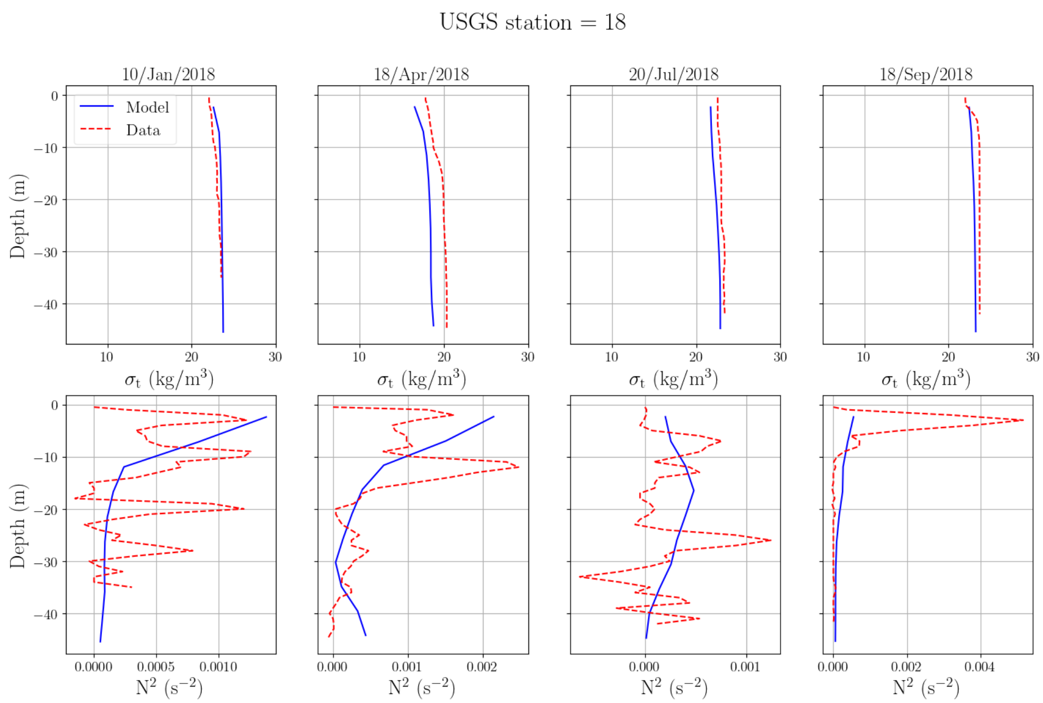

Figures B.1.7. Density profiles and N^2 profiles at station 18 for WY2018

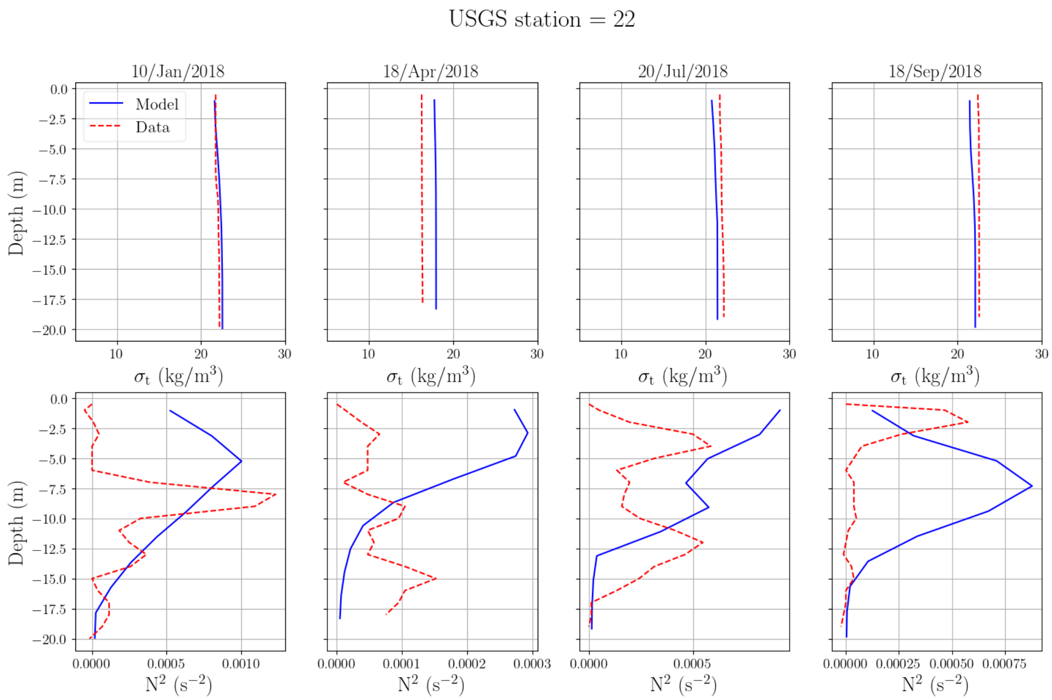

Figures B.1.8. Density profiles and N^2 profiles at station 22 for WY2018

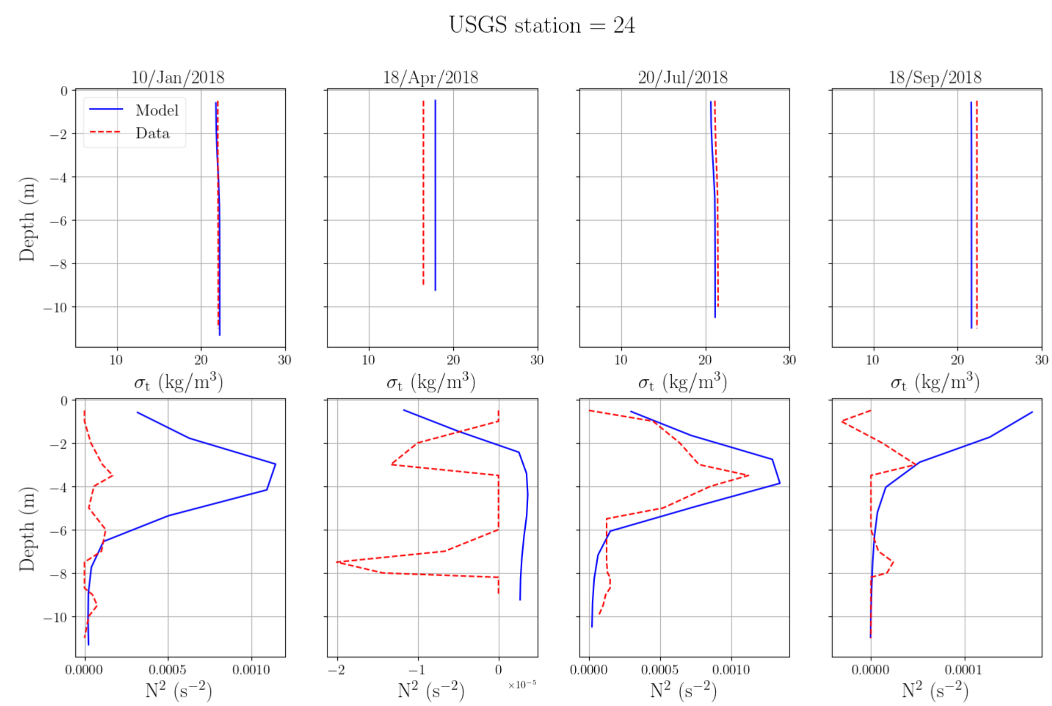

Figures B.1.9. Density profiles and N^2 profiles at station 24 for WY2018

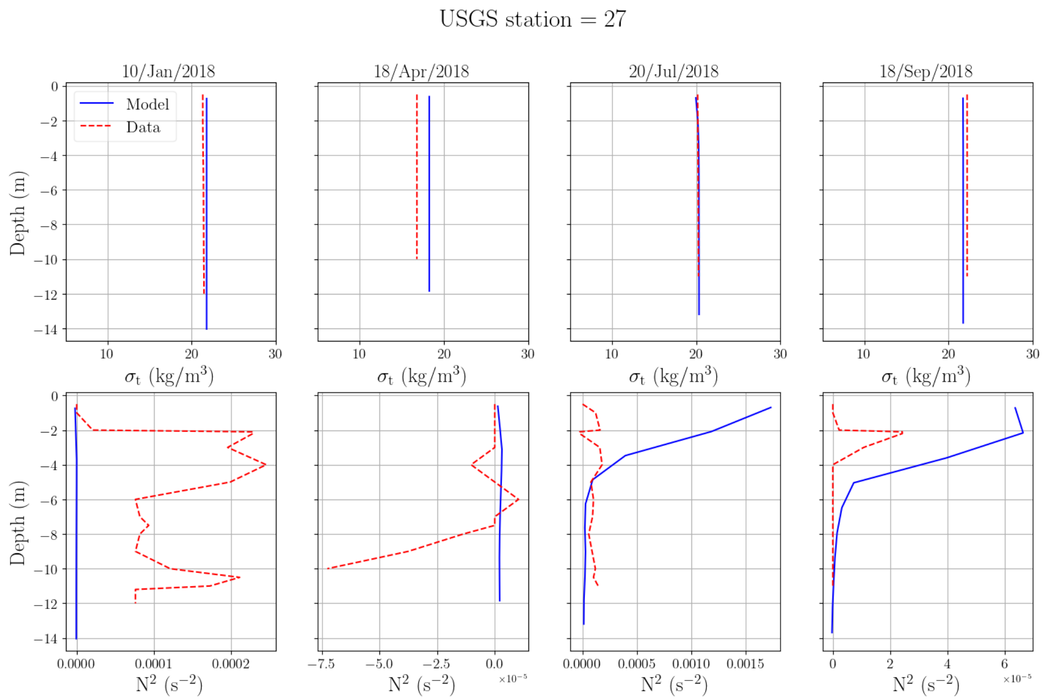

Figures B.1.10. Density profiles and N^2 profiles at station 27 for WY2018

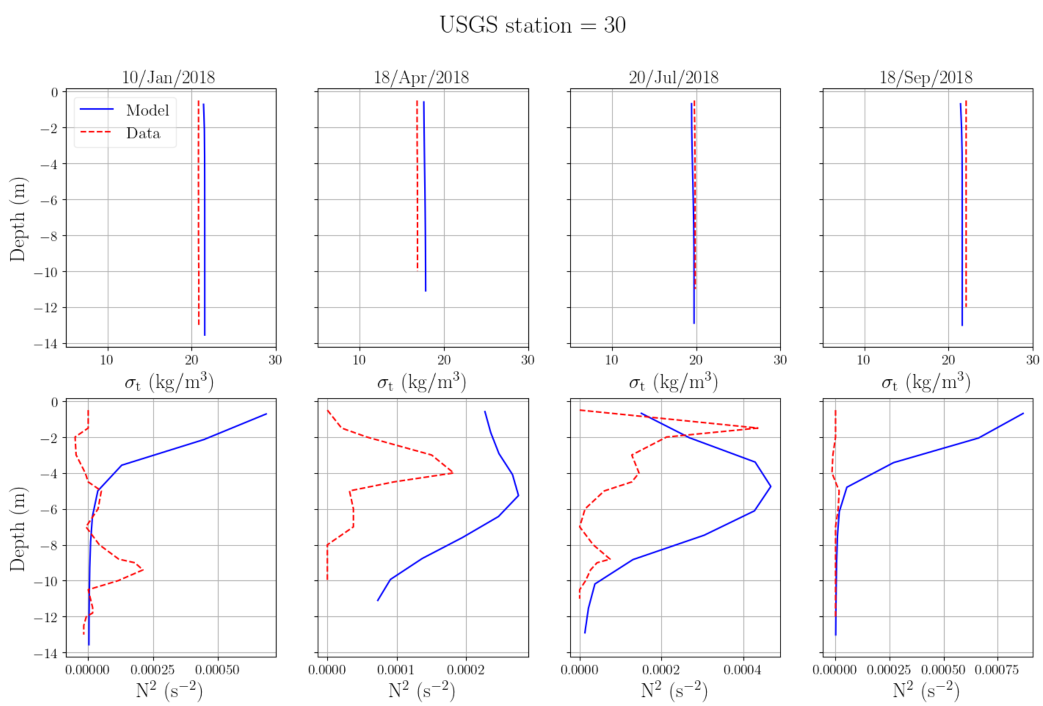

Figures B.1.11. Density profiles and N^2 profiles at station 30 for WY2018

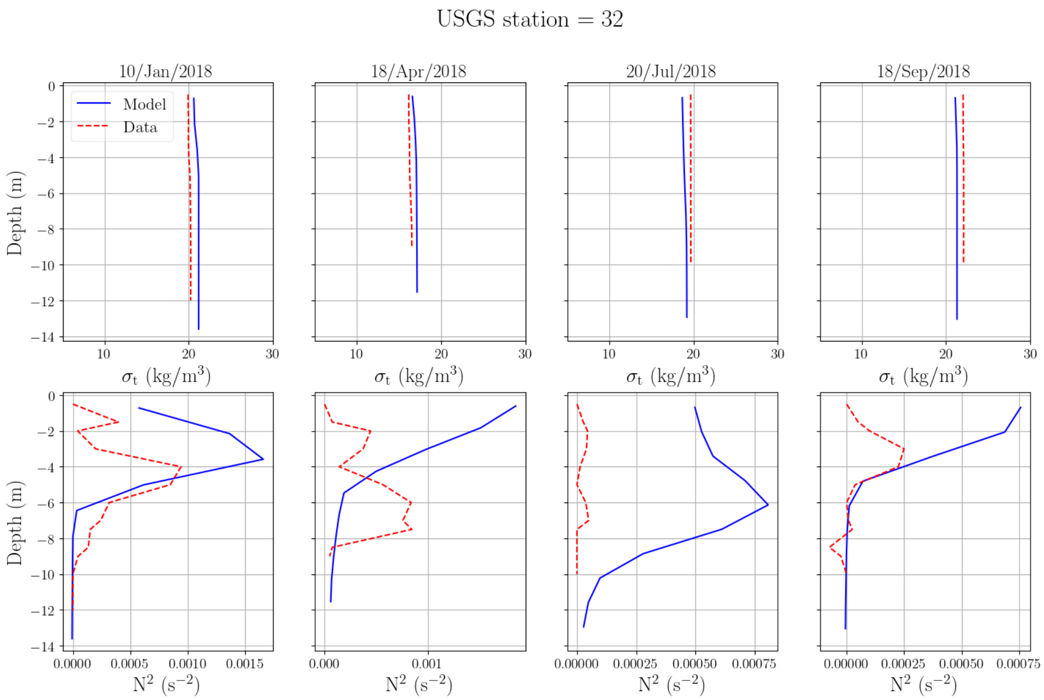

Figures B.1.12. Density profiles and N^2 profiles at station 32 for WY2018

WY2017

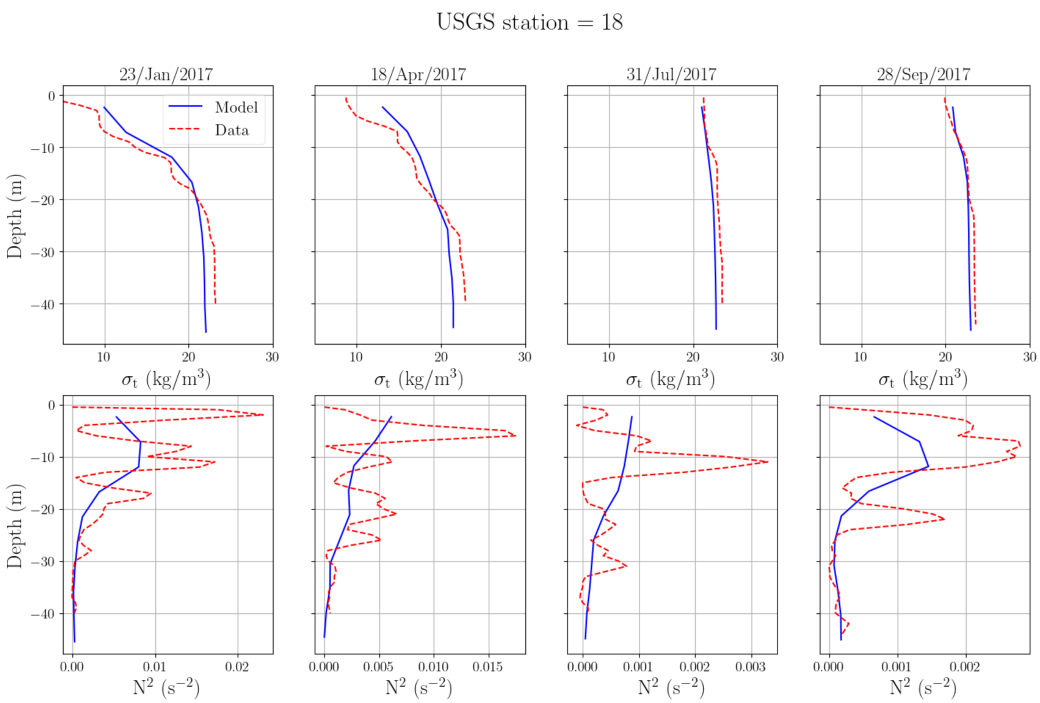

Figures B.1.13. Density profiles and N^2 profiles at station 18 for WY2017

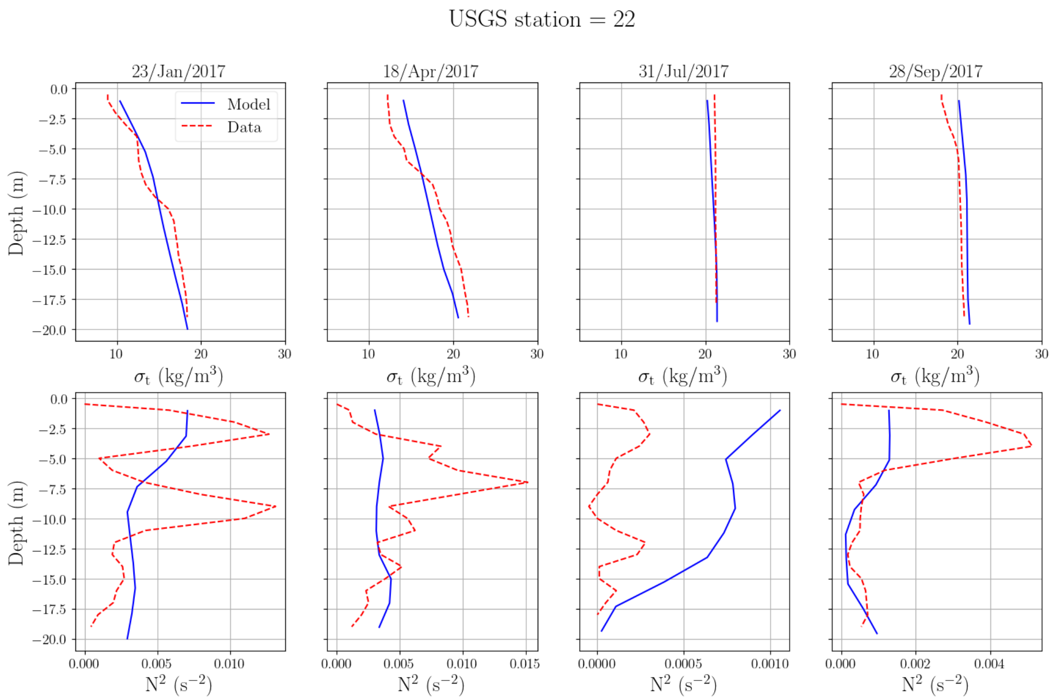

Figures B.1.14. Density profiles and N^2 profiles at station 22 for WY2017

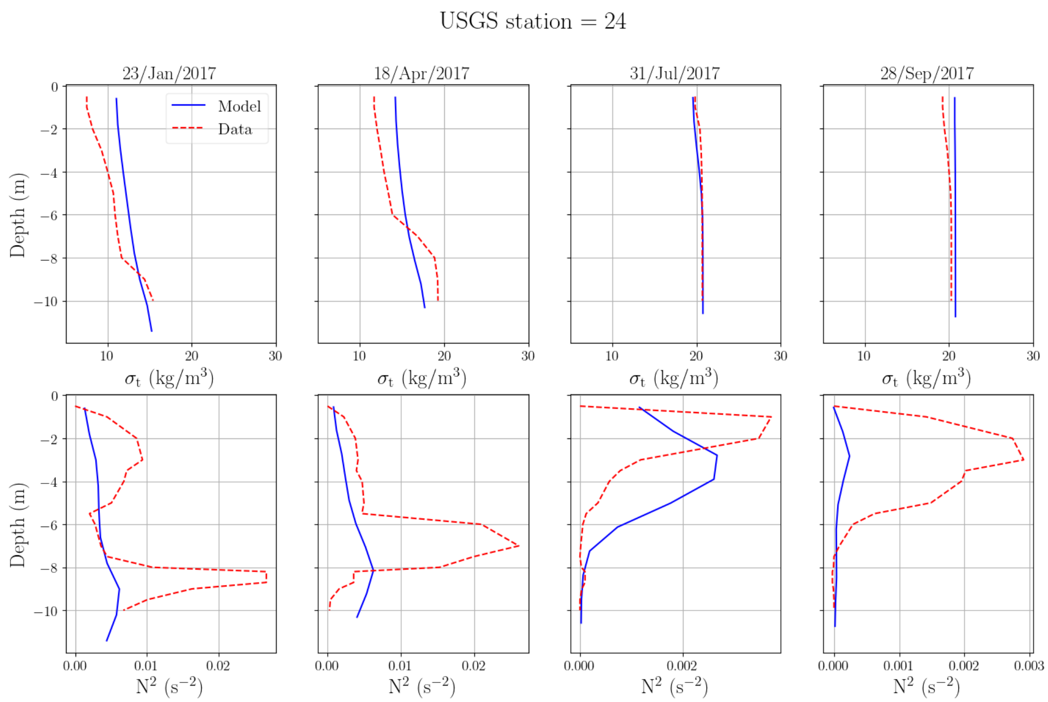

Figures B.1.15. Density profiles and N^2 profiles at station 24 for WY2017

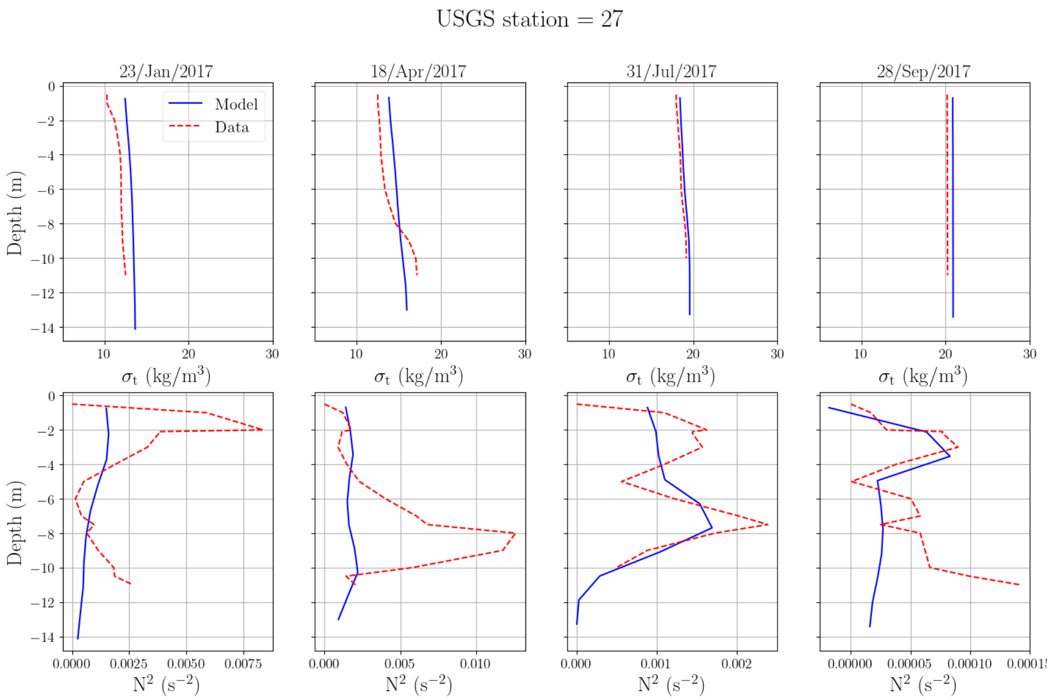

Figures B.1.16. Density profiles and N^2 profiles at station 27 for WY2017

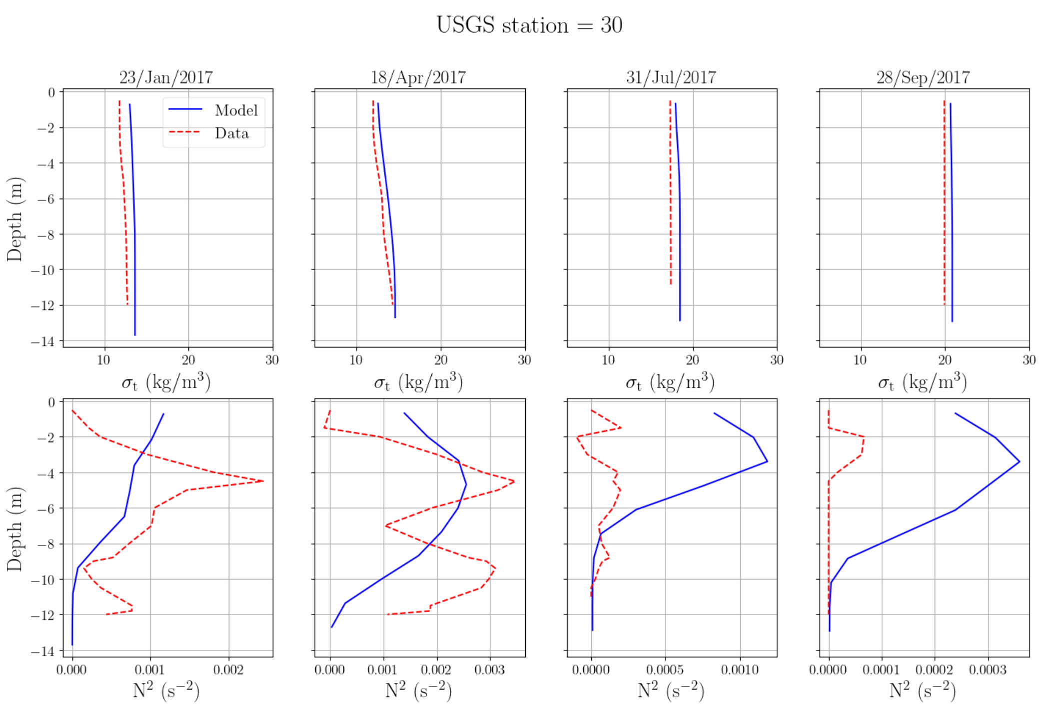

Figures B.1.17. Density profiles and N^2 profiles at station 30 for WY2017

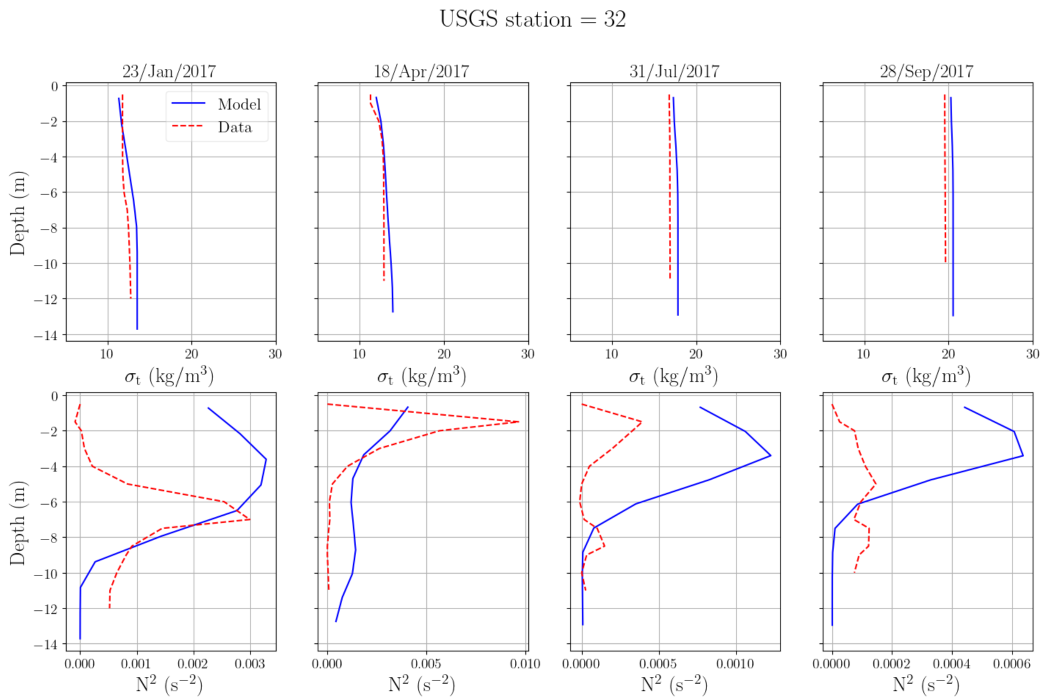

Figures B.1.18. Density profiles and N^2 profiles at station 32 for WY2017

WY2013

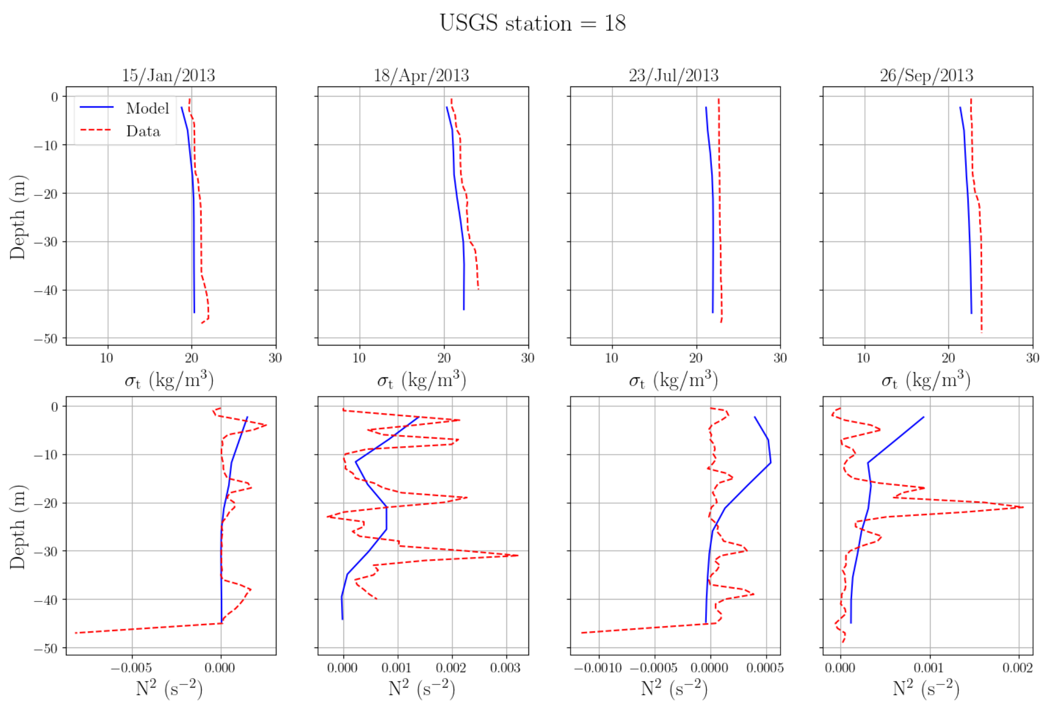

Figures B.1.19. Density profiles and N^2 profiles at station 18 for WY2013

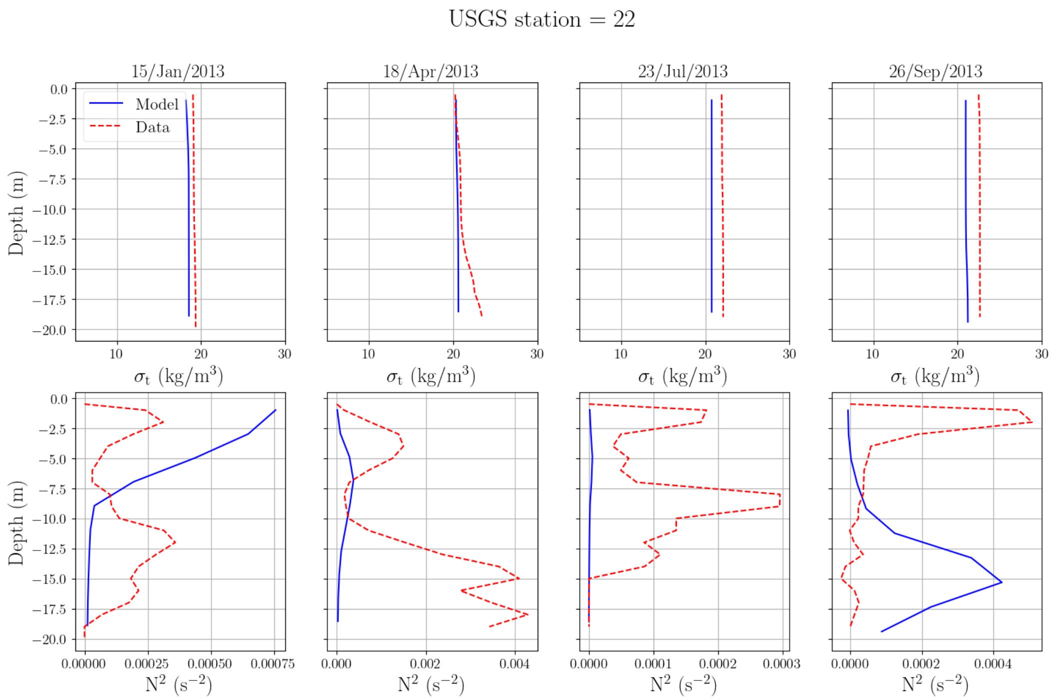

Figures B.1.20. Density profiles and N^2 profiles at station 22 for WY2013

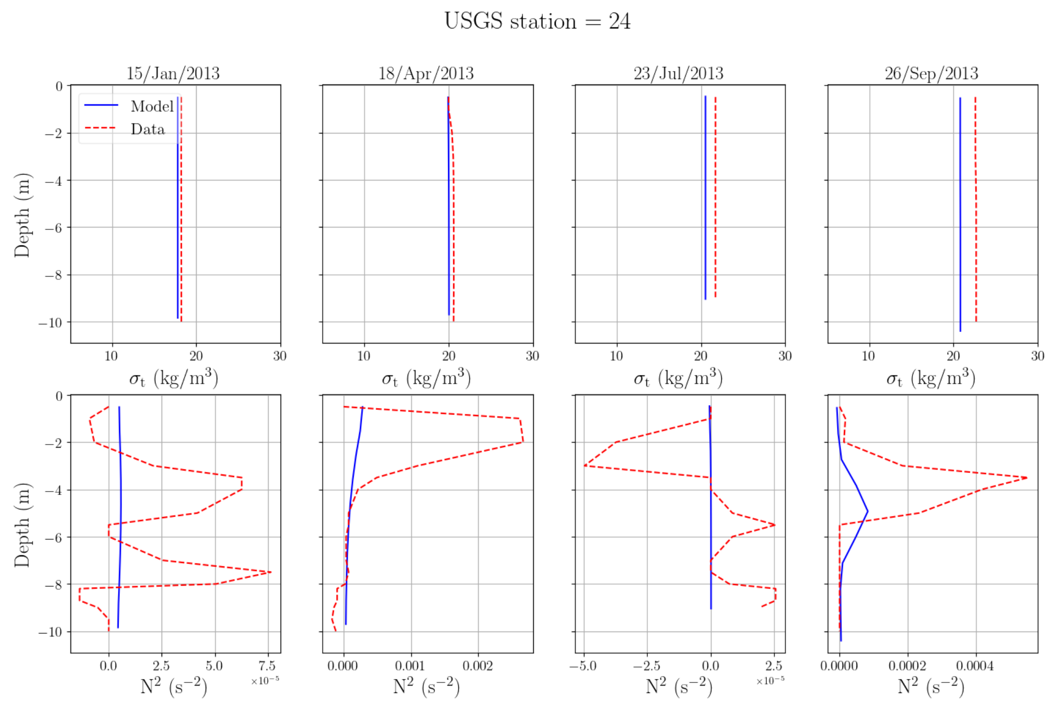

Figures B.1.21. Density profiles and N^2 profiles at station 24 for WY2013

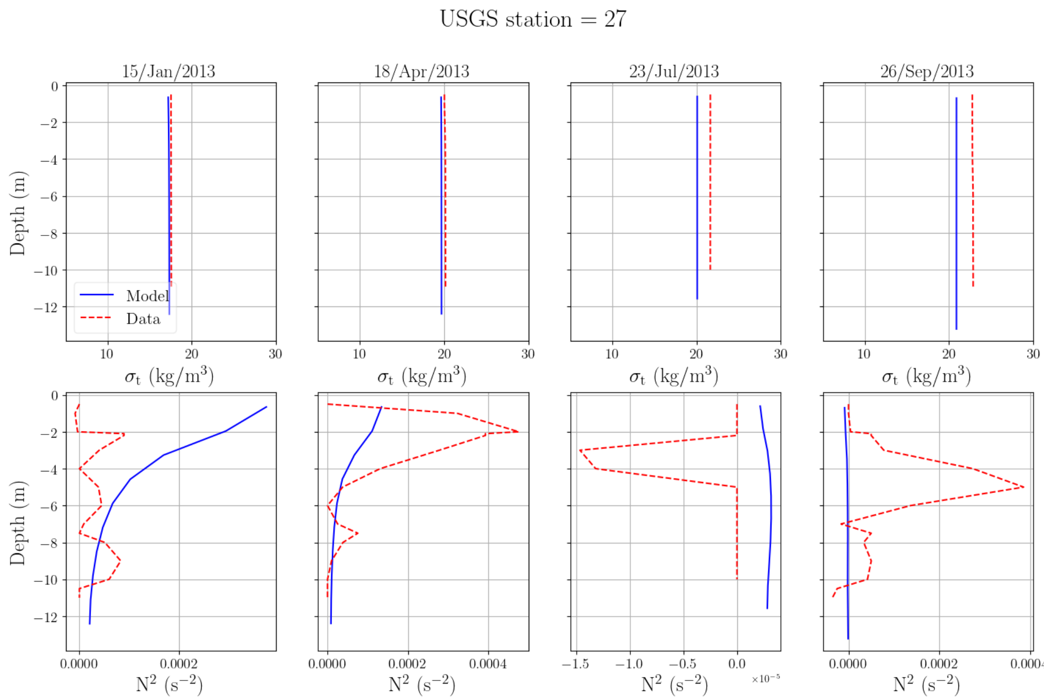

Figures B.1.22. Density profiles and N^2 profiles at station 27 for WY2013

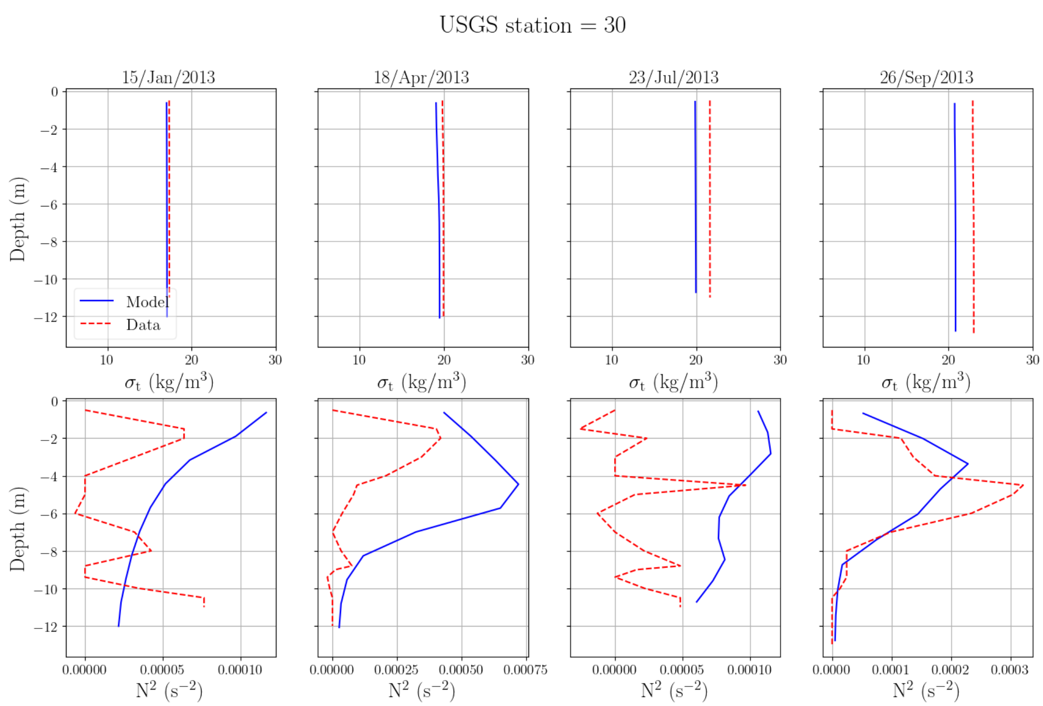

Figures B.1.23. Density profiles and N^2 profiles at station 30 for WY2013

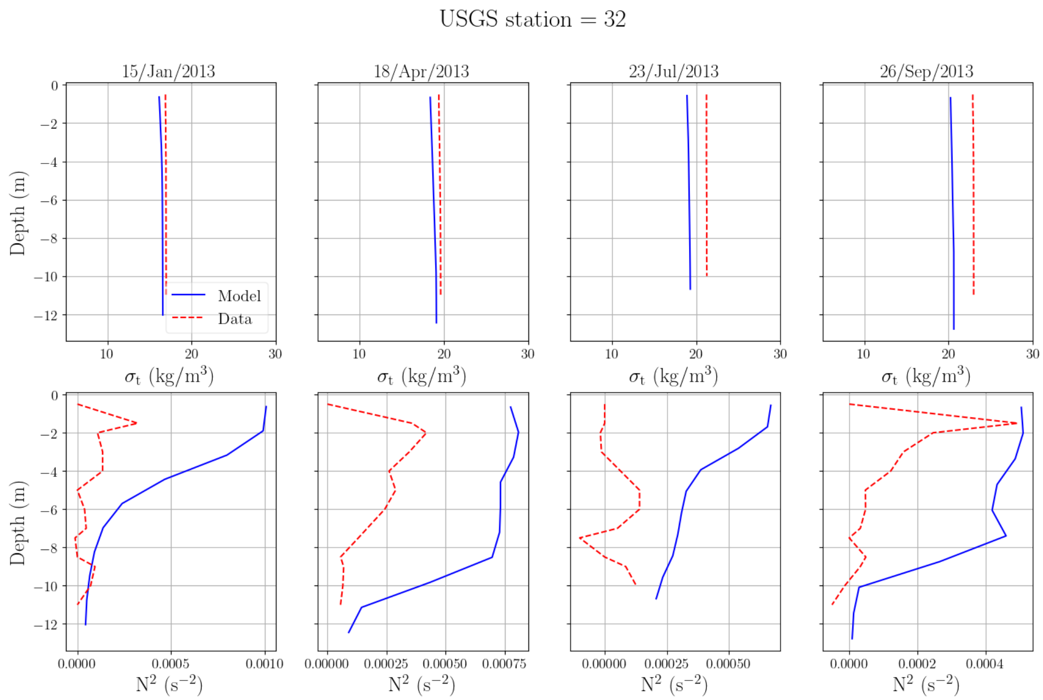

Figures B.1.24. Density profiles and N^2 profiles at station 32 for WY2013